1 1/1 7/94

ELECTRON Attachment TO MOLECULES AT LOW ELECTRON ENERGIES

A. Chutjian[1], A. Garscadden[2], and J. M. Wadehra[3]

TABLE OF CONTENTS

ELECTRON ATTACHMENT TO MOLECULES AT LOW ELECTRON ENERGIES

A. Chutjian[1], A. Garscadden[2], and J. M. Wadehra[3]

[1]Jet Propulsion Laboratory, California Institute of Technology
Pasadena, CA 91109 USA

[2]Air Force Wright Laboratory
Wright-Patterson Air Force Base, OH 45433

[3]Physics Department, Wayne State University,
Detroit, MI 48202

1. INTRODUCTION

One of the most efficient ways of producing negative ions is by the process of dissociative electron attachment to molecules, Here, a diatomic or polyatomic molecule dissociates, by the impact of a low energy electron, into component atoms (or smaller molecular species) while the incident electron attaches itself to one of the dissociating fragments. For certain molecular species the cross section for dissociative attachment (DA) is strongly dependent on the initial rovibrational level of the target. The cross section for DA can be enhanced several orders of magnitude simply by rovibrationally exciting the molecule initially. This excitation could itself be caused by the incident electron, In fact, in the resonance model described below the processes of dissociative electron attachment and rovibrational excitation by electron impact are treated as consequences of two alternative channels for decay of the resonant state. This strong relation between dissociative attachment and vibrational excitation has been emphasized in a number of reviews (Massey 1976,1 980; Smirnov 1982, Kazanskii and Fabrikant 1984, Wadehra 1986, Gauyacq 1987, Domcke 1991).

The usual way of describing, in the resonance model, the physics of DA to molecule AB is *via* the formation of a temporary bound state of the electron-molecule system. The electron in this molecular anion state AB^- (also called the resonance state) can autodetach with a finite lifetime (related to the width Γ of the resonance), leaving behind a vibrationally-excited neutral molecule. On the other hand, if the

lifetime of the resonance is long enough, the anion AB^- can dissociate into A + B-, leading to the process of dissociative electron attachment, Schematically, one has

$$e_i + AB\ (v_i) \rightarrow AB^- \begin{cases} \rightarrow A + B^- \\ \rightarrow e_f + AB\ (v_f)\ . \end{cases} \qquad (1)$$

The final level of quantum number v, can be either discrete (corresponding to excitation of the molecule) or could lie in the continuum (corresponding to dissociation of the molecule).

A possible scenario of the resonance model is depicted in Fig. 1. Shown schematically are the potential energy curves of the neutral molecule AB (labeled V_0) and of the resonant state AB^- (labeled V-), The two potential curves cross at an internuclear separation $R = R_s$ such that, for $R \geq R_s$, the autodetachment of the electron is energetically not permitted. The resonance turns into a stable bound state of AB^-, and R_s is referred to as the stabilization radius, Before the incident electron is captured, the nuclei are rovibrating in the level (v_i, J_i) under the influence of the potential $V_0(R)$. After electron capture, the nuclei of the anion move under the influence of V-(R), The probability of electron capture to form the resonant molecular anion state depends on the internuclear separation. This probability is maximum at an internuclear separation (labeled R_c in Fig, 1 and referred to as the capture radius) at which the energy separation between the two potential curves is equal to the energy of the incident electron. If the potential curve V^- is repulsive in nature, the nuclei in the anion state begin to separate such that the electronic potential energy is converted into nuclear kinetic energy. If autodetachment of the electron occurs at some specific internuclear separation R the neutral molecule is left in a rovibrationally excited level due to the gain in the nuclear kinetic energy (indicated by a vertical dotted line in the figure), The exact rovibrationally excited level (v_f, J_f) achieved by the molecule depends on the gain in the kinetic energy of the nuclei as well as on the relevant selection rules. Depending upon the lifetime of the resonance the nuclei may separate to an internuclear separation larger than R_s beyond which autodetachment of the electron is energetically not possible. Dissociative attachment may then occur resulting in the formation of a stable negative ion.

During the lifetime of the resonance the time spent by the incident electron ($\hbar/\Gamma \sim 10^{-14}$s) in the neighborhood of the molecule is much larger than the normal transit time ($\sim 10^{-17}$s for a 10-eV electron). There are various mechanisms which can be responsible for temporarily confining the electron. These include a centrifugal

potential barrier if the target molecule is in an electron configuration with nonzero angular momentum (shape resonance), or an excitation of the target molecule whereby the incident electron is left with insufficient energy to escape (Feshbach resonance). The lifetime of the temporary trapping of the electron is determined by the width Γ of the resonance. Various limits of the resonance are classified by comparing its lifetime $\hbar/\Gamma$ with the average vibrational period 1/w of the nuclei in the resonant state. The condition $\hbar/\Gamma << 1/w$ corresponds to the *impulse limit*, since it implies that the nuclei have little opportunity to vibrate during the lifetime of the resonance, The other extreme $\hbar/\Gamma >> 1/\omega$ corresponds to the *compound-state limit* wherein the nuclei make a large number of vibrations during the resonance lifetime. The *boomerang limit* $\hbar/\Gamma \sim 1/w$ *is* characterized by interference between a single outgoing and a single reflected nuclear wave.

A few salient features of the resonance model are worth noting. First, the processes of DA and vibrational excitation are treated on an equal footing. The investigation of one leads, in a natural way, to information on the other. In fact, the optical theorem (which is essentially a conservation-of-flux statement) relates the cross sections for these two processes within the resonance model, Second, in the qualitative discussion above we have considered only the formation of a single resonant state, For some molecules and for a certain range of incident electron energies it is possible to form more than one resonant state. Furthermore, autodetachment of the electron in the resonance can lead to more than one final electronic state of the neutral. In either case the total resonance width can be partitioned into a sum of partial widths, each corresponding to a transition between the anion state and an electronic state of the neutral, Third, it was tacitly assumed above that the transition between the temporary anion and the electronic state of the neutrals is a spontaneous one, without any change in nuclear positions or velocities (a Franck-Condon transition). This *local* description of the resonance is valid when the incident electron energy is much greater than the spacing of vibrational levels, or when the incident energy is considerably above threshold. These conditions are not met at low electron energies, and the proper description of the resonance is a *nonlocal* one involving, in its mathematical formulation, an integrodifferential equation with a nonlocal complex potential.

With the advent of several new experimental techniques in the past decade, one has been able to explore the electron attachment properties of diatomic and polyatomic molecules at very low electron energies (below 100 millielectron volts) with resolutions of 5 meV and less. This work has highlighted the fact that for some

diatomic molecules, and for several broad classes of polyatomic molecules, the attachment in this energy range is dominated by an s-wave threshold law. In this case, the attachment cross section $\sigma_A(\epsilon)$ is predicted to vary as $\epsilon^{-1/2}$, where ϵ is the electron energy. Thus, the cross section diverges in the limit of zero electron energy. Such was noted by Wigner in a completely different application (thermal neutron capture by light nuclei) (see, for example, Bethe 1935, Wigner 1948). As is the strength of threshold-law analysis, the same behavior is applicable in dissociative; and nondissociative, electron capture by some molecules. S-wave electron attachment is one of the rare cases in molecular physics where one encounters an infinite cross section.

The diatomic molecules studied to date, in the energy range O-100 meV have been HI, DI, HCI, Cl_2, and F_2. The polyatomic molecules have been SF_6, butanedione, pentandione, so-called "superacids", members of a class of perfluorinated carbon compounds, chlorohalocarbon compounds, and even the explosives molecules RDX, PETN, and TNT, In fact, the s-wave phenomenon is at the heart of two new types of explosives detectors under study: the thermal neutron analyzer (TNA) now deployed at some airports, and the reversal electron attachment detector (READ) presently under development. One wonders if Bethe and Wigner knew they were touching on problems of explosives detection when pondering threshold laws!

Presented herein is a summary of several experimental techniques which have been extensively used in the study of low-energy electron attachment. These are, as single-collision methods, the high-Rydberg collisional ionization, rare-gas photoionization, crossed-beams and the reversal electron attachment detector (READ) techniques; and as multiple-collision methods the Cavalleri electron density sampling (CEDS), electron swarm, flowing- afterglow/Langmuir-probe (FALP) and microwave conductivity/pulsed radiolysis (MCPR) techniques. We present a brief summary of these methods, and show that results from these methods can be combined and compared to give new insights into the mechanism of electron attachment. We then give a practical application of the s-wave phenomenon to trace species detection.

II. THEORETICAL METHODS

1. Basic Equations in the Resonance Model

The projection-operators technique is used to derive the integrodifferential equation, with complex potentials, governing the dynamics of the nuclei in the resonant state (O'Malley 1966), From a conceptual point of view a resonance can be treated as a discrete bound state of the electron-molecule system embedded in, and interacting with, the continuum states of the target molecule (Fano 1961, Bardsley *et al 1966).* The total Hamiltonian of the electron-molecule system can be written as a sum of the nuclear kinetic energy operator $T_N(R)$ and the electronic Hamiltonian H_{el}:

$$H = H_{el}(q, R) + T_n(R) \quad . \tag{2}$$

Here q stands collectively for all the electronic coordinates including those of the incident electron, The complete wave function $\Psi(q,R)$ of the system satisfies the Schrödinger equation,

$$(H - E)\Psi(q, R) = 0 \quad . \tag{3}$$

E is the total energy of the system, including the internal energy (electronic as well as rovibrational) of the target molecule, and the energy of the incident electron. P and Q are projection operators in the electronic part of the Hilbert space

$$P = \int |\epsilon\rangle\langle\epsilon| d\epsilon \quad , \quad Q = |d\rangle\langle d| \tag{4}$$

and they project out, respectively, the discrete resonant state $|d\rangle$ embedded in the continuum, and the continuum states $|\epsilon\rangle$ representing a free electron (with energy ϵ moving in the direction ?) and the neutral target molecule. The continuum states are energy-normalized with density-of-states taken as unity. The operators P and Q satisfy the standard requirements of projection operators, namely,

$$P^2 = P, \quad Q^2 = Q, \quad P + Q = 1, \quad PQ = QP = 0. \tag{5}$$

Assuming that the Born-Oppenheimer approximation is valid for the wave functions in the configuration space, the electronic functions $\langle q|d\rangle = \phi(q,R)$ and $\langle q|\epsilon\rangle = \psi_\epsilon(q,R)$ are slowly varying functions of the parameter R. This implies that the electronic projection operators P and Q commute with the nuclear kinetic energy operator $T_N(R)$ and, therefore, PHQ = $PH_{el}Q$. Furthermore, using the notation that $\langle ,.. \rangle_q$ represents integration over all electronic coordinates, one can define

$$\langle d|H_{el}|d\rangle_q = V^-(R) \ ,$$

$$\langle \epsilon|H_{el}|\epsilon'\rangle_q = (T_N + V_0(R) + \epsilon)\,\delta(\epsilon - \epsilon') \ , \qquad (6)$$

$$\langle d|H_{el}(q,R)|\epsilon\rangle_q = V(\epsilon,R) \ .$$

Here $V^-(R)$ and $V_0(R)$ serve as the electronic energies of the anion resonant state and of the neutral target state of the molecule, respectively. The matrix element $V(\epsilon,R)$ which mixes the discrete electronic state $|d>$ with the continuum states $|\epsilon>$ converts the discrete state into a resonance. If E_v is the internal vibrational energy of the target molecule, then

$$[T_N + V_0(R)]\,|v\rangle = E_v|v\rangle \ . \qquad (7)$$

Here $\langle R|v\rangle = \chi_v(R)$ is the nuclear wavefunction of the vth vibrational level of the target molecule. If the total wave function Ψ is split, using the projection operators, into parts $P\Psi$ and $Q\Psi$, that is

$$\Psi = P\Psi + Q\Psi \ , \qquad (8)$$

then both parts include nuclear as well as electronic degrees of freedom, For asymptotically-large separation between the target molecule and the incident electron, the part $Q\Psi$ vanishes while the part $P\Psi$ behaves as a product of the wave functions of the target molecule and of a free electron. In the configuration space the part $Q\Psi$ takes on a specially simple product form $\phi(q,R)\xi(R)$, where $\xi(R)$ is the nuclear wave function of the resonant anion state and $\phi(q,R)$ is a square-integrable electronic part of the wave function that depends only parametrically on the internuclear separation R. The coupled inhomogeneous equations satisfied by functions $P\Psi$ and $Q\Psi$ are obtained by substituting Eq. (8) into Eq. (3) and then projecting into P and Q spaces:

$$P(H - E)\,P\Psi = -PHQ\Psi \ , \qquad (9a)$$

$$Q(H - E)\,Q\Psi = -QHP\Psi \ . \qquad (9b)$$

A formal solution of the inhomogeneous Eq. (9a) is the sum of the homogeneous solution $P\psi_p$ and a particular solution with correct boundary condition:

$$P\Psi = P\psi_p + G_p PHQ\Psi = P\psi_p + [P(E - H + i0^+)P]^{-1} PHQ\Psi . \qquad (10)$$

Here 0^+ is a vanishingly small positive number that accounts for the outgoing-wave boundary conditions in the open channels. The homogeneous solution correlates with incoming waves in the electron scattering channel and represents asymptotically a free electron with energy ϵ_i incident on the target molecule in vibrational level v_i, that is, $P\psi_p \rightarrow |\epsilon_i\rangle |v_i\rangle$. We note in passing that the dependence of the matrix element $V(\epsilon_i, R)$ on the direction $\hat{\epsilon}_i$ of the incident electron appears only through the plane wave representing the incident electron, One can, therefore, make the approximation

$$V(\epsilon, R) = V(\epsilon, R)\, Y_{lm}(\hat{\epsilon}) , \qquad (11)$$

where $Y_{lm}(\hat{\epsilon})$ is the spherical harmonic in the leading contributing term in the expansion of the plane wave representing the electron. Substituting for $P\Psi$ from Eq. (10) in Eq. (9b) gives

$$Q\,(H + HG_p PH - E)\, Q\Psi = -QHP\psi_p ,$$

which can be rewritten, using Eqs. (4) and (6) as

$$[T_N + V^-(R) - E\,]Q\Psi + QH_{el} G_p\, PH_{el}\, Q\Psi = -QH_{el} P\psi_p . \qquad (12)$$

On premultiplying Eq.(12) by $\langle d| \langle R|$ and using the closure relation $\int dR' |R'\rangle \langle R'| = 1$ as well as the completeness relation $\sum |v\rangle \langle v| = 1$ for the nuclear states in the last term of the left-hand side, one obtains the differential equation satisfied by $\xi(R)$, the nuclear part of the wave function of the resonant anion state,

$$[T_N + V^-(R) - E\,]\xi(R) +$$

$$+\sum_{\Psi} \int d\epsilon \int dR'\, V(\epsilon, R)\, \chi_v(R) \left(\frac{1}{E - E_v - \epsilon + i0^+}\right) \chi_v^*(R')\, V^*(\epsilon, R')\, \xi(R') =$$

$$= -V^*(\epsilon_i, R)\, \chi_{v_i}(R) . \qquad (13)$$

On using the Dirac identity

$$\frac{1}{x + i0^+} = P\frac{1}{x} - i\pi\delta(x) \qquad (14)$$

and the approximation of Eq, (1 1) to carry out the integration over ?, Eq.(13) can be recast in the nonlocal form,

$$[T_N + V\text{-}(R) - E]\xi(\boldsymbol{R}) + \int d\boldsymbol{R}' K(\boldsymbol{R}, \boldsymbol{R}')\,\xi(\boldsymbol{R}') = -V^*(\epsilon_i, R)\, xvi(R). \tag{15}$$

This is the fundamental integrodifferential equation governing the motion of the nuclei in the resonant anion state. It can also be derived using techniques such as the theory of configuration interactions (Bardsley 1968). The nonlocal kernel K(R, R') is explicitlv where

$$K(\boldsymbol{R}, \boldsymbol{R}') = \sum_v \chi_v^*(\boldsymbol{R}')\,\chi_v(\boldsymbol{R})\,[\Delta(R, R';\ E-E_v) - \frac{i}{2}\Gamma(R, R'; E-E_v)], \tag{16}$$

$$\Gamma(R, R';\ E-E_V) = 2\pi V(E-E_v, R)\, V^*(E-EV,\ R'), \tag{17a}$$

and

$$\Delta(R, R';\ E-E_v) = P\int d\epsilon \frac{V(\epsilon, R)\, V^*(\epsilon, R')}{E-Ev-c} = \frac{P}{2\pi}\int d\epsilon \frac{\Gamma(R, R';\ d}{E-E_v-\epsilon}, \tag{17b}$$

The shift A and width Γ of the resonance depend on ϵ_v (≡ E - E.) which is the energy of the scattered electron following the transition O + v in the target molecule. The nonlocal integrodifferential Eq. (15) for ξ(R) can be approximated by a local ordinary differential equation if the coupling matrix element V(ϵ,R) is almost independent of the energy ϵ. This, for example, will be case if the incident electron energy is large compared to the vibrational spacings of the target molecule: it then becomes reasonable to replace ϵ_v in Eq. (16) either by the incident electron energy ϵ_i, or by the local electron energy V-(R) - V_o(R). The nonlocal kernel of Eq. (16) then becomes a local function,

$$K(R, \boldsymbol{R}') = \delta(\boldsymbol{R}-\boldsymbol{R}')\,[\Delta(R;\epsilon_i) - \frac{i}{2}\Gamma(R;\epsilon_i)], \tag{18}$$

and ξ(R) satisfies an ordinary differential equation

$$[T_N + V^-(R) + \Delta(R;\epsilon_j) - \frac{i}{2}\Gamma(R;\epsilon_j) - E]\ \xi(R) = -V^*(\epsilon_j, R)\chi_{v_i}(R) \quad . \tag{19}$$

Here,

$$\Gamma(R;\epsilon_j) = 2\pi |V(\epsilon_j, R)|^2 \quad , \tag{20a}$$

and

$$\Delta(R;\epsilon_j) = \frac{P}{2\pi}\int d\epsilon \frac{\Gamma(R;\epsilon)}{\epsilon_j - \epsilon} \quad . \tag{20b}$$

2. Cross Sections for Dissociative Attachment

The cross section for 'the DA process e -t AB → A + B" is obtained by comparing the outgoing flux of ion-atom pairs to that of the incident electrons. Let $\hbar$K and $\hbar$k$_i$ represent the momentum of the relative motion of the ion-atom system (reduced mass M) and of the incident electron (mass m), respectively, For large ion-atom separation the outgoing ion-atom flux, averaged over the orientations of the molecule, is

$$\frac{1}{4\pi}\int d\hat{R}\ \frac{\hbar K}{M}|\xi(R)|^2 R^2 = \frac{1}{4\pi}\ \frac{\hbar K}{M}|\xi(R)|^2 \quad ,$$

where ξ(R) is the radial part of ξ(R). Assuming energy-normalization of the plane wave representing the electron, the incident electron flux is

$$\left(\frac{mk_i}{8\pi^3\hbar^2}\right)\frac{\hbar k_i}{m} \quad .$$

Hence, the cross section for dissociative electron attachment is given by

$$\sigma_{DA} = \frac{2\pi^2\hbar^2 K}{k_i^2 M}|\xi(R)|^2 \quad . \tag{21}$$

Both local and nonlocal differential equations have been numerically solved for the nuclear wavefunction ξ(R) to obtain DA cross sections for a number of molecules (Wadehra 1986, Wadehra 1990, Atems and Wadehra 1990, Domcke 1991).

3. Other Theoretical Methods

A number of other theoretical approaches have been used for investigating the process of dissociative electron attachment to molecules. Here we provide a brief description of some of these investigations.

A. Use of Fadeev Equations

The system of Fadeev equations is a mathematical embodiment of a three-body system in which the three particles interact *via* two-body potentials. If the process of DA to molecules AB is treated as a three-body rearrangement process e + AB → eA + B then the set of Fadeev equations can be used to describe this process provided the interaction of the electron with AB is replaced by the interaction of the electron with individual fragments A and B as if they were isolated field centers. This appears to be a reasonable approximation as long as the incident electron energy is below the threshold for electronic excitation, The Fadeev-equations approach has the merit of including multipole scattering effects in a three-body system in a concise and consistent manner. Drukarev and Pozdneev (1 980) and Pozdneev (1 982) have used this formalism to obtain DA cross sections in isotopes of H_2, halogen molecules, and in the hydrogen halides.

B. The /?-Matrix Technique

The well-developed R-matrix formalism for calculating scattering parameters in collisions of electrons with diatomic molecules at fixed internuclear separation can be modified so that the restriction on nuclear motion is relaxed, This makes it possible to use the R-matrix technique for obtaining both vibrational excitation (Schneider *et a/ 1979a)* and DA (Schneider *et a/* 1979b) cross sections. A small R-matrix radius divides configuration space into an internal and an external region such that, in the internal region, a compound state of N + 1 electrons is postulated -- analogous to the resonance model. Assuming the Born-Oppenheimer approximation is valid (*i e,* effects due to coupling of the electronic and nuclear motions is negligible) it becomes straightforward to evaluate all relevant expressions using slight modifications of the computer codes employing fixed-nuclei methods. It has been explicitly demonstrated (Fabrikant 1990) that the two different mathematical approaches using the resonant compound state (the nonlocal complex potential approach and the R-matrix approach) are equivalent. The practical difference is that in the R-matrix approach there is no need to assume analytical behavior of the level shift and width functions, since the

complete energy dependence is contained in the expression for the continuity of the logarithmic derivative of the electronic wavefunction at the R-matrix radius. Actual numerical calculations of DA and vibrational excitation have been carried out for HF (Fabrikant *et al 1992)* and N_2 (Schneider *et a/ 1979a)* molecules.

c. Additional Theoretical Techniques

Gauyacq (1 985) has used a nonresonant formalism, based on the effective-range theory and the zero-range potential approximation of Demkov (1 964), to investigate DA in H_2. In this formalism no resonant state of H_2^- is explicitly introduced as an intermediary, In the nonresonant mechanism the incident electron induces vibrational excitation by nonadiabatic effects which can cause the molecule to stretch enough to reach the crossing point of the neutral and anion potential-energy curves (the stabilization radius in the resonance model). This, in turn, assures electron capture into a bound state of the dissociated fragment. The interaction between the incident electron and the fixed-nuclei molecule is represented, in the effective-range approximation, *via* the introduction of a boundary at $r = r_c$. For $r > r_c$ the electron is assumed to feel only a long-range potential which is taken to be the dipole plus quadruple polarization potentials. The short-range interaction is replaced, in the spirit of the zero-range potential, by a single number dependent on the internuclear separation R; and which represents the logarithmic derivative of the radial wavefunction at $r = r_c$. Using a single adjustable parameter it was possible to reproduce the experimentally-observed enhancement of DA cross sections in vibrationally-excited H_2.

4. Angular Distributions

The angular distributions of electrons that are resonantly scattered by a molecule were theoretically analyzed, almost simultaneously, by Read (1 968) and O'Malley and Taylor (1 968), The expressions derived contain a few (normally two) adjustable parameters so that it becomes necessary to utilize some information from experimental measurements of angular distributions to obtain, theoretically, the correct magnitudes of the differential cross sections (DCS). Some of the assumptions made in the theoretical analysis were:

(i) the rotation of the molecule is insignificant during the lifetime of the resonance,

(ii) the projection of the electronic angular momentum on the molecular axis (μ, A,

and A, for the incident electron, the initial target state and the resonant state, respectively) is conserved and this conservation selects a single μ value, namely, $\mu = |\Lambda_r - \Lambda_t|$,

(iii) the electron-molecule interaction is spherically symmetric andspin-independent,

(iv) the electron-molecule scattering is dominated by a single resonance so that the nonresonant scattering as well as scattering due to other resonances can be neglected. Thus, the angular distribution of the DA process is governed by a single spherical harmonic $Y_{L\mu}$ (or a superposition of a few spherical harmonics of orders equal to or higher than L and with the same μ).

Using these assumptions, detailed expressions for the DCS of the two complementary processes of DA and vibrational excitation were obtained by O'Malley and Taylor and by Read. An equivalent derivation of the DCS for the resonant vibrational excitation process has been provided by Chang (1 977). Differential cross sections for the specific DA process can be expressed in the form,

$$\sigma_{DA}(\Omega) = \frac{4\pi^3}{k_1^2} \exp(-p) \sum_{\Lambda_r} |T_{DA}|^2 \qquad (22a)$$

where the transition moment is of the form

$$T_{DA} = \sum_{L=|\mu|}^{\infty} Y^*_{L\mu}(\Omega)\, \mathbb{R}\,, \qquad (22b)$$

where R represents the radial dependence of the scattering. For some specific molecules (such as H_2, N_2, CO, NO, O_2, CO_2, and a few hydrocarbons), explicit angular distributions for resonantly scattered electrons were predicted by Bardsley and Read (1968) using Eqs. (22a) and (22 b).

In the case of electron scattering from polar molecules (e.g. HCl, HF and NaCl) the electron-molecule interaction is not spherically symmetric. For large electron-molecule separations the interaction is dominated by the dipole field of the polar molecule. The assumption (iii) is clearly violated and one has to abandon the use of spherical harmonics. In order to investigate the angular dependence of DA in polar molecules, Teillet-Billy and Gauyacq (1984) essentially replaced spherical harmonics $Y_{L\mu}$ by dipolar angular modes $\phi_{L\mu}$ which are eigenfunctions of the angular part of the electron-dipole interaction system. Since an electron is more likely to approach a

dipole from its positive end, the introduction of a dipolar field results in an asymmetry to the forward and backward electron scattering. The corresponding asymmetry in the DCS'S naturally depends on the dipole moment.

To date, a number of experiments have been carried out to investigate the angular distribution of negative ions formed by DA in various diatomic and polyatomic molecules (Van Brunt and Kieffer 1970, 1974; Hall *et a/ 1977,* Tronc *et al 1977, 1979, 1988;* Azria *et al* 1980, Azria 1984, LeCoat *et* a/ 1985, 1991; Abouaf *et* a/ 1985). For homonuclear diatomic molecules, these angular distributions are symmetric about 90°. For heteronuclear diatomic molecules with permanent dipole moments, such as CO and HCl, there is an asymmetry in the angular distributions.

5. Semiclassical Approximation and the Isotope Effect

A solution of the local radial equation for $\xi(R)$ in the semiclassical approximation contains the usual WKB factor

$$exp\left[-Im \left| \int_{R_c}^{R_s} \sqrt{\frac{2M}{\hbar^2} [E - V^-(R) - \Delta(R;\epsilon_i) + \frac{i}{2}\Gamma(R;\epsilon_i)]\, dR} \right| \right]. \qquad 23a)$$

For a narrow resonance (small Γ and A) this factor can be approximated by

$$\exp\left(-\int_{R_c}^{R} \frac{\Gamma(R)}{\hbar} \frac{dR}{v(R)} \right), \qquad 23b)$$

where $v(R) = \sqrt{2[E - V^-(R)]/M}$ is interpreted as the relative velocity of the outgoing ion-atom pair. Thus, for a narrow resonance, the DA cross section can be approximated by $\sigma_{DA} = \sigma_{cap} S$. Here σ_{cap} is interpreted as the cross section for the formation of the resonance by electron capture, and the second factor S, commonly called the survival factor,

$$S = \exp\left(-\int_{R_c}^{R_s} \frac{\Gamma(R)}{\hbar} \frac{dR}{v(R)} \right), \qquad (24)$$

is the probability that the nuclei in the resonant state separate from the capture radius R_c to the stabilization radius R_s without autodetachment. The survival factor measures

the probability that the resonance survives long enough to assure that the process of DA will transpire.

The semiclassical cross section $\sigma_{DA} = \sigma_{cap} S$ also permits physical insight to the isotope effect in DA. The effect of replacing either one or both of the nuclei in a molecule by their heavier isotopes would be most noticeable for a light molecule such as H_2 because of the relatively larger change in reduced mass. To understand the isotope effect we note that the survival factor S, which is strongly mass dependent, can be approximated by exp $(-\Gamma\tau/\hbar)$ where τ is the time taken by the nuclei to separate from R_c to R_s. Simple kinematical considerations suggest that this time τ is proportional to $M^{1/2}$. Thus nuclei of the heavier isotope, taking longer time than, nuclei of the lighter isotope to separate to R_s, experience a stiffer competition from autodetachment. In effect this reduces the cross section for DA in the heavier isotope of the molecule. In particular, fully quantum-mechanical calculations (Wadehra 1984) show that the peak cross sections for DA in D_2 and T_2 are smaller (by factors of 527 and 65217, respectively) than the corresponding cross section for H_2. The mass dependence of the attachment cross section (the isotope effect) is therefore $\sigma_{DA} \propto$ exp (- constant $\bullet$ M"*). As an example, the value of the ratio

$$\frac{in\ [\sigma_{peak}\ (H_2)\ /\sigma_{peak}\ (T_2\ )\ 1}{in\ [\sigma_{peak}\ (H_2\ )\ /\sigma_{peak}\ (D,\ )\ 1}\ ,$$

using numerically-calculated attachment cross sections, is $ln(65217)/ln(527) = 1.769$. If the isotope effect discussed above were valid, this ratio should be

$$\frac{(M_{T_2}^{1/2} - M_{H_2}^{1/2})}{(M_{D_2}^{1/2} - M_{H_2}^{1/2})} = \frac{\sqrt{3} - 1}{\sqrt{2} - 1}$$

whose value is 1,767, The two values are quite close, showing the validity of the isotope-effect formulation.

6. Klots's Analytical Formula

The long-range interaction between the incident electron and the target molecule is of the form

$$V_{pol}(r) = -\frac{\alpha e^2}{2r^4}$$

where a is the static dipole polarizability of the molecule, Using classical arguments one can see that for a given electron energy $\epsilon = \hbar^2 k^2/2m$ there is an impact parameter b_o such that for $b < b_o$ the electron and molecule are drawn together in an unstable orbiting motion. This provides the classical capture cross section (Langevin 1905) $\sigma_{cap} = \pi b_o^2$. Fully quantum- mechanical calculations using the polarization potential provide a capture cross section which, in the limit $\epsilon \to$ O, is twice as large as the classical Langevin cross section, and is given by (Vogt and Wannier 1954) as

$$\sigma_{\cap} = 4\pi a_o^2 \left(\frac{\alpha Ry}{a_o^3 \epsilon}\right)^{1/2},$$

where a_o and Ry are the Bohr radius and the Rydberg, respectively. This form of the capture cross section led Klots(1 976) to propose the following analytical form for the attachment cross section

$$\sigma_{DA} \quad (\epsilon) \frac{\pi\ Ry a_o^2}{\epsilon}\left(1 - \exp\ -4\ \left(\frac{\alpha\epsilon}{a_o^3 Ry}\right)^{1/2}\right),$$

which agrees with the capture cross sec ion for $\epsilon \to$ O and extends to the "geometrical" cross section π/k^2 at larger values of ϵ. This analytical form is seen to be an excellent fit to the experimental electron attachment data in the millielectron volt energy range (Klar et *a/* 1992b).

III. EXPERIMENTAL METHODS

1. Electron Energies Below 0.5 eV

A. High-Rydberg Collisional Ionization

Consider the reaction

$$X(nl) + AB \to X^+ + AB^-\ (or\ A + B^-)\ , \qquad (25)$$

where X(*nl*) is usually a xenon or rubidium atom in a high-Rydberg state, and the target AB can be any thermal-energy electron-attaching species such as SF_6, CCl_4,

c-C_7F_{14}, *etc* (Stebbings 1976, West *et a/ 1976,* Foltz *et a/ 1977,* Hildebrandt *et a/ 1978,* Beiting *eta/* 1979, Dunning 1985, 1987, Kalamarides *eta/ 1987,* Kalamarides et *a/* 1990a, Ling *et a/ 1992).* The so-called "free-electron model" (Hickman *et a/ 1* 983, Matsuzawa 1983) predicts that the attachment rate constant of AB in Eq. (25) will be equal to that for attachment of free (continuum) electrons having the same velocity distribution as the Rydberg electrons. In essence, the high-Rydberg atom, for sufficiently large *n,* is a carrier of a free electron, of energy equal to its ionization potential minus binding energy.

One form of apparatus using Xe(*nl*) or Rb(*nl*) atoms is shown in Fig, 2. Here, Rb atoms effuse from an oven, and are intersected at right angles by a frequency-stabilized, single-mode pulsed dye laser. Two-photon excitation populates $n^2S_{1/2}$ and $n^2D_{5/2}$ levels, where $10 \leq n \leq 110$. The laser output is modulated (~ 3μs width at ~ 20 kHz repetition rate). Excitation takes place in the presence of the attaching gas in a field-free region, The lack of any observable shifting or splitting in the *n*D levels of ^{85}Rb is taken as is evidence that stray electric fields in the excitation-attachment region are negligible. Such fields can significantly alter the ionization potential of the Rb(*n*D) atom, and hence the effective Rydberg electron energy.

Collisions between the target and Rydberg atom are allowed to occur in a field-free region for a variable time t (1-10 μs) after the laser pulse. The number of atoms remaining after the delay time are sampled by selective field ionization (SFI). The SFI signal S(t) is proportional to the number N(t) of remaining atoms, and the rata constant k(v) for atom destruction is related to N(t) by

$$N(t) = N(0)\, e^{-bt} \qquad (26)$$

where $b = A_{eff} + k(v)[AB]$, $A_{eff} = \tau_{eff}^{-1}$ is the effective spontaneous radiation rate, and [AB] denotes the density of target AB. Measurement of b *vs* [AB], extrapolated to zero pressure, gives both A_{eff} (intercept) and k(v) (slope). The rate constants k(v) are then converted to cross sections *via* the relation

$$k(v) = \int \sigma_A(v)\, v f(v)\, dv \qquad (27)$$

where f(v) is the Rydberg electron velocity distribution, and σ(v) the attachment cross section for the "quasi-free" electrons. The electron energies accessed by this technique are about 0.1-40 meV. The higher energy is limited by post-attachment interactions (Kalamarides *et a/ 1989,* Popple *et a/ 1992,* Ling *et a/* 1993, Carman et *a/ 1993),* and the lower by a diminishing Rydberg population and the increasing effect

of stray electric fields.

Applications of this technique have been made to the measurement of negative-ion lifetimes, and the study of energy partitioning between the DA fragments (Walter 1989, Kalamarides *et al* 1989, 1990a, 1990b). Measurements of the velocity distribution (through time-of-flight) and angular distribution (through images on a position-sensitive detector) provide data on fragment lifetimes, and the effects of Coulomb attraction of the intermediate negative-ion state with the K^+ core. The collisional dynamics have been modeled in terms of the velocity distribution of the reactants, the lifetime and decay energetic of the intermediate state, and the electrostatic interaction between the final negative and positive ions (Ling *et al 1990).*

More recent applications involve the collisional ionization of very -high-n Rydberg atoms [K(np), where $100 \leq n \leq 400$] in which the energy is provided through rotational de-excitation of the polar target (Ling et *a/ 1993a,* 1993b). Cross sections in HF, NH_3, CH_3I and CH_2Br_2 have been found to vary as ϵ^{-1}, whereas the Born approximation gives a variation as $\epsilon^{-1/2}$. The difference has been ascribed to the large fractional change in momentum transferred to the electron during the long collision time. At these low energies, approaching ~ 13.6/4002 = 85 μeV, one also observes differences in the energy dependence for rotationally-inelastic scattering between targets having small (H_2S, 0.97D) and large ($C_6H_5NO_2$, 4.22D) dipole moments (Frey *et al 1* 994).

Experimental Considerations

1. Reducing stray magnetic and electrostatic fields is essential for eliminating electron spiraling and acceleration effects. The former is accomplished by high-permeability metal shields; the latter by use of six large-area copper electrodes. Any residual electric fields are reduced to less than the 10 μeV level by applying small bias potentials to the electrodes (Ling *et a/ 1992).*

2, Since the nature of the collision complex $X^{\bullet\bullet}$-AB is not well understood, the exact electron energy extant during the electron transfer is not clearly defined, especially if some lowering of the X*" ionization takes place during the collision.

3. Cross section data can be positioned on the energy axis according to either the average kinetic energy <c>., or the median kinetic ϵ_m of the Rydberg electron (Kalamarides *et a/ 1990,* Ling *et a/ 1992).* As pointed out by Klar et *a/* (1992b)

this energy difference, for n = 400, can be $\langle \epsilon \rangle_{nl} = 85\ \mu$eV or $\epsilon_m = 10\ \mu$eV, hence leading to some ambiguity.

4. Proximate collisions with low $n(\leq 40)$ atoms have shown some post-collision interaction (PCI). At even lower ns 20 the free-electron model breaks down due to the collisional and post-collisional interaction between X** and AB (Kalamarides *et al 1989,* Zheng et *a/ 1988,* Carman et *a/ 1993).* One must have a good diagnostic for the onset of PCI effects.

5. A separate measurement of total Rb^{+} signal must be made to determine to extent, if any, of direct collisional stripping of the high-Rydberg atom. This rate is subtracted from the total excited-atom depletion rate.

6. Absolute target pressures are required, and some error is introduced in calibration of a Bayard-Alpert gauge at higher pressures, for use at the low target pressures.

B. The Rare-Gas Photoionization Method

This technique utilizes the sharp $^2P_{1/2}$ photoionization threshold in atomic krypton or xenon to generate continuum electrons of energies in the range 1-200 meV with resolutions of 4-6 meV (FWHM) (Ajello and Chutjian 1979, Chutjian 1981, Chutjian *et al 1984,* Chutjian and Alajajian 1985a,b, 1987a,b, Alajajian and Chutjian 1986), The acronym *TPSA* was used, for Threshold Photoelectron Spectroscopy by Electron Attachment since the technique was originally applied to measurements of threshold photoelectron spectra (Chutjian and Ajello 1977, 1980; Ajello *et al 1980).* A schematic diagram of the apparatus is shown in Fig, 3. Kr atoms in the presence of the target AB are photoionized within a collision box by narrow-band photons from a He-Hopfield continuum lamp and a l-meter VUV monochromator. The ionization step

$$\hbar\omega + Kr\,(^1S_o) \rightarrow Kr^{+}\,(^2P_{1/2}) + e\,(\epsilon) \qquad (28)$$

produces electrons e of energy ϵ where ϵ is given by the difference $\epsilon = \hbar\omega - E_t$ for photon energy $\hbar\omega$ and threshold ionization energy E_t (14.666 eV in Kr). The electrons then attach to the admixed target by

$$e\,(\epsilon) + AB \rightarrow AB^{-}\,(or\ A + B^{-}) \qquad (29)$$

The resulting ions are extracted from the collision region with a weak or near-zero electric field, estimated to be about 1.5 mV/mm (Alajajian *et al* 1988). The ions are mass-analyzed, and the signal stored *via* multichannel scaling. The production $P(\epsilon)$ of negative ions at electron energy ϵ can be written symbolically as

$$P(\epsilon) = S \otimes (\sigma_1 \times \sigma_A) \ . \qquad (30)$$

Here, S is the spectrometer slit function, σ_1 the Kr photoionization cross section, σ_A the electron-attachment cross section, and where the symbol $\otimes$ denotes convolution. If sources of broadening other than the spectral resolution S are present then the production of ions will be affected according to

$$P(\epsilon) = S \otimes b \otimes (\sigma_i \times \sigma_A) \ , \qquad (31)$$

where b is a function describing the other sources of broadening (Read 1975). These can be multiple, energy-changing electron-wall collisions (either inelastic or superelastic) prior to attachment, patch fields on the repeller or collision chamber, insulator surface charges or inhomogeneous draw-out fields.

For deconvolution from the spectral slitwidth, the lineshape is parametrized in the form

$$\sigma_A(\epsilon) = N[a(\epsilon^{-1/2} e^{-\epsilon^2/\lambda^2}) + e^{-\epsilon/\gamma}] \ , \qquad (32)$$

The parameters *a* and λ are determined from the lineshape unfolding, γ from the high-energy (ϵ > 10 meV) part of the lineshape, and/V by normalization to the thermal attachment rate constant at 300 K. For the latter, one uses the expression

$$k(\bar{\epsilon}) = (2/m)^{1/2} \int_0^\infty \sigma_A(\epsilon)\, \epsilon^{1/2} f(\epsilon)\, d\epsilon \ , \qquad (33)$$

where $k(\bar{\epsilon})$ is the thermal attachment rate constant at mean electron energy $\bar{\epsilon}$ = 38.78 meV (300 K), *m* the electron mass, and where $f(\epsilon)$ is the Maxwellian electron energy distribution function (EEDF). Values of $k(\bar{\epsilon})$ are obtained from other techniques, such as the multiple-collision Cavalleri, swarm, *FALP*, or *MCPR* methods outlined below. The normalization is only meaningful, of course, if the attachment channels described by Eq. (29), and those measured in $k(\bar{\epsilon})$, are the same.

This approach has been refined by Klar et *a/ (1* 992a, 1992b, 1994), and extended to lower electron energies with sub-meV (< 0.4 meV, FWHM) resolution.

The acronym f. *PA* (Laser Photoelectron Attachment) has been attached . Excitation is made from the metastable Ar($4s\ ^3P_2$) level by one laser to the Ar($4P\ ^3D_3$) level. A second laser is used to excite from this level to either ns or *nd* Rydberg levels, or to the $Ar^+(^2P_{3/2})$ continuum (free electrons). With attachment of free electrons to SF_6 one observes both the s-wave phenomenon, and vibrational excitation of $SF_6(\omega_1)$. Below the $^2P_{3/2}$ ionization threshold one also observes collisional ionization from $Ar^{**}(ns,nd)$ Rydberg atoms. Darrach *et al* (1 994) are presently extending the original VUV approach to lower electron energies and sub-meV resolution by direct laser ionization to the $Xe^+(^2P_{1/2})$ continuum in a single step using a tripled 276 nm light from a Nd:YAG laser and a pulsed noble-gas jet to generate 92 nm radiation,

Experimental Considerations

1. The broadening function *b* due to stray electric fields in the collision region must have a width significantly smaller than the photon slitwidth (less than 5 meV, FWHM). For resolution less than about 3 meV pulsed extraction fields will have to be used to obviate problems of stray fields, unknown contact potentials, and incomplete extraction of negative ions (Alajajian *et al* 1988).

2. Eq. (32) gives the appropriate normalization *N* if the particular channel giving rise to the cross section $\sigma_A(\epsilon)$, as measured under single-collision conditions, is also the only channel contributing to $k(\bar{\epsilon})$, as measured under multiple-collision (swam *FALP,CEDS*) conditions. If more than one DA channel is open, then $k(\bar{\epsilon})$ is a sum over all open channels, including collision-stabilized channels, whereas *N* represents only a single-channel normalization constant (Alajajian and Chutjian 1987),

3. Systematic errors are introduced when obtaining *N* through $k(\bar{\epsilon})$ *via* Eq. (33). The systematic errors arise from the considerable disagreement in the literature in values of $k(\bar{\epsilon})$ for many molecules.

4. The Kr photoionization technique does not require knowledge of particle densities. However, care must be taken to ensure that target and krypton pressures do not drift during a lineshape measurement. Also, checks must be made to see that the negative-ion signal rate is linear in target and krypton pressures, consistent with single-collision conditions.

5. There exists approximately a 1,8 meV error in the electron energy scale due to

grating calibration uncertainties. The VUV ionization scheme for electron production is not practical at energies below about 1-2 meV, whereas one of various laser-ionization schemes can yield greater resolution and intensity at the lower, sub-meV electron energies.

c. Crossed-Beams and Beam-Gas

Crossed beams of low energy electrons and attaching targets, and electron beams on static-gas targets, are effective techniques for measuring DA channels, branching ratios, lifetimes, and peak electron energies. In cases where the energy resolution is comparable to the natural width of the feature, so that deconvolution errors are small, cross section data can be obtained. However, the various techniques are limited to electron energies above about 0,1 eV. Uncertainty in the incident electron beam lineshape and electron energy scale (usually 0,2 eV or greater), along with diminishing electron current, are further limitations to application below 0.1 eV.

Several types of apparatus have been developed using a magnetically-confined, retarding-potential electron gun (Hadjiantoniou et *a/ 1973,* Spyrou *et a/ 1985),* an electrostatically-focused gun (Chantry 1982), or trochoidal monochromator (Stamatović and Schulz 1970, Scheunemann *et a/ 1980,* Kurepa et *a/ 1974).* Detection of negative ions can be by time-of-flight methods (TOF), mass spectrometry, and mass-unresolved current measurement.

A configuration utilizing a trochoidal monochromator, static-gas target and mass analysis is shown in Fig. 4 (Scheunemann eta*l 1980),* This apparatus has been used to measure attachment widths, energy locations and branching channels at energies approaching zero electron volts, with a resolution of about 70 meV. Electrons are emitted from a hairpin filament, and focused by lens elements R, B_1, B_2, B_3 onto the entrance aperture of the trochoidal deflector formed by an electric field E between plates C_1, C_2. A bandwidth of electrons at the exit aperture S_1 is accelerated or decelerated, and focused by elements S_1, S_2, S_3 onto the static gas target. The incident electron current is measured by transporting the beam *via* elements D_1, D_2 to a Faraday cup at A. Negative ions are extracted along the -x direction, mass analyzed, and detected by a multiplier. The confining magnetic field B is $1.6 \times 10^{-2} T$.

The TOF apparatus with magnetically-confined gun of Hadjiantoniou *et a/ (1* 973) is shown schematically in Fig, 5. This apparatus has been successfully used

to measure peak energies, branching ratios and negative-ion lifetimes at incident electron energies below 1 eV, with a resolution of about 0.15 eV. The electron source is a pulsed, retarding-potential difference (RPD) gun formed between the filament F and the five following grids. Electrons are confined by the axial magnetic field parallel to the incident electron beam. The RPD gun is pulsed every 100 μs with a 1 μs width. After about 0.5 μs from the end of the gun pulse, the backing plate is pulsed negatively to eject negative ions from the collision region into the flight tube. Focusing and acceleration grids are used to direct the ions down the tube to the multiplier-detector, Deflectors and a lens in the flight tube ensure focusing of the ion beam.

The flight time t of ions having the same charge but different masses M is given b y $t = L\,(M/2\,E)^{1/2}$, where L is the flight length and E the ion kinetic energy, By measuring flight times of two ions in the drift tube one can relate an unknown mass M_x to that of M by $M_x = M(t_x/t)^2$ where t_x is the flight time of M_x.

Measurement of autoionization lifetimes are made by ejecting surviving negative ions at the horizontal deflection plate (Fig, 5), A voltage pulse after a given flight time t ejects all remaining ions, and only energetic neutrals are transmitted to the electron detector. N^T denotes the sum current of neutrals and negative ions at the detector, and is the number of negative ions that entered the flight tube at $t = 0$. If, after time t, the number of energetic neutrals reaching the detector is N^0, then the difference N^T-N^0 is the number of negative ions N that survived the distance D from the acceleration grid to the pulsed plate. Assuming an exponential decay law characterized by a simple lifetime τ, one has that

$$\tau = -t \,/\, ln\frac{NT-NO}{NT} = -t \,/\, ln\frac{N^-}{NT},$$

where the time t is just $D(M/2E)^{1/2}$. Measurements of $/n(N/N^T)$ at several flight times t (different acceleration energies E) will yield τ.

Experimental Considerations

1. The use of an electrostatically-focused gun, RPD gun or trochoidal monochromator limits the measurement of reliable cross sections to energies above - 0.1-0.2 eV. This limit is placed by effects of surface charges, patch fields, and space charge.

2. The energy width of the incident electron beam (~0.1eV) makes deconvolution results insensitive to the true shape of the cross section. As an example, all beam measurements of the shape of the SF_6 resonance at zero eV have yielded only the instrumental bandwidths.

3. The uncertainty in electron energy scale is about 0.05-0,08 eV, which becomes a significant source of error at energies below ~ 0.5 eV.

D. The Reversal Electron Attachment Detector (*READ*)

In order to combine the properties of high electron densities at low energies, a method was introduced (Bernius and Chutjian 1989, 1990, Orient et *a/ 1985)* wherein one decelerates, then reverses, electron trajectories directed into an electrostatic mirror to obtain zero and near-zero electron energies. The approach is illustrated in Fig. 6. The *READ* consists of an electron gun column (V1-V7), an electrostatic mirror using shaped electrodes (V5-V7), and ion extraction optics (V5-V8). A paraxial beam of electrons is collimated and focused into the mirror which decelerates the beam to zero radial and longitudinal velocity at the reversal plane (R). Effects of space charge, especially at the electron emitter and reversal region, were included in the lens-system design. Attachment under single-collision conditions occurs to a beam of molecules directed at R. The electron gun is pulsed with about a 50°A duty cycle. A reversed electron beam is established in the first half cycle during which attachment takes place. The second half cycle, with the primary electron beam pulsed off, is for ion extraction and focusing into a mass analyzer. It is also possible to accommodate several pulses in the ion extraction "pipeline": one extraction pulse may be initiated before the previous extracted ion bundle has reached the detector, hence increasing the duty cycle of the system even further.

The position of the reversal plane R is adjusted electrostatically, Movement to the right (Fig, 6) results in higher-energy electrons traversing the target so that non-zero energy resonances can be accessed as well. In fact, the electron beam in this case traverses the target twice: once upon deceleration into the mirror, and again on acceleration away from it. Many of these properties have been illustrated, anti detection limits, ion space-charge effects, and applications discussed (Bernius and Chutjian 1989, 1990, Boumsellek *et a/ 1991,* Boumsellek and Chutjian 1992). A variation of this technique using a gridded structure has also been demonstrated (Boumsellek *et al 1993).*

Experimental Considerations

1. Because of nonlinear ion space-charge effects, the detected ion signal scales nonlinearly with target density (Boumsellek and Chutjian 1992). As such, *READ* is useful as a high-sensitivity trace-species monitor when only detection is desired ("go/no-go"), and not necessarily knowledge of the analyte concentration.

2. Space charge is also critical in the cathode-extraction region, where the equipotentials must be as parallel as possible to the emitter surface in order to avoid electrons hitting subsequent apertures (Brewer 1967).

3. An ensemble of reversal planes is present at R, corresponding to the energy width of the electrons from the emitter F. Each zero-energy electron plane, however, contributes to the signal if it lies within the depth of field of the subsequent ion-extraction optics.

4. In terms of energy resolution, *READ* has a width (~ 300 meV) 50-100 times broader than the rare-gas photoionization method (- 5 meV), but currents are factors of -107 larger.

E. The Cavalleri Electron Density Sampling (*CEDS*) Method

The *CEDS* technique has been extensively used by Crompton and co-workers to measure thermal attachment rate constants (Cavalleri 1969, Gibson *et al* 1973, Hegerberg and Crompton 1980, Crompton and Haddad 1983, Petrovic' and Crompton 1985, Orient *et al 1989).* A schematic diagram of the apparatus is shown in Fig. 7. A cylindrical cell contains a mixture of the target AB and N_2. The N_2 pressure is several kPa and, for strongly-attaching molecules, the relative concentration of AB is less than 10 ppm. An X-ray flash of a few μs duration is transmitted through a thin beryllium window to produce electrons within the cell. After a delay time t (during which the electrons are depleted by attachment) an *rf* field is applied *via* external electrodes. The excited, residual electrons excite the N_2 to produce optical emissions which are then detected by the phototube. The intensity of emission is proportional to the number of unattached electrons. About 4 x 10^4 X-ray shots at a 1 Hz rate are required for good statistics. Electron and ion densities are kept small, and the total pressure high, so that effects of ambipolar diffusion are

avoided. Measurements of the rate constant are made over a range of temperatures by heating and cooling both the target and electrons in the collision region.

The electron population $n(t)$ in the cell is described in the form

$$N(t) = N_0 e^{-t/\tau}$$

where $\tau^{-1} = DA^{-2} + \nu_a$ for an attaching gas. Here D is the diffusion coefficient, A the diffusion length described by the cell geometry (Crompton and Haddad 1983), and ν_a the attachment collision frequency proportional to the N_2 density. The quantity τ^{-1} can be related to the attachment rate constant by the expression

$$\tau^{-1} = \tau_D^{-1} + k(\bar{\epsilon})\,[AB]\,, \tag{34}$$

where τ_D^{-1} is the free diffusion rate of electrons, $k(\bar{\epsilon}) = \nu_a/[AB]$ is the attachment rate constant at=, and [AB] the number density of target {attaching) gas, If we denote the number density of the buffer gas as N and the fractional target concentration as $f \equiv [AB]/N$, then the attenuation rate in Eq. (34) can be written as

$$\tau^{-1} = \tau_D^{-1} = k(\bar{\epsilon})\, f\, N, \tag{35}$$

and if one multiplies Eq. (35) by N, then one obtains

$$N\tau^{-1} = N\tau_D^{-1} + k(\bar{\epsilon})\quad fN^2. \tag{36}$$

Rate constants can be obtained either from Eqs. (35) or (36). If τ_D^{-1} is measured in a separate experiment in the buffer gas (NJ, then the product $k(\bar{\epsilon})fN$ is obtained from Eq. (35) by measurement of τ^{-1} at a single density Nand concentration f. Also, from Eq. (36), measurement of $N\tau^{-1}$ vs N^2 yields a straight line of slope $k(\bar{\epsilon})f$.

Experimental Considerations

1. Because of the large attachment rates at thermal energies ($\bar{\epsilon}$ - 40 meV), measurements in SF_6, $CFCl_3$, perfluorinated and chlorhalocarbon compounds, *etc* must be made at very low concentrations, Hence f is in the range (l-5) x 10^{-6}. This quantity must be measured precisely, and care taken that its value does not change during the measurement (eg, through chemical reaction, photodissociation, or leaks).

2. Experiments are done in a static gas cell so that values of f can be affected

during an experiment by destruction of the target by X-ray or *rf* pulses; or by selective target adsorption on the cell wall. These effects are usually evident in observing a time dependence of emitted light or rate constant from run-to-run, Adsorption and condensation, or wall reactions and dissociation may be especially important at low (200 K) or high temperatures (600 K) when temperature dependencies of $k(\bar{\epsilon})$ are measured.

F. The Electron Swarm Method

The electron swarm technique measures $k(\bar{\epsilon})$ as a function of mean electron energy and E/N, where E is the magnitude of the swarm electric field E and N the carrier gas density (Christophorou 1971, Hunter and Christophorou 1984, Spyrou and Christophorou 1985). One solves the Boltzmann equation, in some degree of approximation, to obtain the EEDF $f(\epsilon, E/N)$ at the mean energy $\bar{\epsilon}$ of the swarm.

A schematic diagram of the apparatus used by the Oak Ridge group is shown in Fig. 8, Bursts of electrons from an alpha-particle emitter are allowed to drift to the anode under the influence of a uniform E field (directed upward in Fig. 8). The alpha-particle trajectories are well collimated so that the starting plane of the swarm is well defined, The cathode is a planar alpha-particle emitter in ^{252}Cf or ^{239}Pu producing particles of energy 6.1 MeV/particle or 5.1 MeV/particle, respectively. The decay of each ^{252}Cf alpha particle produces $\sim 2 \times 10^5$ electrons within a time of -5 ns (at 133 kPa N_2 pressure).

Each current burst induces a voltage pulse at the output amplifier at a specific E/N value. The pulse-height distribution is first recorded as a function of E/N with only buffer gas (N_2 or Ar) in the drift tube. A small quantity (usually 10^{-5} to 10^{-8} the buffer gas density) of the target AB is added, and the ratio of pulse heights recorded as a function of E/N. This ratio is then used to obtain the quantity $\eta(\bar{\epsilon})/[AB]$, the attachment coefficient. is units of cm^2. The rate constant $k(\bar{\epsilon})$ is related to $\eta(\bar{\epsilon})/[AB]$ by $k(\bar{\epsilon}) = \eta(\bar{\epsilon})w/[AB]$. Here w is the electron drift velocity usually obtained in a separate measurement using pure buffer gas. The transit time τ_1 of the swarm is measured, and the drift velocity given by $w = d/\tau_1$ where d is the known drift distance between the planar source and anode. The drift region is enclosed in a stainless steel pressure vessel capable of standing pressures to 10 MPa, and capable of being heated and cooled to measure temperature dependencies in $k(\bar{\epsilon})$.

The quantity $k(\bar{\epsilon})$ is an average of the attachment cross section $\sigma_A(\epsilon)$ over the

electron energy distribution function in the swarm. These are related by the usual expression

$$k(\bar{\epsilon}) = (2/m)^{1/2} \int_0^\infty \sigma_A(\epsilon)\, \epsilon^{1/2} f(\epsilon, E/N)\, d\epsilon \qquad (37)$$

where $f(\epsilon, E/N)$ is the electron energy distribution function at the reduced electric field E/N, Effects of the swarm-cell temperature on $k(\bar{\epsilon})$ are present *via* the particle density N and hence E/N, as well as *via* the Boltzmann population of molecular rotational-vibrational levels which affect $\sigma_A(\epsilon)$ (Orient and Chutjian 1986, Orient *et al 1989).*

From Eq. (37) $k(\bar{\epsilon})$ is seen to be an average of $\sigma_A(\epsilon)$ over the swarm distribution function $f(\epsilon, E/N)$. In order to unfold $\sigma_A(\epsilon)$ one must know $f(\epsilon, E/N)$ at every E/N for which $k(\bar{\epsilon})$ is measured. The $f(\epsilon, E/N)$ cannot be measured directly, and are determined from solutions to the Boltzmann transport equation (Huxley and Crompton 1974). These solutions in turn require a large body of elastic and inelastic scattering cross sections for the carrier gas (N_2 or Ar), again assuming that the target gas has negligible effect on $f(\epsilon, E/N)$ (an assumption that is easily verified experimentally). The scattering data required are elastic scattering cross sections; rotational, vibrational and electronic excitation cross sections; and ionization (direct and dissociative) cross sections. The $f(\epsilon, E/N)$ are thus dependent on the quality of the cross-section base for the carrier gas, Many of these data have been summarized up to 1983 in Trajmar *et al 1983,* and for N_2 summaries can be found in Phelps and Pitchford 1985a, 1985b. Other reviews of basic data may be found in Tawara *eta/(1* 985, 1990) and Hayashi (1981),

Assuming one has calculated a reliable set of $f(\epsilon, E/N)$ from the transport equation, one then requires an unfolding procedure in Eq. (37), This procedure (McCorkle *et a/ 1980,* Christophorou et *a/ 1971)* involves the solution of Eq. (37) for $\sigma_A(\epsilon)$ at each E/N at which $k(\bar{\epsilon})$ is measured. Successive iterations between $\sigma_A(\epsilon)$ and $k(\bar{\epsilon})$ are carried out until a "best-fit" between measured and fitted rates is obtained. Specifically, one defines the attachment rate $R(\bar{\epsilon}_j)$ at the j^{th} value of the mean electron energy and the electron distribution function $F(\bar{\epsilon}_j, \epsilon)$ at the same $\bar{\epsilon}_j$, and the monoenergetic attachment rate $M(\epsilon)$. This last quantity eventually becomes the electron velocity-weighted cross section $\epsilon^{1/2}\sigma_A(\epsilon)$ at the end of the iterations. It is that rate which would have been measured if all the electrons in the swarm had the same energy. The three quantities are related through the expression

The iterative procedure is started by some judicious choice of $M(\epsilon)$, either as the experimental $k(\bar{\epsilon})$, or as a constant value up to some energy ϵ_{max} beyond which $\sigma_A(\epsilon)$

$$R(\bar{\epsilon}_j) = \int_0^\infty M(\epsilon)\, f(\bar{\epsilon}_j, \epsilon)\, d\epsilon. \qquad (38)$$

makes negligible contribution to the rate,

After each iteration a series of weighting factors $w(\bar{\epsilon}_j)$ is obtained from the experimental rate $R_{exp}(\bar{\epsilon}_j)$ and calculated rate $R_{calc}(\bar{\epsilon}_j)$ where

$$w(\bar{\epsilon}_j) = R_{exp}(\bar{\epsilon}_j) / R_{calc}(\bar{\epsilon}_j)$$

These weights are then used to correct the starting $M(\epsilon)$ by

$$M_{new}(\epsilon) = M_{old}(\epsilon) \left[\frac{\sum_j w(\bar{\epsilon}_j) F(\bar{\epsilon}_j)}{\sum_j F(\bar{\epsilon}_j, \epsilon)} \right] \text{''}$$

This new function is introduced into Eq. (38) and the iteration carried out until the quantity

$$\frac{\sum_j [R_{exp}(\bar{\epsilon}_j) - R_{calc}(\bar{\epsilon}_j)]^2}{\sum_j [R_{exp}(\bar{\epsilon}_j)]^2}$$

is a minimum,

A recent development to the "continuous" swarm technique described above is a time-resolved approach in which the initial electron burst is created in 0.6 nsec-wide pulses from a N_2 laser striking the cathode surface (Datskos *et al* 1993a, 1993b). The prompt electrons quickly thermalize with the buffer gas (N_2) which establishes a characteristic EEDF $f(\epsilon, E/N, T)$. The time development of the drifted electron current at the anode is monitored, This current consists of the electron loss *(due* to attachment to the surrounding target-N_2 mixture), and sometimes electron gain (delayed in time, resulting from autoionization of the molecular product). The time development yields the electron attachment frequency t_a^{-1} and the electron detachment frequency t_d^{-1}. Knowledge of the mean electron energy $\bar{\epsilon}$ from the Boltzmann solution yields attachment rate constants from $k(\bar{\epsilon}, T) = t_a^{-1}(\bar{\epsilon}, T)/N_a$, where N_a is the number density of the attaching target. Rate constants for SF_6 and c-C_4F_6 have been reported in which both the target internal energy is changed (T between 300 and 600 K), as well as the mean electron energy ($\bar{\epsilon}$ between 0,19 and 1.0 eV)

(Datskos *et al* 1993b).

Experimental Considerations

1. Errors arise in the deconvolution procedure *via* Eq. (38) to obtain $\sigma_A(\epsilon)$ from $k(\bar{\epsilon})$. There are two sources of error: one associated with calculation of $F(\bar{\epsilon}_j,\epsilon)$ at each $\bar{\epsilon}_j$, and the other in the convergence of the iteration procedure itself. Calculation of the $F(\bar{\epsilon}_j,\epsilon)$ in turn depends upon the level of aPProximation to the Boltzmann equation (two-term, four-term, *etc,* or whether angular distributions of scattering are incorporated); and to the accuracy and completeness of the scattering cross section data base. In many cases, N_2 for example, accurate excitation cross sections near threshold are not available, and are obtained by extrapolation.

2. When comparing rates or cross sections to data from single-collision experiments (e. g., high Rydberg ionization or rare-gas photoionization techniques) a difference in interpretation may arise. Data obtained by swarm methods refer to a negative-ion product distribution formed by multiple-collisions which can result in stabilization of negative ions. When this stabilization is not present (in the single-collision experiments) the distributions, and hence the associated rates and cross sections, may be different.

3. Because of diminishing electron density at lower energies, swarm-unfolded cross sections at energies below about 50 meV will have a relatively larger uncertainty in experiments carried out at 300K and above.

4. There are the usual sources of statistical errors in measurements of the rates $k(\bar{\epsilon})$. These are errors associated with measurements of the attaching and buffer gas pressures, drift distance, cell temperature, electron swarm transit time, electric field, and average, amplified electron signal pulse height. The total quadrature error is about 5% at the 2σ level. The error in the electron energy scale is approximate 20 meV.

G. The Flowing-Afterglow/Langmuir-Probe (*FALP*) Technique

The *FALP* technique has been developed by Smith, Adams and coworkers (Adams, *et al* 1975, Smith *et al* 1975, Smith and Plumb 1972, Smith and Adams

1983, 1984) to measure ion-molecule, ion-ion, electron-ion and electron-molecule collision phenomena in a flowing-afterglow plasma. Data have been reported for thermal attachment rate constants (Smith *eta/* 1990, 1989, Adams eta/ *1985,* Smith *et al 1984,* Alge *eta/ 1984),* dissociative recombination (ion) product distributions and rate constants (Adams et al 1991, Herd *et a/* 1990, Smith and Adams 1987, Adams *et a/ 1988, 1984,* Alge *et a/ 1983),* dissociative recombination using spectroscopic detection of the neutral products (Adams 1994), and ion-molecule rate constants (Španěl *et al 1993,* Smith *et al 1992,* Mayhew and Smith 1990, Smith and Adams 1985, Adams and Smith 1985), In the *FALP* approach one generates an afterglow plasma in a fast-flowing helium carrier gas of -0.1 kPa pressure by means of a microwave discharge located upstream. Argon atoms are added to the plasma to quench any metastable He atoms, and a small quantity of the target gas (ppm concentrations) is added downstream. A schematic of the apparatus is shown in Fig 9 for mass-spectrometric detection of the ion distribution. Techniques also include use of emission spectroscopy, laser-induced fluorescence, and REMPI to detect neutral products (Adams 1994).

The following discussion addresses *FALP* applications to electron-attachment measurements [see Smith and Španěl (1 994) for a review], At the point of addition of the target AB one generates a large axial gradient of the electron density due to continual depletion by attachment to AB. Neglecting ambipolar diffusion, the rate of electron loss (or negative-ion formation) can be written as

$$\frac{\partial n_e}{\partial t} = -k(\bar{\epsilon})\, n_e\, [AB]\ , \qquad (39)$$

where n_e is the electron density and $k(\bar{\epsilon})$ the attachment rate constant, However, in practice, the *FALP* technique requires relatively high ionization densities or n_e *(10^7-10^8* cm^3) because of the limited sensitivity of the probe, Thus, ambipolar diffusion cannot be neglected, and the appropriate continuity equation becomes (Adams *et a/ 1975,* Smith *eta/ 1984)*

$$\frac{\partial n_e}{\partial t} = v_p \frac{\partial n_e}{\partial z} = D_{ae} \nabla^2 n_e - k(\bar{\epsilon})\, n_e\, [AB]\ , \qquad (40)$$

where D_{ae} is the electron-positive ion (Ar^+) ambipolar diffusion coefficient. Under assumptions that (i) the positive ion density n^+ is reduced by diffusion only (rather than diffusion and recombination), (ii) that diffusive losses of n^+ occur almost entirely in the fundamental mode (*i.e.*, sufficiently downstream), and (iii) there are no volume

negative-ion losses due to diffusion, detachment or recombination, Eq. (40) can be solved in the form (Smith *et al 1984)*

$$\frac{n_e(z)}{n_e(0)} = \left(1 - \frac{\nu_D}{\nu_a}\right)^{-1} \left[\exp\left(-\frac{\nu_a}{v_P} z\right) - \frac{\nu_D}{\nu_a} \exp\left(-\frac{\nu_D}{v_P} z\right)\right], \quad (41)$$

where $v_D = D_{ee}/\Lambda^2$, and $v_a = k(\bar{\varepsilon})[AB]$. Here, A is the characteristic diffusion length described by the flow-tube geometry (Huxley and Crompton 1974, Mason and McDaniel 1973).

Measurement of $k(\bar{\varepsilon})$ in Eq. (41) requires measurement of, first, the relative values of $n_e(z)/n_e(0)$ *vs z* (position along flow tube), This is done (see Fig, 9) by a small, movable Langmuir probe which traverses most of the distance between the attaching gas inlet port and the quadruple mass spectrometer. Second, the quantity v_D is determined in a separate experiment in an argon-helium electron-ion afterglow plasma, and knowledge of the cell geometry. Third, the spatial variation $\partial n_e/\partial z$ is related to the time variation $\partial n_e/\partial t$ by measuring *UP.* This quantity is obtained by pulse-modulating the microwave discharge, and measuring the velocity of passage of the plasma disturbance down the flow tube using the Langmuir probe. Fourth, the attaching gas density n_m is obtained by measurement of flow rate through a known conductance into the *FALP* tube,

Experimental Considerations

1. When absolute values of n_e are measured, errors are introduced by uncertainties in the Langmuir probe area, and the plasma potential (Smith and Adams 1983, Godyak 1991), This error is minimized in measurements of $k(\bar{\varepsilon})$ since only relative values $n_e(z)/n_e(0)$ [Eq. (41)] are needed.

2. Errors are also present in measurements of v_D and *up* (Adams *et al* 1975). While errors in measurement of [AB] are small, they can be large in cases of highly viscous targets such as H_2SO_4 (Adams *et al 1986).* Errors are also introduced in the curve-fitting procedure to obtain $k(\bar{\varepsilon})$ from ln v_e vs z data, since the fitting will be sensitive to the individual errors in v_D, [AB] v_p and $n_e(z)/n_e(0)$.

3. Care must be taken to ensure that the energetic electrons in the microwave region have truly reached a Maxwellian distribution; that superelastic collisions

with excited He atoms are not a source of electron heating; and that the gas atoms themselves are not heated by the discharge.

H. The Microwave-Cavity /Pulsed-Radiolysis (*MCPR*) Technique

The *MCPR* technique has been developed by Hatano, Shimamori and coworkers to measure k($\bar{\epsilon}$), thermal rate constants in a Bloch-Bradbury (BB) sequence (attachment followed by third-body stabilization); and for attachment to van der Waals molecules (Shimamori and Hatano 1976, Toriumi and Hatano 1985, Shimamori and Hotta 1986), In this technique a pulsed, high-energy electron beam of - 1-3 ns duration impinges on a thin tungsten foil, The collision area becomes a source of X-rays which in turn irradiate a high-pressure (10-100 kPa) gas mixture within a microwave resonator (Fig. 10), The resonator itself can be thermally heated or cooled in the temperature range 77-373 K to measure temperature dependencies of the attachment rate constant (Shimamori and Nakatani 1988).

Electrons generated in the cavity are rapidly thermalized, and the cavity Q and resonant frequency are altered, The changes are proportional to the electron density, and are detected by differentially-amplified signals which monitor the klystron and cavity frequencies. The product of the observed electron lifetime and target density, τ_0[AB], can be related to the direct (collisionless) rate constant k, and the three-body (quenching) rate constant k_M by the expression

$$\tau_0 [AB] = k_1^{-1} + (k_M [M])^{-1}, \qquad (17)$$

where [M] is the pressure of the buffer gas, Measurements of τ_0[AB] *vs* [M]$^{-1}$ then yield k_M (slope) for each collision partner, and k, (intercept).

In addition to changing the target's thermal population (heating and cooling the gas cell) Shimamori et *a/ (1* 992a, 1992b) have added a second, high-power microwave source to effect additional heating of the electrons within the cavity. An Maxwellian EEDF is set up in a Xe buffer gas. The mean electron energy $\bar{\epsilon}$ is a function of the applied heating microwave power. The conductivity of the cavity is measured as a function of time after the X-Ray burst, and is related to the e-Xe momentum-transfer collision frequency *via* the e-Xe elastic momentum-transfer cross sections (especially near the Ramsauer minimum) and the (assumed) Maxwellian EEDF in the cell. The significance of this added excitation channel is that one now has a means of altering both the internal energy of the molecular target [to study $\sigma_{v,J}(\epsilon)$ as a function of v, J], as well as the mean electron energy [to study $\sigma_{v,J}(\epsilon)$ as a function

of $\bar{\varepsilon}$].

Measurements of $k(\bar{\varepsilon})$, using electron heating in the energy range $0.03 \leq \bar{\varepsilon} \leq$ 3.0 eV, have been reported by Shimamori et *al (1 991)* for CCl_4, $CHCl_3$, C_6H_5Cl, and BCl_3. Recent *MCPR* results include single measurements at room temperature (SO_2, Shimamori *et al* 1993; C_6F_5X and C_6H_5X for X== 1, Br, Cl, and F Shimamori et a/ 1993).

Experimental Considerations

1. Measurements over a wide pressure and temperature range, and use of isotopic substitution, are often needed to support a unique attachment mechanism [e. g., Bloch-Bradbury vs van der Waals attachment (Shimamori and Hotta 1983, 1984)].

2. Observational times of electron density in the cavity are limited to the range 1 μs (to allow electrons to thermalize) to $\lesssim$ 50 μs (to mitigate against loss effects of ambipolar diffusion and attachment to impurities) (Hatano *et a/ 1982)*. This in turn restricts the measurable range of rate constants.

3. Care must be taken to ensure that the heating of electrons occurs uniformly over the volume of the collision cell.

4. Conversion of the electron collision frequency to a mean electron energy is indirect, and involves uncertainties in the Xe momentum-transfer cross section at the Ramsauer minimum; as well as assumption of a Maxwellian electron energy distribution in the cell,

5. Because of the sealed microwave cavity, care must be taken to ensure that the X-rays, subsequent high-energy electrons, or even room light, do not introduce breakdown products in the cavity,

2. Higher Electron Energies (0.5-10 eV)

A. Detection of the Outgoing Electron

"There is a large array of experimental techniques directed towards the study of

elastic and inelastic electron scattering from atoms and molecules. Many of these techniques have been reviewed previously (Trajmar and Register 1984). Variations exist in the degree of refinement of the electron optics system, in the incident electron energy range, residual energy range, energy and angular resolution; and whether use is made of coincidence techniques between, for example, scattered electrons, electrons and emitted photons, or (at higher electron energies) between electrons and the ionized target. Related experimental techniques have also been used to detect ejected electrons in high-resolution photoemission studies.

The most frequently-used approach in the study resonances and attachment at higher electron energies is the use of a 127° or 180° electrostatic monochromator with associated entrance and exit optics to define the energy, resolution, and angular width of the incident electron beam. This is combined with a similar electron energy analyzer to analyze and detect the scattered electron. The target is usually taken as a beam effusing from a hypodermic needle, a capillary array (e. g., part of a microchannel plate), or an apertured oven,

An example of one approach is the instrument of Jung et *a/ (1* 982) and Sohn *et a/ (1* 983) which utilizes two 127° electrostatic analyzers combined with a gas-beam target. Resolution through the two analyzers is typically in the range 8-24 meV (FWHM). To achieve low energy and high resolution care was taken to limit (a) residual magnetic fields to about 0.1 mG through correction coils, shielding, and use of non-magnetic materials, and (b) stray electric fields through shielding, cleaning and bakeout, and heating during operation. An example of instruments using 180° hemispherical analyzers is illustrated in Chutjian (1 976, 1979) and Boesten (1 988) where care was taken in the optics design to control the energy and angular properties at the target and subsequent electron analyzer,

A typical geometry using two 127° electrostatic analyzers is shown in Fig, 11 (Jung *et al* 1982). The incident energy is tunable in the range of about 0.5-30 eV, and the range of accepted final energies about O-5 eV. The electron analyzer can be rotated in the angular range -60° to + 140° to measure angular differential cross sections. Also, the electron gun section can be differentially pumped with respect to the target chamber to prevent contamination and fluctuations of the space-charge limited current in the region of the electron emitter (Chutjian 1976, Sohn *et al* 1983).

Combining the low incident electron energies with the high overall resolution of this instrument, Jung *eta/(1* 982) have studied rotational broadening and excitation

in fairly heavy molecules. Pure rotational spectra in CO have been reported for the vibrationally elastic channel ($\Delta v = 0$) at a resolution of 10 meV, at scattering angles between 20° and 65° (Jung *et al* 1982). Measurements such are placed on the cross section scale through a phase-shift analysis of a "standard" cross section, such as that of He (Register et *al 1980),* and use of the relative-flow method to transfer the standard from He to the target gas (Srivastava et *al 1975,* Trajmar *et al* 1983). Alternatively, the calculated cross section for e-He elastic scattering can be used as the primary standard, as has been done by Buckman eta*l (1 991)* for measurement of accurate, near-threshold, pure vibrational excitation cross sections in H_2.

A somewhat different crossed-beams apparatus was used by Cvejanović *et al (1993)* to study pure vibrational excitation in H_20 and D_20 up to very high *n (n* up to 5, or energies up to 3 eV). The excitation proceeds through two resonances: the $^2B_1$ resonance at 6.5 eV, and a broader resonance in the range 4-10 eV, centered near 8 eV. The apparatus had a Herzog-corrected 90° electrostatic analyzer as the electron monochromator, and a double 112° analyzer (Gresteau *et al 1979).*

Inherent to the operation of some electron lens systems in their variable transmissivity as a function of residual (final) electron energy. This is especially true for empirically-designed systems, or when the system is used at very low residual energies (threshold scattering). In these cases, several schemes have been adopted for calibrating the transmission function of the lens system. One involves, close to threshold, use of the Wannier expression for near-threshold ionization of He. Here, the cross section $\sigma(E)$ is related to the outgoing electron energy E by $\sigma(E) \sim E^{0.127}$. One may then correct energy-loss spectra in a range of about O-6 eV residual energy by comparison to the Wannier expression. At higher residual energies, calibration *via* known differential cross sections for the $n = 2$ and $n = 3$ transitions in He is possible. Many of these experimental problems are discussed by Nickel *et al (1* 989).

Recent applications of these basic experimental ideas have been made to the study of threshold photoelectron spectroscopy using high-energy photons from the Daresbury Synchrotrons Radiation Source, King *et al (1* 987) have used a 127° analyzer with an extraction electrode and cylindrical target cage to extract selectively near-zero-energy electrons from the ionized target (Fig, 12). A measure of the energy resolution and selectivity is obtained *via* the threshold $2_{P3/2}$ and $^2P_{1,2}$ ionization peaks in Art. The total widths of the features are a convolution of the photon energy width (17 meV) and the spectrometer resolution (3 meV). Results at low and high residual

electron energies have been published (Zubek and King 1990, Zubek *et a/ 1989),* as well as electron-ion coincidence results using in combination a time-of-flight analyzer to detect with high efficiency the positive ion produced in the photoionization (King 1991, Govers *et a/ 1984).*

Finally, while the detector commonly used in these instruments is the channel electron multiplier, results have been reported, at both high and low incident and final electron energies, utilizing a multianode detector which allows detection of a range of electron energies simultaneously (Hatfield *et a/ 1989),* The detector, at the exit plane of electrostatic 180° spherical analyzer, records the radial position of electrons, and hence their energy.

B. Detection of the Outgoing Negative Ion

Because of the electrostatic nature of practically all electron scattering instruments in use (no momentum-focusing devices present), systems used to detect elastically- or inelastically-scattered electrons can also be used to focus and detect negative ions (Trajmar and Hall 1974), Differences lie in the fact that (a) a momentum- or velocity-filtering device [e. g., a small, shielded magnet (Schermann *et a/ (1* 978)] must be used to separate the ions from electrons, (b) conventional mass spectrometers (quadruple or otherwise) can be used as the analyzer, (c) timing considerations are different when pulsed formation/detection is used (microseconds for ions, vs nanoseconds for electrons), (d) care must be given to accelerate the ion to a high energy (usually about 1 keV) prior to final detection by the channel electron multiplier or microchannel plate (a 100V potential is sufficient for electrons), and (e) surface patch-field variations are less important,

A timely application of such a device to the study of dissociative attachment from high vibrational levels of H_2 has been made by Hall *eta/ (1* 988) and Popović *et a/ (1* 990). A schematic of the instrument is shown in Fig, 13. Electrons from a hairpin tungsten filament are accelerated, focused, and energy-selected by a conventional 127° electrostatic filter (Marmet and Kerwin 1960), The target in this case is a hydrogen beam, effusing from a hot oven, consisting of a mixture of vibrationally-excited molecules (up to v= 9, 10 and 13 for H_2, HD, and D_2, respectively). These molecules are formed within the oven by recombination of hydrogen atoms on a cold, metallic wall. The atoms are generated in turn by dissociation of H_2 on the incandescent hairpin filament (Hall *et a/ 1988).*

Negative ions H^- (or D-) are produced by DA through the $^2\Sigma_u^+$ resonance, with two major differences from the well-known, ground-state phenomenon: (a) the DA threshold is moved to much lower energies by the internal *v,J* excitation, and (b) the DA cross section is greatly enhanced by the rapid increase in the H_2" resonance lifetime with internuclear separation. In the competition between autoionization and internuclear separation, the latter now has a fighting chance.

A spectrum of the H^- yield as a function of electron energy has been reported (Popović *et al* 1990), and levels up to v"=9 can be detected. In the general case, this vibrational limit will be determined by the point of crossing between the neutral and negative-ion potential energy curves, the population in the H_2 beam, the lowest electron energy that can be focused by the electron monochromator, and the lowest ion energy detectable by the analyzer,

In a different experiment, recent work in UV laser-excited H_2 has yielded evidence for H" formation through attachment of laser-produced electrons to highly-excited molecular states, These could be the E,F states, HR molecules, or some "super-excited states (SES") above the ionization continuum formed through decay of doubly-excited states of H_2 (Pinnaduwage and Christophorou 1993, 1994; Pinnaduwage *et al 1991) (see* also Sec. *IV. 1*).

In applications where angular distributions of the outgoing ion are not of interest, one may use magnetic confinement of the incident electron beam, and electrostatic extraction of the outgoing negative (or positive) ion (Orient and Srivastava 1983, Krishnakumar and Srivastava 1990). The advantages here are that, thanks to the confining solenoidal magnetic field, one has higher space-charge limited electron currents, and one may access lower electron energies. A recent version of this approach is illustrated in Fig, 14. Fast pulsing of the electron gun allows one to attach electrons to the molecular-beam target in a field-free region. During the "electron-off" cycle, ions are extracted out of the collision region by rapid biasing of the repeller and extractor grid, Care was taken in the measurements to ensure that all of the ions were extracted from the target region. Results for the DA process O/N_2O in the electron energy range O-5 eV have been reported (Krishnakumar and Srivastava 1990). Calibration to the cross section is again accomplished by using the relative-flow technique (Srivastava *et a/ 1973,* Trajmar et *a/ 1983)* and comparison to a previously-measured "standard", such as the DA process O^-/O_2.

In earlier work on $e\text{-}CO_2$ resonance excitation Orient and Srivastava (1 983) used

two magnetically -confined electron beams directed in opposite directions to (a) vibrationally excite CO_2, and (b) dissociatively attach from the vibrationally-excited CO_2 ground state. A peak in enhancement of the 4.4 eV $^2\Pi_u$ resonance was found with $\sim$1eV electrons, corresponding to about 0,1 eV vibrational excitation in the $C0_2$ target.

Because of the relative simplicity of the extraction optics, one may reverse extraction potentials, and alter the biasing of the quadruple mass analyzer to detect positive ions. Cross sections for direct and dissociative ionization in a variety of molecular targets have been reported by Orient and Srivastava (1 987).

Experimental Considerations

1. In order to obtain accurate scattering intensities, care must be given to (a) the angular resolution of the electron analyzer optics (especially for DCS which exhibit sharp minima, or are sharply forward-peaked); (b) the energy transmission of the analyzer optics, especially for features near threshold where the electron energy change is a large fraction of the starting energy; (c) when measuring DCS, the changing scattering volume with scattering angle,

2. Conversion of scattering intensities to cross sections is often made by the relative-flow method, In this, one relies on the accuracy of the secondary standard used. Careful adjustment of flow rates must also be made to give equal Knudsen numbers for the target and standard gases. Finally, scattering from the target, present as background, is obtained by rerouting the target beam, and subtracting the signal from the same pressure of target present as background.

3. When extracting ions from a magnetic field, care must be taken to ensure complete extraction. This can usually be done by calculating ion trajectories under the given conditions of experimental geometry and voltages,

4. Because of the low incident and final (threshold) electron energies care must be taken to eliminate magnetic fields to the 0.5 mG level or better, and to reduce stray electric fields (patch fields, penetrating fields from high-voltage lens elements, *etc*) to values less than several meV.

5. Even with high resolution, rotational transitions are still overlapped, and errors

are incurred in the deconvolution procedure. Accurate measurement of the lineshape and *a priori* knowledge of line locations are needed to obtain accurate scattering intensities.

IV. RESULTS IN LOW-ENERGY ELECTRON ATTACHMENT

1. Electron Attachment to Photon-Excited Molecular States

Using a 0.2-eV energy width electron beam and a quadruple mass spectrometer, the production of negative ions to ground and electronically-excited SO_2 was studied in a (single collisions) triple crossed-beams apparatus: electrons, ground-state SO_2, and *308* nm photons from a pulsed XeCl laser (Jaffke *et al 1993).* The DA process from ground-state SO_2

$$e + \tilde{X}\,(^1A_1)\,SO_2 \rightarrow SO_2^{-*} \rightarrow SO + O^-$$

has a maximum at 4.55 eV, In the presence of the exciting photon, one has the DA excitation assisted by the transition

$$h\nu + \tilde{X}\,SO_2 \rightarrow \tilde{B}^1B_1\ (\ +\ \tilde{A}^1A_2\ )\ SO_2^{-*} \rightarrow SO + O^-\ ,$$

The threshold for DA is shifted to a lower energy, in this case $\leq$ - 0.2 eV, and the excited-state DA cross section is found to be roughly two orders of magnitude larger than that of the ground state, The yield of O^- from the ground and excited states of SO_2 is shown in the series of spectra in Fig, 15, with laser on and laser off (Jaffke *et al 1993).* Observations of photon-enhanced attachment were first reported, in two variations of swarm experiments, for thiophenol (Christophorou et *al 1987,* Pinnaduwage *et al 1989)* and for several amines (Pinnaduwage *et al 1991),*

Recent results of H^- formation from laser-excited H_2 (Pinnaduwage and Christophorou 1993, 1994) are interesting in that they bear on processes in volume-production H^- sources (see Sec. V. 6). Production of H^- is postulated *via* a so-called SES mechanism in which photons are used to produce both (a) low-energy electrons from photoionization of H_2, and (b) prepare an intermediate state (E, F states, Rydberg states, or the SES). Electron attachment from the excited states (very likely the E,F or Rydberg states) provides an extra channel for H^- formation, in addition to that *via* vibrationally-excited $H_2(X)$ produced with electrons and surface recombination. This channel may also be responsible for the discrepancy noted by Berlemont e? *al* (1 993)

between calculated vibrational and H^- number densities in hydrogen discharges.

2. Electron Attachment in HI and DI

The spectroscopic constants of the diatomic molecules HI and DI are known to high accuracy, One easily calculates that the zero-energy dissociative attachment (DA) process in HI should be exothermic by 5.3 meV, and that in DI endothermic by 35.5 meV. Thus DA in DI is allowed *via* rotational levels J" populated at elevated temperatures. The DA cross sections for both HI and DI were measured using the Kr photoionization technique (Alajajian and Chutjian 1988). The HI cross sections were obtained by normalization to k($\bar{\epsilon}$) of Smith and Adams (1 987) using the *FALP* method; and DI cross sections obtained through an intercomparison technique (Alajajian and Chutjian 1987). Results of Carman *et a/ (1* 993) using Rydberg electron transfer have given comparable cross sections in the energy range (ϵ < 45 meV) where PCI effects are absent. Stable HI^- and DI^- have also been detected,

Measurements of the T-dependence of DA signal in DI relative to HI have been carried out (Chutjian *et a/ 1990),* The effect of increasing 1^- signal in DI, relative to 1^- in HI, was accounted for by the increase in the Boltzmann population of DI(*J"*) levels with T. Shown in Fig. 16 is the experimental relative enhancement in 1^- signal, along with the calculated expected increase in population of higher *J"* levels, It would be interesting to exploit this effect to rapidly "turn on" a DA process by, for example, laser-exciting "cold" DI to a *v,J level* above its DA threshold. This could be used as a gaseous opening switch wherein the plasma is made less conductive by converting electrons to negative ions,

The attachment and temperature effect in terms of potential energy curves is shown in Fig, 17. The interpretation of the electron attachment process implied in the curves of Fig. 17(a) anti (b) is that of attachment through a resonant $^2\Sigma^+$ state of Hi-. An alternative explanation can be attachment *via* a diabatic mechanism through an electronic state made bound by Born-Oppenheimer neglected terms in the Hamiltonian (Crawford and Koch 1974, Carman *et al 1993).* Such a potential-energy curve is shown schematically in Fig. 17(c). *Ab initio* calculations of Chapman *et al* (1 988) indicate a resonance crossing into the neutral ground state at too high an energy (-0.2 eV or ~0.6 eV for a "diffuse" or "tight" basis set, respectively) to give rise to the zero-energy attachment peak [Fig. 17(d)]. This energy location depends on the size of the basis set. It appears to be lowered by the enhancement of the diffuse

component of the basis set approaching, presumably, the state HI (X) -t e wherein the adiabatic mechanism takes hold.

3. Electron Attachment in F_2

Zero-energy electron attachment to F_2 to produce F^- has been a source of controversy for nearly a decade. One expects the relevant electronic states to be $F_2(X^1\Sigma^+_g)$ and $F_2^-(X^2\Sigma^+_u)$ (Hazi *et a/ 1981,* Bardsley and Wadehra 1983), By symmetry, the negative ion cannot support an s-wave, and the first allowed is p-wave. This would lead to a threshold cross section varying as $\epsilon^{1/2}$ (Wigner 1948), vanishing at zero energy.

A rising cross section has been detected in every experiment on F_2. The results are summarized in Fig, *18,* Here one sees that beam (., Chantry 1982), swarm (o, McCorkle *et a/ 1986),* and Kr photoionization data (—, Chutjian and Alajajian 1987a) are in quite good agreement for such an experimentally intractable molecule, Possible reasons for this apparently s-wave behavior are that (a) some ungerade character from higher-lying negative-ion states is admixed with the $F_2(X)$ state, (b) electron-rotation (coriolis) interaction mixes gerade states, and (c) nonadiabatic terms mix the $^1\Sigma^+_g$ and $^2\Sigma^+_u$ states when the Hamiltonian is expressed in electronic coordinates relative to the separated nuclei (Pack and Hirschfelder 1968), Or, the answer could be simply that (d) one has not gone low enough in energy, because threshold laws never specify the energy at which threshold behavior is attained] Measurements are currently in progress at JPL with a new approach (Darrach *et a/* 1993) to extend the energy limit to below 5 meV, at a resolution of 0.5 meV, to determine if the cross section is still rising, or falling.

4. Attachment to SF_6 and Its Temperature Dependence

Cross sections and rate constants for electron attachment to SF_6 have been reported using many of the techniques outlined in Sec. II (Datskos *et a/* 1993b). Attachment to form the parent ion SF_6 is s-wave, as confirmed in four different cross-section measurements (Zollars *et a/ 1985,* McCorkle *et a/ 1980,* Chutjian and Alajajian 1985a, Klar *et a/* 1992a, 1992 b). The s-wave behavior has also been treated theoretically in terms of electron capture through non-adiabatic coupling to the nuclear motion (Gauyacq and Herzenberg 1984). Theory also predicted the ω_1 vibrational excitation observed by Klar *et a/ (1* 992a).

The puzzle in SF_6 appeared to be rather in the rate constant, and its T dependence. The matter was resolved through combining results of a calculation (Chutjian 1982, Orient and Chutjian 1986), with the T-dependence of k(T) as measured by four different techniques.

Using the theory of O'Malley (1 966) one may write the attachment cross section $\sigma_A^{v\omega,J}(\epsilon)$ for the v^{th} harmonic of the ω^{th} normal mode, and rotational level J, as

$$\sigma_A^{v\omega,J}(\epsilon) = (4\pi^2 g/k^2)(\Gamma_a/\Gamma_d)\,|\chi_{v\omega,J}(R_\epsilon - i\,\Gamma_a/\Gamma_d)|^2 \times e^{-\rho(\epsilon)}\,, \quad (43)$$

where k is the electron momentum, Γ_a and Γ_d are the autoionization and dissociation widths, respectively, g is a spin degeneracy factor, $e^{-\rho(\epsilon)}$ the survival probability, and R_ϵ is the turning point in the final negative-ion state at energy ϵ. The quantity $\chi_{v\omega,J}$ is the complex overlap integral between the vth vibrational level in the $\omega$the normal mode, and the quasicontinuum of SF_6^- states represented by a modified δ-function (see Orient and Chutjian 1986 for details). This cross section of each v,J level must in turn be summed, at each T, over all significantly populated states S of the system, or

$$\sigma_A(\epsilon) = \sum_S \sum_{v\omega} \sum_J b_{v\omega,J}\,\sigma_A^{v\omega,J}(\epsilon)\,. \quad (44)$$

A particular state S consists of the set of excitations of one or more normal modes w, with v quanta of excitation in each mode.

Comparisons of the calculated $\sigma_A(\epsilon)$ from Eq, (44) with swarm (McCorkle at al 1980), high-Rydberg ionization (Zollars *et al* 1985), and Kr photoionization results (Chutjian and Alajajian 1985) can be found in Orient and Chutjian (1 986). We turn our attention herein rather to the rate constant as a function of T. This can be calculated by combining Eqs. (44) and (43) at each T, and comparing that result to the large body of experimental data, This theoretical comparison is shown by the solid lines in Fig. 19. One sees that the rate constants are "well-behaved": a rate constant exhibiting s-wave behavior (ℓ = O) becomes constant as T is lowered (put $\sigma_A(\epsilon) \sim \epsilon^{-1/2}$ in Eq. (33) to see this), while that varying as p-wave ($\ell = 1$) vanishes as $T \to 0$ K.

Experimentally, from examining beam-gas (A, Spence and Schulz 1973), swarm (O, Fehsenfeld 1970), and *CEDS* data (D, Petrović and Crompton 1985) one would conclude that a constant cross section had, in fact, been attained; but in a much

higher temperature range, between 200 and 600 K, and not in the expected theoretical limit T → 0 K. An explanation for this constancy at the higher T came from the calculation, and from another piece of evidence. There are two channels open in the SF_6 attachment: one to produce SF_6, and the other to produce $SF_5^- + F$. When one adds to the calculated rate constant for the SF_6^- channel alone, the measured rate constant for the second channel (Smith *et a/* 1984, Fehsenfeld 1970), one then obtains the curves (····) shown. To summarize, the constant rate constant in the range *200-600* K was not the true s-wave behavior, but only a compensation of a falling SF_6^- rate constant by a rising SF_5^- -I- F one, The true s-wave behavior will be apparent if $k(\bar{\epsilon})$ can be measured at T<200 K.

Finally, we point out that the *FALP* results (., Smith et *a/ 1984)* could not be reconciled with either theory or the other experiments.

5. Attachment to $CFCl_3$ and CCl_4 and their Temperature Dependencies

The discrepancy between *FALP* results and measured cross sections for SF_6 led to a similar examination of cross sections and rate constants in $CFCl_3$ and CCl_4. One would expect that for these molecules the rate constant should not exhibit a peak at higher temperatures, The cross section in SF_6 is falling with energy, and a Maxwellian EEDF simply places more electron population towards higher energies [smaller $\sigma_A(\epsilon)$] as T is increased, and hence the rate constant should decrease.

To test this hypothesis, a series of calculations was carried out on $CFCl_3$ and CCl_4 (Orient *et a/ 1989)* to compare with earlier measurements (Chutjian eta*/ 1984,* Chutjian and Alajajian 1985a). Simultaneously, a series of *CEDS* measurements of $k(\bar{\epsilon})$ *vs* T for $CFCl_3$ and CCl_4 were made by Crompton and co-workers,

Results for $CFCl_3$ are shown in Fig. 20, One sees again good agreement of the calculated (s-wave) cross section (—, the shading is the error in the underlying experimental cross section), *CEDS* experiments (■, Orient *et a/ 1989),* and swarm results (◯, McCorkle *et a/ 1980), FALP* results (V, Smith *et a/ 1984)* appear to give a peak in the rate constant near 450 K which is difficult to reconcile either with *CEDS* results or theory,

V. APPLICATIONS

1. Gaseous Dielectrics

Electronegative gases have long been studied by the electrical power industry for use as insulators and in high power switches, especially switch-off devices. An effective gas dielectric is considered by the research community (Christophorou and Pinnaduwage 1990) as a gas that defines an electron energy distribution function f(E) and ionization and attachment cross section $Q_i(E)$ and $Q_a(E)$ that minimize the quantity given by

$$\int_{G_1}^{\infty} f(\epsilon)\epsilon^{1/2} Q_i(\epsilon)\, d\epsilon - \int_{0}^{\infty} f(\epsilon)\epsilon^{1/2} Q_a(\epsilon)\, d\epsilon \quad ,$$

or $(Z_i - Z_a)$, where Z_i is the ionization frequency and Z_a is the attachment frequency.

In the engineering community the gaseous dielectric is attractive because of its insulation performance. Also, for ac applications, it has lower polarization losses as compared to liquids; and in contrast to solids many gaseous dielectrics are relatively self-healing if subjected to overvoltage and arcing, The gas dielectric installation is often easier to handle in terms of maintenance, accessibility to components, definition and purity of the material, and the system support required.

In engineering terms, breakdown is also described as an electron-impact generated avalanche whose growth is determined by the *effective* coefficient of ionization $\bar{\alpha}$, which is defined as the difference between Townsend first coefficient of ionization α, and the coefficient of attachment, η.

Sulfur hexafluoride is one of the most important gaseous dielectrics (Trump 1954), An SF_6 gas-insulated substation takes only about 10% the space of similarly rated air-insulated switching station. It has been verified experimentally that $\bar{\alpha}$ is a linear function of the electric field strength and the gas pressure at a reference temperature. For pure SF_6

$$\bar{\alpha}(E,p) = \bar{\beta}E - \bar{K}p \ ,$$

where $\bar{\beta}$ = 27.8 kV^{-1} and $\bar{K}$ = 248 $(bar\text{-}mm)^{-1}$ (Pedersen 1989), Thus the limiting value $(E/p)/_s$ (where $\bar{\alpha}$ = O) is 8.84 kV/cm-bar. The success of SF_6 as a dielectric is due to the direct attachment process at a threshold energy (ϵ_{th}) of zero, or very low electron energy

$$e + SF_6 \rightarrow SF_6^- \qquad (Em = 0.0\ eV),$$

and to the dissociative attachment

$$e + SF_6 \rightarrow SF_5^- + F \qquad (\epsilon_{th} = 0.1\ eV).$$

At electron energies above 0.5 eV the second process is the more important, In addition attachment occurs with the dissociated products of SF_6 such as

$$e + SF_4 \rightarrow SF_3^- + F \qquad (\epsilon_{th} = 0.7\ eV)$$

$$Cj + SFd - SFa + F - \qquad (EM = 0.2\ eV)$$

$$e + F_2 \rightarrow F + F- \qquad (\epsilon_{th} = 0.0\ eV).$$

For E/N < 200 Td, McGeechan *et a/ (1* 975) found that SF_6 is the predominant species, However the conversion of SF_6 ions into F ions exceeds 10% above 360 Td.

As well as having high dielectric strength SF_6 has chemical inertness and low toxicity (the maximum continuous recommended exposure is 1000 ppm). It is thermally stable up to about 500 C and will not burn, While SF_6 mostly recombines after electrical-induced dissociation, Van Brunt and Herron (1 990) have shown that in the presence of oxygen and water vapor, small but important amounts of toxic by-products such as S_2F_{10}, SOF_4, and HF can be formed, Knowledge regarding larger cluster formations promoted by negative ions at high pressures is lacking, and is an area for further research (Van Brunt and Herron 1990). The reduced ionization coefficient for SF_6 and the attachment coefficient have been measured by de Urquijo-Carmona *eta/ (1* 986) and remeasured and discussed by Aschwanden (1985),

There should be significant advantages to gas mixtures that provide large rates of electron attachment across the electron energy spectrum (Christophorou 1978). This requirement usually implies dissociative attachment to remove higher-energy electrons and to satisfy energy-momentum conservation, Given these plausible arguments it is somewhat ironic that the engineering rule-of-thumb for conditions on the right-hand side of the Paschen curve (higher pDs) is that the breakdown field as a function of density of the gas concerned is roughly independent of the gas species

and its electronegativity (Cooke and Cookson 1978)! To first order He and SF_6 are of comparable electrical strength at equal gas densities, even though SF_6 has 16 times the insulation strength of helium at equal pressures, The collected data for uniform fields give the breakdown field E_{BD} as

$$E_{BD} = k\rho \left(1 + \frac{a}{\rho d}\right)^{\frac{1}{2}} .$$

Here k = 1.5 x 10^4 kV-cm^2/gram, p = gas density (grams/cm^3), coefficient a = 10-4, gm/cm^2, and d = gap spacing (cm).

Thus, a 20% SF_6/80% N_2 gas mixture gives about 80% the insulation holdoff of pure SF_6. However it is noted that the SF_6 density corresponds to doubling the N_2 density. This mixture has the advantage of lower cost than pure SF_6, and more reasonable pressures which avoids thick-walled containers that pure N_2 would require to give the same insulating strength, The other important breakdown parameter is the time to breakdown, A similarity relationship, depending on density, is also found to be independent of the electronegative properties of the gas (Cooke and Cookson *1978),*

These engineering approximations demonstrate the importance of isotropic electron scattering and the consequent reduction in drift velocity and on ionization rate. However a detailed approach to electron-molecule collisional and attachment effects as functions of energy is usually necessary to describe gas mixtures, The net ionization coefficient is related to the Townsend coefficients by

$$\frac{\omega_d \alpha}{N} = \left(\frac{2}{m m_e}\right)^{1/2} \int_{\epsilon_I}^{\infty} f(\epsilon)\, \epsilon^{1/2}\, Q_I(\epsilon)\, d\epsilon ,$$

$$\frac{\omega_d \eta}{N} = \left(\frac{2}{m_e}\right)^{1/2} \int_{0}^{\infty} f(\epsilon)\, \epsilon^{1/2}\, Q_a(\epsilon)\, d\epsilon ,$$

$$\bar{\alpha} = (\alpha - \eta) .$$

In principle the condition $\bar{\alpha} \geq 0$ for net volume gain in the gas is independent of the electron drift velocity. However one is dealing with a statistical distribution of a and η, and other things being equal, a lower drift velocity will reduce the probability of breakdown,

The fact that the density argument presented above cannot describe selected gas mixtures is neatly illustrated by some older data of Christophorou (1978). Itis shown that 2-C_4F_6 has a higher breakdown potential than 2-C_4F_8. When both are at a 50% mixture in nitrogen, the 2-C_4F_6 has a V_B of approximately 60 kV for a 7mm plane electrode gap at 600 torr, whereas the denser 2-C_4F_8 has a breakdown potential of approximately 40 kV. Similarly, there are isomeric differences in breakdown potential, and these correlate with the magnitudes of their attachment cross sections.

Basic research has provided many of the electron collision cross sections for N_2 and electronegative gases, so that it is possible to predict the breakdown potentials of the more common gas mixtures to a high degree of accuracy, If the objective is to hold off the highest voltage, then there are obvious advantages to using gases that provide large attachment cross sections, and large collision cross sections that rapidly degrade the electron energy, It is therefore argued (Christophorou *et a/ 1984)* that breakdown is much more determined by the gas mixture possessing large attachment cross sections (to capture the energy-degraded electrons) rather than by a small ionization cross section (few electrons with energy sufficient to ionize the gas mixture).

The description of sustained discharges is more difficult than breakdown for several reasons, There can be discharge-induced chemistry; the diffusion of multiply-charged positive and negative ions leads to simple analytical expressions in only a few special cases; and there is much less information on attachment and ionization of radicals, and a limited data base on detachment of negative ions, The reduced detachment coefficient is defined as

$$\frac{\delta}{N} = \frac{1}{i\ v_{id}} \int_0^\infty Q_d(\epsilon_L)\, \epsilon_L^{1/2} f(\epsilon_L)\, d\epsilon_L \ ,$$

where ϵ_L is the ion energy in the laboratory frame, $f(\epsilon_L)$ is the ion kinetic energy distribution function, v_{id} the ion drift velocity and m_i is the ion mass,

Until recently detachment databases on SF_6 used results of two groups of experiments. The first group employed a spatially well-defined bunch of negative ions that was accelerated in a strong electric field. The electrons were detached in the resulting ion-neutral collisions. This method required the electric field to be sufficiently strong that the detached electrons could be detected by their avalanches (Hansen *et a/ 1983;* O'Neill and Craggs 1973). The second group measured the variation in time lag between the high-voltage pulse and the occurrence of breakdown

as a function of the negative-ion concentration (Niemeyer *et a/ 1989).* Unfortunately results of these two groups do not agree on the values of the reduced detachment coefficient (Hilmert and Schmidt 1991). Newer experiments involve the use of molecular beams (Olthoff *et a/ 1989;* Yichen-Wang et *a/ 1989),* or a swarm method employing a pulsed electric field (Hilmert and Schmidt 1991). Results of this latter experiment are in reasonable agreement with a theoretical curve of Olthoff *et a/ (1* 989), if it is assumed that the SF_6^- ion transforms into SF_5^- and F during application of the high-field pulse, and that detachment occurs predominantly from the F^- ion,

2. Electronegative Discharges

Negative ions in low pressure positive column discharges change the radial density profiles of the other charged particles, increase the impedance and decrease the stability of the discharge. The negative ions tend to be trapped away from the ion sheaths that form on insulating walls and negatively-biased electrodes. Emeleus and Sayers (1 938) succinctly and fairly accurately summarized the effects in their observation that the electronegative gas discharge behaved as an electropositive gas discharge at higher pressure, However at least part of the effects near the cathode sheath are caused by the lower ionization potential and higher ionization efficiency of the electronegative gas compared to the rare-gas buffer.

In a positive-column glow discharge the radial ambipolar fields efficiently retard the radial diffusion of low concentrations of the low-mobility negative ions, At high' negative ion concentrations, the ambipolar field itself is reduced by the negative-ion space charge, However, closer to the insulating boundary the electron-retarding fields confine the negative ions within a reduced radius,

In a capacitively-coupled *rf* discharge the electrode *dc* sheaths and radial ambipolar fields also trap negative ions. These effects may partially explain why wall-sampling mass spectroscopy often fails to detect negative ions from discharges in attaching gases.

Thus negative ions are important in gas-discharge plasmas for several reasons. First, when electron losses by attachment are dominant over losses due to electron-ion recombination and diffusion, it is the balance between attachment and ionization that now determines the required electric field (or normalized E/N value) to maintain a self-sustaining discharge, or to provide the circuit-imposed drift current if the discharge ionization is externally controlled, Second, the rate of change of the

attachment rate with applied field, or the characteristic electron energy is the essential parameter controlling the discharge stability. Third, the negative-ion formation rate is actually the dominant excited-state source term in several rare gas-halogen excimer lasers. Fourth, the reactive radicals responsible for etching of semiconductors often originate in electronegative gases such as the halogens. These applications have prompted studies of various configurations of discharges operated in electronegative gases.

Studies have shown that the proportional solution (Oskam 1958, constant ratio of negative ion density to electron density) was applicable in late-afterglow plasmas, but not when the electron temperature is much greater than the ion temperature, and the ionization rate larger than the attachment rate, Rogoff (1985) has revisited the ambipolar diffusion coefficients originated by Thompson (1 959) (and reproduced by Massey (1 976) without comment), and points out that in three-component plasmas Thompson's coefficients do not permit the negative ions to diffuse in the opposite direction to the electrons as they might do in some circumstances. Also, though not explicit in his paper, Thompson required that

$$\frac{D_e}{\mu_e}\frac{\nabla n_e}{n_e} = \frac{D_-}{\mu_e}\frac{\nabla n_-}{n_-}$$

This constraint is severe and not usually found in electronegative discharges.

Additional boundary conditions must be included in the modeling of the electronegative discharge. One considers the continuity equations for three charged species, and either uses Poisson's equation or assumes quasi-neutrality as in the Schottky approach. The former method is needed to describe the lower pressure free-fall situation, while the latter is more permissible under collisional diffusion conditions. There are now four equations to be solved but typically six boundary conditions (Ferreira *et a/ 1988).* This means that there are now two eigenvalues. The mathematical requirements

$$j_e = \frac{j^* - \sum(\mu_l j_l)_k}{1 + \sum(\mu_l j_l^E)_k / j_e^E}$$

translate into constraints on the physical parameters of the discharge. For example, only certain ionization frequencies and certain on-axis ratios ($\alpha = n_-/n_e$) of negative ion density to electron density are possible.

Effects caused by negative ions are illustrated byexamining the two limiting conditions:

α << 1: When the negative ion density is small the ambipolar field is still controlled by the difference in nobilities of the positive ions and electrons. This ambipolar field ensures equality of the positive and negative fluxes to the insulating boundaries, When the ions have a much lower temperature than the electrons and there are volume losses of negative ions, there can be a radial inward flow of negative ions. The discharge separates into two spatial regimes, The negative ion density profile narrows and creates an annular electron-positive ion plasma. The negative ions are lost by recombination and detachment, and not by diffusion.

α << 1: When the negative ion density is comparable to the positive ion density, the ambipolar field is now determined by any difference in their nobilities, Such differences are small and consequently the radial field is also small, Negative ions can now diffuse to the boundaries. It must also be recognized that when the discharge has high recombination losses, the plasma may choose three-dimensional solutions, Discharges in an electronegative gas such as I_2 display quite exotic standing and moving striations.

The negative-ion profiles for a range of u's, for $T_e >> T_n$, are illustrated in Fig, *21,* Note that the transition between off-axis values of *a* (large) and *a* (small) tends to occur near the walls of the tube, Formally, the transition condition may be defined as (Bell 1993)

$$(\alpha)_{crit} = (T_e - T_n) - \mu_+(T_p + T_n)/\mu_e ,$$

where the T's are particle temperatures and the μ's are nobilities. For T_e = 1 eV, $T_p \simeq T_n$ = 0,03 eV and $\mu_e/\mu_+ = 10^3$, then α_{crit} = 2 x 104, This result implies that the "low negative-ion density" trapping regime includes many discharges of technical interest, and that the negative ions will not be detected at the actual boundaries under *cw* conditions. Thus, experimental mass-sampling of negative ions from plasmas is more successful when the probe is behind the anode, or on the axis of the discharge.

In a low pressure diffusion-controlled electropositive discharge ionization waves often occur because there is a phase delay between a change in the electric field and the subsequent ionization response, In a recombination-controlled discharge this mechanism does not occur because an increase in electron density results in a decrease in the local electric field. In many electronegative gases DA occurs. This

process has a threshold energy and a rate coefficient that usually depends sensitively on (E/N). The (E/N) dependence of DA therefore is similar to that of the ionization rate but with a lower threshold and (often) a steeper initial slope, Under these conditions a decreased field results in decreased attachment and higher electron density. This decreases the electric field and the perturbation grows, Instabilities that negative ions introduce in low pressure glows and in high pressure externally-sustained discharges are discussed in more detail below.

3. Negative Ions in Laser Plasmas: Molecular Gas-Discharge Laser

The direct-current, glow-discharge $C0_2$ laser is limited by the energy density that can be applied to the discharge, and in its pressure scaling by the onset of inhomogeneities and/or the glow-to-arc transition. Transverse-excited atmospheric (TEA) discharges of long pulse duration are similarly limited by the onset of discharge instabilities. It has been found that negative ions reduce the thresholds for these phenomena. The onset of the inhomogeneities is a function of the gas mixture and its prior history, Negative ions such as O^- are formed by dissociative attachment of CO_2. Subsequently more stable negative ions such as NO_2^- and $N0_3$ are formed by electron collisions with compounds formed from products of neutral dissociation of CO_2 and N_2. Analyses (Haas 1973, Nighan and Wiegand 1974, Nighan 1976) have shown that there are several types of plasma instabilities in these discharges which can often be coupled, The fastest-growing are ionization-type instabilities, next are vibrational-relaxation related waves, and finally the thermal instability, Studies have shown that the trigger instability at high-energy loading conditions is the attachment-ionization-recombination mode (also called the domain instability). In CO_2 mixtures the attachment process is dissociative

$$e + CO_2 \rightarrow CO + O^-$$

followed by rapid conversion of O^- to CO_3^-

$$O^- + CO_2 + M \rightarrow CO_3^- + M \ .$$

The O^- density can be reduced by adding amounts of CO or H_2 to the discharge to cause detachment. However the detachment of electrons from CO_3^- is relatively slow so that the main control is *via* interception of the O-. Domain instabilities or ionization-wave striations cause inhomogeneities in the direction of the applied field. Even when they do not lead to arcs they are to be avoided because they limit the optical

homogeneity of the discharge laser. The domain instability occurs in discharges that display a region of differential negative conductivity in their current-voltage response. This effect can occur when the attachment rate is a rapidly increasing function of E/N.

For discharge conditions typical of molecular gas lasers, when there is a local perturbation in the electric field, the characteristic time for electron-density response is much longer than the time for electron-temperature or energy-distribution response, The particle continuity equations can then be linearized to obtain the stability criterion for the attachment instability (Haas 1973). Alternatively, the equations can be solved directly to give the time-dependent behavior of the principal quantities. Nighan and Weigand (1 974) showed that a necessary criterion for the DA instability is

$$(k_a \hat{k}_a / k_i \hat{k}_i) >> 1 ,$$

where $\hat{k} = \partial ln k / \partial ln T_e = (T_e/k)(\partial k/\partial T_e)$. Or, since T_e is a monotonic function of E/N,

$$\hat{k} = constant \quad (E/Nk)\,[\partial k/\partial (E/N)] .$$

The dependence of k_a on E/N is determined by the EEDF, which in turn is determined by the collisional cross sections of the gas mixture. Examples of ionization and attachment coefficients for CO_2 laser mixtures are given by Nighan (1976). Note that, at a selected E/N, the EEDF is essentially independent of the minority species, With respect to the stability of the plasma, because the logarithmic derivatives of the coefficients are also determining parameters the most important attacher is not necessarily that with the largest attachment rate, It is the rate-of-change of attachment rate with electron energy that is most important, The net attachment rate, *i.e.* the attachment rate minus the detachment rate, is also important because it determines the plasma impedance and the operating E/N. H_2 and CO_2 have large rates for detachment of 0-, OH-, NO^- and 02-, However, NO_2^- and NO_3^- do not undergo detachment collisions readily, so that as the gas is dissociated and further processed by the plasma, and more of these ions are created, the energy-loading threshold for instability is decreased. Some of these problems can be alleviated in small-scale CO_2 laser discharge systems by adding xenon to the gas, Xenon has a lower ionization potential than the other components, and a large ionization cross section. A small amount can control the ionization and also reduce the dissociation of nitrogen. In larger scale discharges gas recirculation and homogeneous and heterogeneous catalysts (to promote neutral recombination) assist the stability of the discharge.

While external ionization sources tend to increase discharge stability, Douglas-

Hamilton and Mani (1 973) showed that electron attachment instability was possible in electron-beam ionized discharges at high pressures. A linearized analysis showed that the discharge was unstable unless $v_a > 2v_i$. One can appreciate this relation by considering that, at high pressures, the ionization is through a metastable state, The latter density is proportional to the electron density, hence the ionization frequency is proportional to n_e^2. The attachment frequency is proportional to n_e, so if there is a perturbation in electron density, the discharge stabilizes only if the attachment frequency exceeds twice the ionization frequency. This constraint limits the gas-mixture variation and power loading of excimer lasers.

As diffusion can be neglected the continuity equation for electrons is

$$\frac{dn_e}{dt} = S - \beta n_e - \alpha_r n_e n_+ ,$$

where β is the electron-neutral attachment rate, α_r the electron-ion recombination coefficient, and S is the external ionization source term. This equation is subjected to perturbation analysis in n_e and E to obtain

$$-i\omega \sim E\frac{\partial \beta}{\partial E} - \beta - \alpha_r n_{+o} ,$$

where the o subscript indicates unperturbed values. When recombination still exceeds attachment, the equilibrium ion density is approximately $(S/\alpha_r)^{1/2}$. Instability onset occurs when

$$S \leq S_{crit} = \frac{1}{\alpha_r}\left(E\frac{\partial \beta}{\partial E} - \beta\right)^2$$

and

$$\frac{E}{\beta}\frac{\partial \beta}{\partial E} > 1.$$

Douglas-Hamilton and Mani also demonstrated this instability in a pulsed electron beam sustained discharge in helium plus water vapor; and in the CO_2 laser "triple mixture", (He : N_2 : CO_2 = 3 : 2 : 1), As predicted by the analysis, the discharge showed a sharp *decrease* in *dc* current due to the presence of the attachment instability, This result contrasts with observations on the ionization instability in diffusion-controlled positive columns where, the average current *increases,* In the water-vapor containing mixtures, a variety of hydrated ions are expected [including $H_3O^+ \cdot (nH_2O)$, where n = 1→4, and $OH \cdot (5H_2O)$] especially in the

afterglow of the pulsed discharge.

A more detailed analysis (Douglas-Hamilton and Mani 1974) shows that the instability region is actually a bounded region in the S *vs* E/N space.

4. Oxygen Discharges

The oxygen discharge has been a favorite electric discharge for study. As long ago as 1927, Guntherschulze (1927) identified the O_2 discharge at low pressure as having two distinct forms: one with a high longitudinal electric field at higher currents and low pressures, and a second with a much lower electric field. There were color and spectroscopic differences associated with each form. These discharges were later termed (Seeliger and Wichman 1951) the H(hoch)-form and the T(tief)-form. At a selected pressure, an increase in current eventually causes the discharges to transition from the T- to H- form. The forms can be obtained in the same discharge, and the H-portion is always situated on the anode side of the column, The transition exhibits hysteresis as the current or pressure is changed.

Of the two, it is the T-form that is considered to differ from other molecular gases; the electric field is anomalously low when compared to values observed in other molecular gases. The T-form is always found. to be unstable with large modulations in its parameters, so that reported electric fields and currents are time-averaged values, The I{-form is essentially stable and has an electric field typical of molecular gases.

Thompson (1 959) studied the low pressure discharge (0.04 torr) experimentally and theoretically, He derived effective diffusion coefficients for the three-component plasma which were quoted liberally and uncritically for many years, Sabadil (1 973) made a series of diffusion analyses for the oxygen discharge and also attempted to explain the peculiar instability, which he termed a domain instability in analogy with the Gunn oscillations in semiconductor diodes. Edgely and von Engel (1 980) revisited the oxygen discharge with a rather complete analysis that did not assume quasi-neutrality, The computational difficulties were considerable, and there were only a few comparisons given in their paper. They did not consider recombination or gas-temperature effects. Nobata and Kando (1 979) also studied the charged-particle diffusion profiles, including gas-temperature effects, and compared the analysis with the observable contraction above about 5 torr. Nobata and Kando reconciled some of the previous results in the literature by solving the momentum and continuity

equations instead of assuming a fixed relation between $\frac{\nabla n_-}{n_-}$ and $\frac{\nabla n_e}{n_e}$.

Under the conditions $T_e >> T+, T.$ one has $\mu_+ = \mu_-$, and $\frac{T_e}{AT.}\left|\frac{\nabla n_e}{n_e}\right| > \frac{\nabla n_-}{n_-}$ it was found that the flux of negative ions, positive ions, and electrons each is approximately proportional to the electron density gradient,

$$(nv)_e \simeq -D_o(1 + 2\alpha)\,\nabla n_e ,$$

$$(nv)_- \simeq DO\,\alpha\,\nabla n_e ,$$

$$(nv)_+ \simeq -D_o(1 + \alpha)\,\nabla n_e ,$$

where DO = $\frac{\mu_o k T_e}{eA}$, and A = $1 + [\mu_+ + (\mu_+ + \mu_-)\alpha]/\mu_e$.

When $\frac{\nabla n_-}{n_-} = \left(\frac{T_e}{T_-}\right)\frac{\nabla n_e}{n_e}$ the equations of Thompson are recovered. Note that the sign on the diffusion coefficient for the negative ions indicates that they diffuse radially inward.

The radial electron density profile is calculated from the following equation (45) that is now a function of the attachment rate ν_a, detachment rate ν_d, electron-ion recombination rate α_i, and ionization frequency Z_e:

$$\frac{d2ne}{dr^2} + \frac{1}{r}\frac{dn_e}{dr} + \frac{1}{D_o(1+2\beta)}\frac{d}{dr}[D_o(1+2\beta)]\frac{dn_e}{dr} + \\ + n_e\frac{Z_e - \nu_a - \alpha_e n_+ + \beta\nu_d}{D_o(1+2\beta)} = 0 \qquad (45)$$

Here the quantities are $\beta = n_-/n_e$, the diffusion coefficient DO = $\mu_+ kT_e/eA$, and A = $1 + [\mu_+ + (\mu_+ + \mu_-)\beta]/\mu_e$. The problem with the analytic approach is that β is assumed independent of radius. The approach of Bell (1 993) does not have this limitation, but has not yet been applied to oxygen,

A useful approximation also permitting an analytic solution (Tsendin 1989) is to divide the discharge into two regions: an inner one where the negative ions are trapped and the densities of the charged species are proportional; and an outer

annulus where the negative-ion density is almost zero and the plasma is essentially electropositive,

These results appear to be good approximations for the H-form of the discharge. However, it must be emphasized that the low current T-form has large modulations in its microscopic parameters which are not stabilized by current control,

Dettmer and Garscadden (1 981) investigated the effects of additives on the T-form of the discharge, and found that argon gave only minor effects but that carbon monoxide gave dramatic effects and could eliminate the T-form altogether. Analysis of the results indicated that the mechanism was collisional detachment of the negative ions, principally by the reaction

$$O^- + CO \rightarrow O + CO + e .$$

Chemical-kinetics calculations show that the dominant detachment reactions at a gas density of 10^{17} cm^{-3} and electron density of 10^{11} cm^{-3} are:

$$e + O^- \rightarrow O + e \quad (7.9 \times 10^{-10})$$

$$O_2^{\bullet} + O^- \rightarrow O_3 + e \quad (3.0 \times 10^{-10})$$

$$O_2^- + O \rightarrow O_3 + e \quad (3.3 \times 10^{-10})$$

$$O_2^- + O_2^{\bullet} \rightarrow 2O_2 + e \quad (2.0 \times 10^{-10}).$$

The dominant negative ion is O^- and, neglecting atom quenching, the $O_2(^1\Delta)$ concentration is predicted to approach 20% of the 0_2 concentration at E/N = 50 Td, Therefore it appears that self-stabilization or mode-change of the discharge is caused by the electron and excited-state detachment of O-.

Studies in connection with ozone negative-ion formation and metastables have been carried out by Khvorostovskaya and Yankovsky (1 991),

5. Influence of Negative Ions on Electron Emission

It is well known that oxide cathodes and even matrix cathodes degrade in the presence of small amounts of certain gases, usually called poisoning gases, This

occurs even with matrix cathodes and lanthanum hexaboride-based cathodes. The poisoning process has been usually attributed to physical chemistry and work function changes on the cathode surface, Baranov and Petrosov (1 987) have proposed a new mechanism for the degradation. It is suggested that negative ions in the inter-electrode space build up space charge and change the perveance of the electronic space charge flow. Of course, other mechanisms can coexist with the negative-ion space charge effect operating over a wide parameter range, In a planar diode the Langmuir-Childs relation is

$$j_e + \sum (\mu j_i)_k = P U_a^{3/2} = j_a ,$$

where j_e and j_i are the current densities of the electrons and ions, k is the ionic species, U_a is the anode potential and P is the perveance of the diode. The quantity j" is the vacuum perveance current density in the diode, and $\mu_k = (M_k/m)^{1/2}$ is the ratio of the nobilities of the electrons and ions. Values of μ_k are in the range 10^2 to 10^3. Therefore even when $j_i / j_e \sim 0.1$ %, the difference j' - j_e can be ~10%.

The negative ions can be generated by (a) surface ionization (b) ion sputtering, (c) thermionic emission, and (d) volume attachment (minor importance), Under space-charge limited conduction conditions, if the negative ions are emitted with low energy, the negative ion current is

$$(j_i)_k = (j_i^E)_k \exp (-e U_m / kT_k) ,$$

whew U_m is the potential barrier and j_i^E is the ion emission current density. Then

$$j_e = \frac{J^{**}}{1 + Z(\mu_i^E)_k / j_e^E} ,$$

where j_i^E is the electron emission current density, If the negative ions originate through sputtering and have an energy larger than the potential well U_m, then

Under partial vacuum conditions, ion-sputtering currents of La^- (0.5), B^- (0.3), BO^- (2.79) BO_2^- (4.2) and others can be generated (numbers in parentheses refer to the electron affinity in eV).

Baramov and Petrosov show that this model leads to plausible results for oxygen contamination creating BO^- ions in a diode using a LaB_6 cathode, It appears that surface cathode poisoning is the dominant mechanism below 1600 K and that negative ion space-charge effects are more important above this temperature,

6. Negative Ion Sources

It is much easier to neutralize negative ions than positive ions. Consequently there has been great interest in the development of high-current negative ions in connection with neutral beam injection into tokamaks for heating and for other directed beam applications, The general principles of efficient negative ion formation were projected to be similar to those occurring in solar atmospheres -- a low ionization potential source of electrons and a supply of attaching gas. Experiments gave significant negative ions and gradually understanding of a two-step mechanism for volume sources emerged (Bacal and Skinner 1990). The first step is (A):

$$fast\ e + H_2(X^1\Sigma_g^+; v'=0) \rightarrow H_2^*(B^1\Sigma_u^+, C^1\Pi_u \ldots) + e$$

$$H_2^*(B^1\Sigma_u^+, C^1\Pi_u \ldots) \rightarrow H_2(X^1\Sigma_g^+; v'') + h\nu .$$

Fast electrons excite ground state molecular hydrogen to higher electron states whi ch then radiate back to the ground state and both transitions result in "Franck-Condon" mixing of the vibrational population, The second step is (B):

$$slow\ e + H_2(X^1\Sigma_g^+; v'') \rightarrow H^- + H .$$

Wadehra and Bardsley (1 978) showed that the dissociative attachment cross section was an exceedingly strong function of vibrational quantum number, The two-step mechanism involving different electron energies suggested either two discharge chambers or separation of the processes in time using a pulsed discharge. The negative ion sources are typically divided into two regions using a magnetic filter. Region (A) where fast electrons are accelerated from hot filaments is called the driver region. Region (B) accepts only slow electrons across the magnetic filter and is termed the extractor region, Negative ion densities up to 70% of the positive ion density in the extractor have been reported by Holmes *et al (1985).*

A discrepancy has been noted (Berlemont *et al 1993,* Garscadden and Nagpal 1995) between the measured and calculated $H_2(X\ ^1\Sigma_g^+, v'' \geq 5)$ and H^- number densities. Simple kinetic analysis shows that DA to high-Rydberg states of H_2 is very efficient, and may be responsible for an additional channel of H^- production which could resolve the low value of H^- in the volume-source model,

In order to populate the empty electron affinity level of a hydrogen atom, one needs a source of electrons with energy of 0,75 eV (van 0s *et al 1987,* van 0s 1989). All metals have such electrons in their conduction bands; however, they have a stronger bond in energy with the work function of the metal surface, Even with

cesiated surfaces the work function is larger than the electron affinity of hydrogen. However, when a hydrogen atom is very close to the surface, the affinity level is lowered and electric field broadened due to the interaction with the image of the affinity level in the metal (see Fig, 22). When the atom is very close to the metal surface, the electron affinity level can become lower than the work function and an electron in the conduction band may transfer to the atom. Surface conversion sources that convert positive ions to negative ions have given converter efficiencies of > 4°/0 (Goretskii *et al* 1989). It was found that a pure barium metal converter gave comparable yields to those obtained with cesiated surfaces and avoided some of the insulation problems with condensing cesium. While the cesiated surface has the lower work function, the barium metal has a higher density of electrons in its conduction band.

A third type of high current source has been reported by Goretskii *etal(1989).* It uses a reflex discharge shown in Fig, 23. They propose that this compact configuration is analogous to a two-chamber system. It has a magnetic field parallel to the reflex discharge axis. The density of slow electrons in the discharge column is about 10^{14} c m^{-3}, and of fast electrons about 10^{12} c m^{-3}. Away from the column there are few fast electrons while the thermal electron density falls off gradually. It is postulated that the vibrational excitation of molecules occurs in the discharge column from where they diffuse radially to undergo dissociative attachment by the slow electrons. The authors pay special attention to the gas pumping speeds required for high-current negative-ion sources.

7. Negative Ions and Laser Preionization

For uniform excitation of high pressure excimer lasers such as XeCl and KrF, preionization by electron beams, x-rays or corona discharges, *etc* have been found to be effective, It was observed empirically that a delay of 100 ns to 1 μs of the main pulse with respect to the preionization pulse was necessary to obtain good uniformity, The mechanism of overlapping avalanches is consistent with experimental data, Hsia (1 977) postulated that the preionization electrons are rapidly attached to the halogen donor gas

$$e + F_2 \rightarrow F^- + F$$

$$e + NF_3 \rightarrow F^- + NF_2$$

in a time of nanoseconds or less at typical donor concentrations of 1017 cm^{-3} and the negative ions disappear by three-body recombination, but that a residual negative ion

density of the order of 10^{11} cm"3 extends to 1 μsec. When the electric field of the main pulse is applied, Hsia argued that collisional detachment of the accelerated F^- ions released the preionization electrons. Over a decade later, this interpretation was challenged by Osborne *eta/ (1989).* They showed that Hsia apparently erred in using the *electron affinity* rather than the *reaction threshold* for the collisional detachment of F^- and also omitted the pressure dependence of the negative ion mobility. The corrections result in a factor of 2 in the threshold and a factor of 3 decrease in the mobility with a consequent overall correction in fast F^- density of 10^{13}! Re-analysis of the problem shows that modest amounts of UV radiation appear adequate to provide sufficient photodetachment to explain the preionization. This result is detailed because the original hypothesis has been repealed in the published literature without critical examination.

8. Radio Frequency Discharges for Plasma-Enhanced Processing

The manufacture of high-density electronic circuits relies on plasma-enhanced etching to achieve fidelity of pattern transfer, high anisotropy and rapid etch rates, As the etched material must be volatile at reasonable temperatures, most of the gas mixtures used involve the halogens and consequently electronegative discharges. *Rf* discharges in pure electronegative gases and their mixtures with noble gases are widely used. The gases uses include BCl_3, Cl_2, HCl, HBr, CCl_2, CF_4, $CHCl_3$, $CFCl_3$, HF and SF_6. The oxygen discharge, which also displays electronegative properties, is used in passivation and oxidation applications.

The electrons and ions have markedly different random currents so that a floating electrode in contact with a plasma will self-bias negative until the negative and positive fluxes are equal. When the electrode is driven by an external *rf* potential, the electron current becomes strongly modulated because of the non-linear current-voltage response, however, the same constraint applies. Consequently, the voltage bias becomes larger. Generally, industrial reactors are asymmetric in electrode area, or one of the electrodes in grounded and at the same potential of the metal enclosure (if used). When the *rf*-coupled driven electrode is then smaller than the grounded electrode, it acquires a significant negative *dc* bias to balance the net current through both sheaths, These systems are designed to enhance etch uniformity so that the electrodes are aligned and the discharge has excellent radial symmetry. There is a radial electric field to enforce ambipolarity in the wall current. Under such boundary conditions, negative ions are trapped in the plasma volume and are lost by recombination and detachment but not diffusion, The relative concentrations of

negative ions can be estimated as

$$n_- \cdot \left(\frac{n_e k a}{(n_e k_d + an>} \right) [A] ,$$

where k_a is the attachment coefficient, k_d is the electron impact detachment coefficient, α is the ion-ion recombination coefficient, and $[A]$ is the concentration of attacher. The long trapping times mean that the negative ions can build up to large fractional concentrations of the ion density. Under these conditions, dust or particulate is also often found trapped in the plasma, The sizes of the clusters are typically from tens of Angstroms to several microns, and in some circumstances as large as 10^{-1} cm, A typical dust particle of one micron size contains 108-109 atoms. The particles charge negatively and are electrostatically suspended by the ambipolar and sheath fields against gravity, ion drag and thermophoresis. Particles form rapidly throughout the discharge volume in gases such as CO or SiH_4 where electron-impact induced dissociation produces carbon atoms or silicon atoms, respectively, They also are found in rare-gas *rf* discharges with carbon or silicon electrodes. Under such conditions, the particle material must originate from the electrodes by ion-induced sputtering, The resulting vapor pressures of atomic and dimer carbon are very low, but are many times the equilibrium value. Under such conditions, homogeneous nucleation occurs with the critical size for a stable cluster extending to the dimer. The trapping of dust for hours or days in a plasma indicates that much of the lifetime of the cluster and the particle has to be as a negative ion and a negatively charged particle, The growth kinetics of such negatively charged clusters have been studied by dynamic light scattering and by square wave amplitude modulation of the *rf* excitation (Watanabe and Shiratani 1993), Negative ions are believed to be key species at low pressures for particle formation, During the "off-time" of the modulation they can diffuse to the boundaries or convect with the gas flow, Densities of 60 nm diameter particles are estimated to approach 109 cm^{-3}, Under some conditions the dust attains a surface charge of 103-104 e and sufficient density to change phase to a Coulomb liquid or even solid. While such conditions influence discharge impedance, they are generally to be avoided in microelectronics processing.

9. Mass Spectrometer Sampling of Negative Ions

Axford and Hayhurst (1 990) have carefully reviewed the conditions for mass spectroscopy of flames. It is even more difficult than sampling of plasmas, The pressure transition is from a hot, near-atmospheric pressure flame to a high vacuum

region ($\sim 10^{-8}$ torr) where the ions are mass analyzed and detected. The gas is cooled before it passes through the sampling aperture (typically 0.1 mm diameter) because the sampler is invariably colder than the hot gas. There is even further cooling as the sampled flow undergoes near-adiabatic, supersonic expansion into the first vacuum stage of the mass spectrometer system. Both circumstances can give anomalous and unreal clustering of the parent ions, positive and negative. In order to detect negative ions distinctly from the electron background, it is usually necessary to use an electron-deflecting magnetic field, and/or a small positive bias between the sample nozzle and the burner (or in the case of a plasma, with respect to a reference electrode). It is also usually necessary to sample the flame or plasma on-axis, as well as on the side: space-charge effects and ambipolar fields can concentrate the negative ions at the center of the plasma (see later remarks on three-component plasmas).

Loffer and Homann (1 990) have extracted positive and negative polycyclic aromatic hydrocarbon (PAH) ions, oxygenated PAH ions, and polyhedral carbon ions from premixed benzene-oxygen flames, The OXO-PAH negative ions appear first, with only one oxygen atom, up to mass 413 ($C_{23}H_{13}O^-$), and the even-numbered carbon-atom species dominate. These ions decompose in the flame to PAH. Negative polyhedral ions (C-50 and C-60) have been extracted from these flames just below the sooting threshold. In acetylene-oxygen flames negative PAH ions are not observed, This observation favors the formation of ions in the benzene flame by growth of the phenolate from condensation reaction rather than by large neutral PAHs reacting with O_2^-, 0“, or OH”.

The detection of the polyhedral ions in non-sooting benzene flames means that there must be an additional source of these ions besides nascent carbon particles. The carbon-rich candidates in benzene flames are the PAH polyynes, their ions and OXO-PAH ions, However mass growth of PAH^- and oxo-PAH^- was zero and limited, respectively. Negative polyyne ions are also excluded as sources because of their low concentrations. Therefore it is argued that the polyhedral negative ions are formed from large uncharged hydrocarbons that grow and then become charged. Some of these conclusions may depend on special creation conditions for the larger clusters, and even moreso for the fullerenes.

Research on negative carbon cluster-ions has been spurred on by the icosahedrally-structured molecules, the importance of carbon molecules in sooting, and by carbon grains in interstellar space promoting polyatomic molecule formation. The structure of smaller clusters has been studied by anion photoelectron

spectroscopy (Arnold *et al 1991)* and by Coulomb Explosion Imaging (CEI) (Feldman 1990). The experiment uses a Smalley-type laser-vaporization/pulsed molecular beam source. The ions formed in the laser-generated plasma are sampled by a time-of-f light mass spectrometer. The ion of interest is selectively photodetached by an appropriately-timed pulse from harmonics of a Nd:YAG laser. The energy of the photodetached electrons is measured with a resolution of 8 meV to give the photoelectron spectrum, Since the anion photodetachment is a sudden transition, it is a vertical process and the length of the measured vibrational progression in the electron energy spectrum provides information about changes in geometry between anion and neutral, Up to C_{11}^-, and excepting C_{10}^-, Arnold et *a/ (1 991)* found that the configurations of both states were linear for most of the molecules, with some minor nonlinear contributions that might be ring- configuration isomers, Yang *et a/ (1* 987, 1988) have also used anion photoelectron spectroscopy to measure the structure and electron affinities for carbon molecules C_n up to n = 84, Above n = 10 the molecules were identified as monocyclic ring forms. These experiments show that electron affinities are quite large, being in the range 2-4.4 eV (see Table I).

Table 1. Electron Affinities of Carbon Molecules

Molecules			C_2	C_3	C_4	C_5	C_6	C_7	C_8	C_9	C_{10}	C_{60}
EA (eV)	3.3	2.0	3.9	2.8	4,2	3.4	4,4	3,7	3.9	2.65		

Doubly-charged C_{60} anions with lifetime longer than 1 msec have also been observed (Hettich and Ritchie 1991). The model proposed for the formation of these ions involves negative surface ionization. Doubly-charged anions have also been produced by sputtering of the graphite target with cesium ions (Schauer *eta/ 1990).* To date, no beams of these clusters have been formed. These results are noted because vaporization of carbon molecular clusters and formation of anions will influence electron emission from contaminated filaments (Sec. V B).

In order to study electron attachment to large neutral clusters, very low-energy electrons with a defined narrow energy distribution are required to minimize dissociation of the cluster, Several groups have used high Rydberg-state rare gas atoms which transfer the Rydberg electron to the weakly bound clusters of positive electron affinities. The cluster fragment anions are detected by mass spectroscopy

(Kondoq 1987). Measurements are made as a function of the principal quantum number. Experiments with $(CO_2)_n^-$ revealed that the threshold size for anions was n = 3; f e r n = 11, 12 and 13 the intensities were weak whereas 14 and 16 were magic numbers. The $C0_2$ monomer cannot capture the Rydberg electron because the vertical electron affinity of CO_2 is negative. The vertical EA of $(CO_2)_n^-$ increases with n and becomes positive for n = 3. The cross section for attachment also increases with n because the state density of $(CO_2)_n^{-*}$ and its lifetime for autodetachment increase with n,

Knowledge of reaction mechanisms, thermodynamics, and kinetic rates of formation of stable negative ions is important in calculations of electrical properties of combustion systems, It appears that photodetachment and optogalvanic spectroscopy could be applied to this area to permit higher spatial resolutions and fewer sampling ambiguities.

10. Ignition and Inhibition of Combustion

Hydrocarbon-based flames and other flames and plumes are known to be weakly electrically conducting. The ionization source appears to be chemiionization in the reaction zone as a result of the energetic reactions

$$O + CH \rightarrow HCO^+ + e ,$$

or

$$CH^* + C_2H_2 \rightarrow C_3H_3^+ + e .$$

Subsequent charge transfer reactions create other ions of which the most dominant is often H_3O^+,

$$HCO^+ + H_2O \rightarrow H_3O^+ + CO .$$

Negative ions also have been detected in flames through mass spectroscopy. The initial reaction at higher pressure is identified as

$$e + O_2 + M \rightarrow O_2^- + M ,$$

with subsequent electron transfer to other electronegative radicals found in hydrocarbon combustion (Barnard and Bradley 1985), such as C_2, CH, O, OH, O_3, C_2H, CH_3O_2, and HO_2.

The ignition of a combustible mixture by a spark occurs when the temperature

profile is consistent with that for flame propagation (Barreto, 1979), The initial spark is localized and has a temperature much higher than the flame temperature. Hence the plasma-heated volume must expand and cool to achieve the required condition for ignition (Lewis and von Elbe 1961). The time dependence of the energy input of the spark depends on the electron avalanche growth in the gas mixture, ion bombardment and secondary emission of the cathode, and on circuit parameters.

Thermal ignition of an explosive mixture may be prevented either by increasing the heat removal, or by decreasing the reaction rate (Zel'dovich 1944), Inert gases or dust must be added in sufficient quantity to change the specific heat of the mixture. However it has been found that some gases such as halogenated compounds strongly affect the flame velocity and ignition threshold at concentrations as low as a fraction of a percent, This sensitivity has been attributed to the halogens' removing the reactive radicals (Bellis and O'Neal 1957) or attaching the free electrons (Creiz 1961). Lee (1 963) summarized the flame inhibition effectiveness for 19 electron-attaching compounds and their measured electron attachment coefficients at an approximate electron energy of 0.2 eV (corresponding to a typical flame temperature), It was noted that effective flame inhibitors such as CF_2Br_2, CH_2Br_2 and $CHCl_3$, and antiknock compounds such as tetraethyllead, iron pentacarbonyl and methyl-cyclopentadienyl manganese tricarbonyl all have relatively high electron affinities, even if the correlation with knock inhibition was not exact. However most attachment data are only available for relatively low gas temperature; and data for the appropriate low electron energy are not equivalent to data at the combustion temperature, Christophorou *et al* (1 984) have emphasized the effects of temperature on dissociative attachment and on the total electron attachment rate. At high temperatures the dissociation of molecular negative ions is faster and the lifetime of negative ions is expected be shorter because of the higher internal and translational energy of colliding species, Thus gases which have high attachment cross sections at low temperatures, but low electron affinity, are expected to have low attachment rates at high gas temperatures. In contrast, some species that have low attachment rates at low temperature show strong increases with increasing temperature, somewhat similar to the classical case of the effects of vibration and rotation in hydrogen, These considerations are complicated by the fact that some of the more complex and weaker electron-attaching molecules may dissociate into "good" electron attachers at high temperatures,

Analyses of effects of additives on ignition have been essentially steady-state approaches. They do not take account such interactions as the vibrational-

translational relaxation of the additives. Rapid heat releases caused by, for example, small concentrations of iron pentacarbonyl in vibrationally-excited carbon monoxide, can easily overcome any specific heat effects of the additive,

A number of metals when added to flames produce very stable negative ions, The thermodynamic parameters for a number of species are shown in Table II (after Miller 1973).

Table II. Thermodynamic data for metal-containing negative ions

Ion	Reaction	K_{eq}	Electron Affinity (kJ mole-l)	Ref.
BO_2^-	$HBO_2 + e \rightarrow BO_2^- + H$	1500 exp(-1 0,000/T)	393	A
$HMoO_4^-$	$H_2MoO_4 + e \rightarrow HMoO_4^- + H$	24 exp (500/T)	410	B
MoO_3^-	$HMoO_4 + H \rightarrow MoO_3^- + H_2O^+$	0,85 exp (10,400/T)	250	B
HWO_4^-	$H_2WO_4 + e \rightarrow HWO_4^- + H$	25 exp (1 300/T)	400	c
WO_3^-	$HWO_4 + H \rightarrow WO_3^- + H_2O^+$	0.87 exp (5700/T)	351	c
CrO_3^-	$HCrO_3 + e \rightarrow CrO_3^- + H$	2500 exp (-1 3,400/T)	229	D
$HCrO_3^-$	$CrO_3 + H_2 \rightarrow HCrO_3^- + H+$	1,7 exp (-9000/T)	390	D

11. Electron-Capture Detection of Complex Molecules

The chemical ionization source of a mass spectrometer can be used to produce negative ions by electron capture reactions (referred to as electron capture negative ion mass spectroscopy - ECNIMS) using a nonreactive buffer gas such as methane or argon, Negative ions are efficiently and selectively formed by reactions of electrons with electronegative molecules, Chemical ionization sources can be designed to limit gas conductance so that ion source pressures of around 1 torr can be used, The

buffer-gas ionization is a source of secondary electrons and the buffer-gas cross sections essentially determine the electron energy distribution. The gas also promotes three-body stabilization of negative ions. Many environmental contaminants form negative ions in this manner. Electron-molecule reactions proceed more rapidly than ion-molecule reactions and lower detection limits for certain compounds are observed when using ECNIMS as compared to positive-ion mass spectroscopy,

Mass spectroscopy of negative ions is notoriously difficult due to false signals generated by photoelectrons and other secondary electrons, and even by *positive* ions for a quadruple mass analyzer, Important advances have been the introduction of conversion dynode electron multipliers and the use of pulsed positive ion-negative ion chemical ionization mass spectroscopy, In the former method the system has a conventional positive-ion electron multiplier, however the negative ions are converted to positive ions before they enter the multiplier. The negative ions are accelerated onto a conversion dynode held at high positive potential. The negative ions cause sputtering of metal atoms, some of which may lose electrons and become positive ions; fragment and produce some positive ions; or undergo charge-stripping to produce neutrals and positive ions. The conversion dynode multiplier has eliminated the need to electrically float the detector at high potential, reduced the noise due to stray electrons entering the multiplier, and has improved the detection of the low-energy negative ions encountered in quadruples.

The growing importance of electron-capture negative ion detection spectroscopy is illustrated by the text of Stemmler and Hites (1 988) which contains ECNI mass spectra of 361 compounds, The mass spectra were measured on a MS system, The compounds were selected to include the major classes of environmental contaminants such as those found on the US Environmental Protection Agency's priorily pollutant list, Compound classes of environmental importance include halogenated benzenes and phenols; nitrobenzenes and related dinitro herbicides; polycyclic aromatic hydrocarbons; halogenated biphenyls, dioxins, and dibenzofurans; DDT derivatives; and hexachlorocyclopentadiene pesticides. Many of these compounds display spectra which show marked isomeric dependence. Some of the effect is due to dependence on vapor pressure, especially the presence of dimers at lower temperatures, and some to the dissociative attachment process being bond-dependent. To date most of the results are empirical,

A. The Reversal Electron Attachment Detector

The fact that an electron attachment cross section actually tends towards infinity at energies approaching zero can be ample fuel for the imagination, Conventional ion sources and glow discharges usually have mean electron energies well above this limit, and hence can provide only a small fraction of the available EEDF to attach to species such as SF_6, $CFCl_3$, CCl_4, *etc.* To utilize these large cross sections the *READ* concept was developed. In effect, at these low energies one is attempting to provide a "match" between the peak of the electron-energy distribution function and the energy at the cross-section peak of the target resonance state.

One practical use of this device is that explosives molecules also have the interesting property of attaching zero-energy electrons! The *READ* can be used to detect some of the explosives-of-choice, such as RDX, PETN and TNT, Shown in Fig. 24 is the zero-energy attachment spectrum of the explosive PETN (Boumsellek *et al* 1991 b). Controlled substances (heroin, cocaine, marijuana, *etc*) also attach at energies which are hyperthermal (hence inaccessible to the conventional *ECD),* but which have been detected in *READ* measurements. Work is currently underway to measure the sensitivity of *READ* to detection of these species using an atmospheric-interface device, such as the molecular jet separator, Trace detection of molecules has also been demonstrated through higher energy resonances, such as the 6,2 eV resonance in O_2 (Man *et a/* 1993).

B. Glow-Discharge Ionization

Techniques have been developed based on the formation of a glow-discharge plasma containing the analyte species in ambient air, The plasma is formed at pressures of 0.2-1.0 torr in a differentially-pumped chamber, and ions are extracted through a small aperture through a second differentially-pumped focusing system into a quadruple, ion trap, *etc* mass spectrometer (McLuckey *et a/ 1988,* 1989), Operation with both positive and negative ions is possible through appropriate choice of optics polarity. Detection sensitivities of 1-2 parts-per-trillion have been reported for 2,4,6-trinitrotoluene (McLuckey *eta/ 1988),* Detection sensitivity for negative ions has been measured as a function of the skimmer-entrance aperture distance, cathode (entrance plate) voltage, and total plasma pressure (Chambers *eta/ 1993).*

Variations of this technique using Ar support gas and radiofrequency, rather than direct-current discharges, have been demonstrated (Watson et *a/ 1993,*

McLuckey eta/1992). These have seen application to the measurements of mass spectra of species present on solid conductors (brass and steel standards) and nonconductors (glasses).

c. Droplet Ionization

The so-called electrospray and ion-spray techniques have been developed as interfaces for capillary liquid chromatography-mass spectrometry (Fenn *et a/ 1990,* Blades *et a/* 1991, Ikonomou *et a/ 1991,* Kebarle and Tang 1993). The techniques involve the formation of micron-sized charged particle droplets through electrophoretic charging of the droplets. In positive-ion operation the positively-charged droplets drift towards a cathode aperture (capillary inlet), during which time they "evaporate" to form gas-phase species which are analyzed with a conventional mass spectrometer system. In the negative-ion mode an additional sheath gas is combined with the sheath liquid-analyte mixture. The purpose of the gas is presumed to be to scavenge electrons and suppress corona-discharge formation (Smith *et a/ 1988),* The various mechanisms involved in the electrophoretic charging, droplet evaporation and discharge suppression appear to be tentative, and worthy of further study,

12, Radiocarbon Dating

The comparison of the amount of radiocarbon (^{14}C) in a sample with that in contemporary living matter permits an estimate of the absolute age of the sample (Libby *et a/ 1955).*

Radiocarbon ^{14}C is a radioactive isotope with a half-life of 5730 ± 40 years. The naturally-occurring isotopes of carbon are 12C and ^{13}C and are not radioactive, ^{14}C decays by emission of a beta-particle (0.156 MeV) to nitrogen ^{14}N.

The method depends on the relatively constant formation rate of ^{14}C from ^{14}N by neutron bombardment in the upper atmosphere,

$$^{14}N + n \cdot {}^{14}C + p .$$

The ^{14}C atoms react with oxygen molecules to form ^{14}C carbon dioxide, which becomes dispersed throughout the atmosphere and hydrosphere, and eventually the biosphere. These are reservoirs for the I*C, ^{13}C and ^{14}C isotopes in the percentage ratios 98,9:1.1:10-10 (Goffer 1980),

Whenever living matter dies and no longer exchanges carbon dioxide with the reservoirs the input of ^{14}C ceases and the concentration of radiocarbon will decrease with time, The determination of the amount of radiocarbon by means of its radioactivity is quite difficult, The radioactive carbon in living matter averages only 13.5 disintegrations/minute/gm of contained carbon, Careful shielding and long counting times are required to obtain good statistics on small samples of older carbon. A large improvement can be obtained by using a particle accelerator to directly count the number of ^{14}C atoms relative to the number of ^{12}C or ^{13}C atoms, However, the probable presence of ^{14}N atoms (differing by one part in 10^5 in mass from ^{14}C) in any sample means that this measurement is not straightforward if positive-ion mass spectroscopy is used,

One can use negative-ion mass spectroscopy to determine the ^{14}C more accurately. One takes advantage of the fact that nitrogen does not form a long-lived negative ion, Negative-ion accelerator mass spectroscopy, while quite elaborate and expensive, has reduced the data acquisition time to minutes from the days required if measuring the beta decay. The negative ions, produced using a Cs sputter-ion source, are extracted at energies of 30-50 kV, mass-analyzed and accelerated to energies of tens of MeV and further analyzed, For ^{14}C measurements the isotopic ratios' $^{14}C/^{12}C$ and $^{13}C/^{12}C$ must be measured to a precision of 1 % relative to a known standard. In order to handle the large dynamic range from the abundant stable isotopes to the rare unstable isotope, special pulsed-injection methods or accurate attenuation must be used to avoid space-charge effects (Bonani *et al 1986).* Ion sources and accelerator configurations used for ^{14}C dating have been described by Middleton *et al (1* 989) and by Bronk and Hedges (1 987), These configurations typically produce 20 microampere of l*C negative ions with a high-intensity sputter source using CO_2 gas as the dating sample,

13. Isotope Dating

Other isotope dating analyses that rely on negative ion accelerator mass spectroscopy include ^{26}Al, ^{10}Be and ^{36}Cl. ^{26}Al is detected relatively easily since the only isobar, ^{26}Mg, does not form stable negative ions. However the efficiency of making negative ions of aluminum (usually from $A1_20_3$ mixed with silver) is low (Bonani *et a/* 1986), and there may be opportunities for significant improvement in negative-ion sources using aluminum or aluminum compounds. Be does not form a stable negative ion (Bonani *et a/ 1986)* and the analysis of ^{10}Be therefore uses BeO mixed with copper powder to obtain a fast negative molecular ion beam of BeO. This

beam is then stripped and dissociated by passing it through a thin (1 0 micrograms/cm^2) carbon foil, Boron oxide also forms negative ions so it is necessary to remove the isobar ^{10}B with an absorber cell (Bonani *et a/ 1986).* The detection of ^{36}Cl from AgCl samples is made difficult by contamination from sulfur which also readily forms negative ions, The ^{36}S background has been suppressed by a factor 103 through measurement of energy losses of the isobars at 48 MeV in a four-stage counter telescope (Bonani *et a/ 1986).*

14. Role of H⁻ in the Opacity of the Solar Atmosphere

The first definitive study of radiative transfer in stellar atmospheres was that by Chandrasekhar (1 960), He emphasized the importance and usefulness of local thermodynamic equilibrium in the calculation of radiative transfer in the solar atmosphere, as opposed to a microscopic analysis of each individual radiative, collisional and absorption process. Chandrasekhar cites H⁻ absorption as a process that previous microscopic models probably would have neglected.

Although the neutral hydrogen atom is by far the most abundant atom, for late-type stars (Lotz 1970), continuous absorption by ground state atomic hydrogen only onsets at λ = 912 Å. Absorption of visible radiation does occur from excited states of hydrogen; however, as these levels are greater than 10 eV above the ground state, then for electron temperatures of approximately 6000 K or so, typical of our sun, the populations of the higher principal quantum number states are small. For some time it was considered that the main causes of the continuous absorption in stellar atmospheres were the more common metallic elements (ionization potential, eV): Na (5.12), Mg *(7.61),* Ca *(6.09),* Fe (7.87), Si (8.15) and hydrogen beyond its series limit. However, this interpretation led to serious discrepancies, especially in the wavelength dependence of the solar emission. A resolution was given by Wildt (193$Ja, 1939b, 1941) who recognized the importance of H" in causing continuous absorption, The hydrogen atom concentration is high and free electrons are provided by ionization of the above-listed low ionization potential elements, The solar atmosphere has been estimated to have of the order of one metal atom for 104 hydrogen atoms, The electron affinity (EA) of hydrogen is 0.75 eV and, therefore, photoionization of H⁻ is a mechanism for continuous absorption at wavelengths shorter than 16,550 Å. The photoionization cross section was considered by Wildt and later by Massey and Bates (1940). These derivations gave the general trend, but not good agreement with observation. A later study by Chandrasekhar and Breen (1946) provided values for the bound-free absorption cross section as a function of

temperature (4200 -7200 K). There is also a contribution by free-free absorption that becomes important in the infrared and is the main absorption process at wavelengths longer than 1.4 microns at 6300 K. Subsequent calculations using Hylleraas treatments (Schwartz 1961), variational and close-coupling treatments (Geltman 1962, Stewart 1978) gave good agreement with beam experiments (Branscomb and Smith 1955).

An estimate of the absorption by H^- per neutral hydrogen atom can be made using the Saha-Lindemann equation applied to the reaction (AHer 1965)

$$H + e \leftrightarrow H^- .$$

In general, the Saha equation is

$$\frac{n_{r+1}}{n_r} P_e = \frac{(2\pi m)^{3/2}}{h^3} (kT)^{5/2} 2 \frac{Z_{r+1}(T)}{Z_r(T)} \exp -\left(\frac{I_r}{kT}\right). \qquad (45)$$

Here T is the equilibrium temperature, n_r is the density of atoms ionized r times, I_r is the ionization energy from state r to $r+1$, P_e is the electron pressure, and $Z_r(T)$ is the partition function for the ion Z_r.

For the photodetachment of H-,

$$\frac{n_o}{n} P_e = \frac{(2\pi m)^{3/2}}{h^3} (kT)^{5/2} \frac{2Z_o(T)}{Z_-(T)} \exp -\left(\frac{EA}{kT}\right)$$

or

$$\log\left(\frac{n_-}{n_o} P_e\right) = 0.48 - 2{,}5 \log T - \log \left[\frac{2Z_o(T)}{Z_-(T)}\right] \cdot \frac{5040(EA)}{T}$$

$$= -0.12 + \frac{5040(EA)}{T} - 2{,}5 \log T \qquad (46)$$

if P_e is measured in dynes cm^{-2}. For H", EA = 0.75 eV and setting θ = 5040/T,

$$\log\left(\frac{n_-}{n_{0_1}}\right) = 0.75\,\theta - ;\log o + \log P_e - 9.376 = \log \Phi(\theta)\,. \qquad (47)$$

The $\log \Phi(\theta)$ is a slowly varying function of θ (Goldberg and Pierce 1959). The absorption of the hydrogen plasma is shown in Fig, 25, The main contribution in the visible spectrum arises from bound-free absorption of the negative ion. The maximum in the cross section of 4 x 10"^{17} cm^2 occurs about 0.85 microns, The theoretical absorption coefficient of H^- per hydrogen atom is also illustrated for a chosen LTE condition of 6300 K (after Chandrasekhar 1960). It is noted that under solar atmosphere conditions, the fractional negative ion concentrations are very low compared to those found in nonequilibrium low pressure discharges,

In stars whose composition is much different from that of the sun, it has been suggested (Branscomb and Pagel 1958) that other negative ions may be of importance, especially in carbon stars. It appears that C" (electron affinity 3.1 eV) would contribute to absorption in the latter case, that OH^- (1 .78) may be important in late M and S stars, and CN^- (3.1) may contribute more absorption than C_3 in late N type stars. Branscomb and Pagel remarked that the laboratory photodetachment and absorption measurements of molecular negative ions are usually for the ground vibrational state; whereas in a stellar plasma, higher vibrational levels also are populated. Therefore, the apparent absorption threshold would be shifted to longer wavelengths if the vibrational energy spacings of the negative ion are larger than those of the neutral molecule, The negative ions 0^- and O_2^- were evaluated as unimportant in any stars, Black (1 988) has reviewed the potential roles of various negative ions in interstellar space. While many negative ions could be important intermediates in the gas phase chemistry (Dalgarno and McCray 1973), confirmation will be difficult because of low concentrations and meager knowledge of their spectra, Black suggests that the reaction

$$H^- + O_2 \rightarrow HO_2 + e$$

may be the only important source of HO_2 and then if the O_2 concentration can be gauged, HO_2 observations would measure H^-, and possibly its contribution to H_2 formation in the absence of grains and surface recombination.

15. Negative Ions in the Earth's Atmosphere

The oxygen negative ions are important in aeronomy. There are detailed reviews on the topic (Wayne 1992, Swider 1985). The ionosphere has several characteristic regions whose electron densities typically are 10^6 cm^{-3}, F-region or above 150 km; 106 cm^{-3}, E-region, 100- 150 km, and 10^3 for the D-region around 70 km (all daytime values), The nighttime values for the E and F regions are about an order of magnitude lower, and almost zero for the D region. The radiative formation and destruction of the oxygen negative ions must be included in the electron continuity equation for the earth's upper atmosphere.

Negative atomic oxygen ions are formed above 90 km primarily by radiative attachment. Below 90 km, formation of O_2^- by three body electron attachment reactions occurs, In sunlight the electrons are easily photodetached [$EA(O^-) = 1.3$ eV), $EA(O_2^-) = 0.44$ eV].

The oxygen ions are not all that stable and also experience collisional detachment with many species including O atoms and the O_2 1_A state, which have especially fast rate constants,

$$O^- + O \rightarrow O_2 + e$$
$$k = 1.9 \times 10^{10}\ cm^3\ sec^{-1}$$

$$O_2^- + O \rightarrow O_3 + e$$
$$k = 3.3 \times 10^{10}\ cm^3 sec^{-1}$$

$$O^- + O_2(^1\Delta) \rightarrow O_3 + e$$
$$k = 3 \times 10^{10}\ cm^3 sec^{-1}$$

$$O_2^- + O_2(^1\Delta) \rightarrow O_2 + O_2 + e.$$
$$k = 2 \times 10^{10}\ cm^3 sec^{-1}$$

The terminal negative ions in the atmosphere are therefore species such as the more stable CO_3^-, HCO_3^-, NO_3^- molecules, and the water-vapor clusters $C0_3$" $(H_2O)_n$ and NO_3^- $\bullet(H_2O)_n$. The diurnal variation in the electron density is mainly by indirect processes: *via* photolysis of O_2 and 0_3 and subsequent collisional detachment of the oxygen negative ions by O atoms. Around 8 km the Air Force Geophysics Laboratory has

measured a relatively dense layer of negative ions with masses greater than M/e = 134, These may be mainly hydrated ions of HCO_3^-.

Many negative-ion photodetachment cross sections have been measured accurately by Leopold eta/(1 985). The radiative attachment cross sections then can be derived from the photodetachrnent cross sections by detailed balancing,

$$Q_{det} = \left(\frac{mcv:v}{hv\ ,}\right)^2 \frac{g_o}{g_-} Q_{att} .$$

Radiative attachment is constrained by the angular momentum state of the electron experiencing attachment. The atomic cross section varies linearly with electron velocity near threshold for attachment into a bounds state and inversely with velocity for a *p* state, Knowledge of the atomic and molecular radiative cross sections of negative ions, in addition to their binding energies, is needed to describe the emission continua of many sources including stars, laboratory plasmas and relaxing flows,

16. Injection of Electronegative Gases into the F-Region

Bernhardt *et a/ (1* 986) have used trace amount of SF_6 in ionosphere modification experiments to probe the F-region properties and kinetics, In this example, "trace" means 18 kilograms (7.4x 10^{25} molecules) that were released from a Nike-Tomahawk rocket at 350 km into an ambient electron concentration of 105 cm^{-3}. This produces ionospheric disturbances that may be observed in the infrared and the visible spectrum, and can also be probed with radio waves. The short time response is to produce a three component plasma because of electron attachment to SF_6 mainly forming SF_5^- (EA of parent = 3.7 eV), SF_6^- (0.8 eV) and F^- (3.4 eV), with branching ratios depending on the electron and gas temperatures, At room temperature the cross section for F^- formation exceeds that for SF_5^- only if the electron energy is above 2.5 eV. Experiments by Chen and Chantry (1 971) showed that for electron energies between O and 1 eV, the molecular negative ions are dominant and F^- was undetectable until the gas temperature reached 600 K and then increased rapidly, At gas temperatures of 2000 to 3000 K the dominant ion is F-. Thus the gas temperature fluctuations in the thermosphere result in marked changes in the negative ion and in the attachment rate. The long time response is to produce a plasma depletion volume because of a significant reduction in the ion and electron densities by the increased ion-ion recombination rates. Bernhardt provides a comprehensive table of the ionospheric reactions stimulated by the release of SF_6. The most important are:

$$SF_6^- + O + \text{''} \quad SF_6 + O^{**} + 12.81\ eV \qquad (48)$$

$$SF_5^- + O^+ \rightarrow SF_5 + O^* + 9.91\ eV \qquad (49)$$

$$F^- + O^+ \rightarrow F + O + 10.2 eV \qquad (50)$$

all with fast rate constants about 5 x 10-B cm^3 see-l,

The point is that the excited oxygen O(^{5}P) atoms, mainly from reaction (48), produce 777,4 nm emission which was observable from a flying laboratory at 9144 km and from a ground station, Although the concentration [SF_6^-] is typically only 0,1 [$SF_6$1 it is mainly responsible for the 777.4 nm airglow radiation from oxygen. The SF_6 acts as a gas catalyst promoting the recombination of 0^+ and electrons, The *net* effect of attachment and reaction (48) is

$$SF_6 + e + O^+ \rightarrow SF_6 + O^{**} .$$

Weak emission at 6300 nm from O(^{1} D) atoms was also observed, although it had been anticipated to exhibit the major enhancement. Analysis of the electronegative gas perturbations thus provides microscopic information about the F-region over large scale lengths, (The airglow cloud is estimated as 25 to 30 km in radius 1 minute after release.) Other electronegative compounds with temperature-dependent attachment rates that have been considered for creating negative ion clouds include CF_3Br and $Ni(CO)_4$.

It has also been shown (Bernhardt 1984) that the negative ion plasma will be marginally unstable to the gradient drift instability. Earlier theoretical studies by Smith (1965) indicated a strong influence of negative ions on whistler waves. At low collision frequencies, it was predicted that the dispersion of the waves would be modified by negative ions, The effects on the group refractive index would be most dramatic as the wave frequency approached the ion cyclotron frequency, The negative ion and the whistler wave are in resonance at the gyrofrequency which is not the case for the positive ion. Therefore relatively small line integrals of negative ions over the propagation path have significant effects on the whistler waves and Smith cites experimental reports to suggest that they have been observed.

ACKNOWLEDGEMENTS

We thank Dr S Boumsellek for his comments on aspects of this report, This work was carried out in part at the Jet Propulsion Laboratory, California Institute of Technology. AC "was supported by the Federal Aviation Administration through agreement with the National Aeronautics and Space Administration. JMW acknowledges support from the Air Force Office of Scientific Research and the National Science Foundation,

REFERENCES

Abouaf R, Teillet-Billy D, Azria Rand Girard P *1985 J Phys B: At Mol Phys 78 3017*

Adams N G 1994 *Int J Mass Spectry Ion Process 1321*

Adams N G, Herd C R, Geoghegan M, Smith D, Canosa A, Gomet J C, Rowe B R, Queffelec J L and Morlais M 1991 *J Chem Phys 944852*

Adams N G, Smith D and Herd C R 1988 *In? J Mass Spectry Ion Process 84243*

Adams N G, Smith D, Viggiano A A, Paulson J F and Henchman M J 1986 *J Chem Phys 846728*

Adams N G, Church M J and Smith D 1975 *J Phys D: Appl Phys 81409*

Adams N G and Smith D 1985 *Astrophys J 294 L63*

Adams N G, Smith D and Alge E 1984 *J Chem Phys 87 1778*

Adams N G, Smith D, Alge E, and Burden J 1985 *Chem Phys Lett 176460*

Ajello J M and Chutjian A 1979 *J Chem Phys 77 1079*

Ajello J M, Chutjian A and Winchell R 1980 *J Electron Spectrosc Rel Phenom 78197*

Alajajian S H, Bernius M T and Chutjian A 1988 *J Phys B: At Mol Opt Phys 27 4021*

Alajajian S H and Chutjian A 1986 *J Phys B: At Mol Phys 792393*

Alajajian S H and Chutjian A 1987 *J Phys B: At Mol Phys 202117*

Alajajian S H and Chutjian A 1988 *Phys Rev A 373680*

Alge E, Adams N G and Smith D 1983 *J Phys B: At Mol Phys 761433*

Alge E, Adams N G and Smith D 1984 *J Phys B: At Mol Phys 773827*

Aller L 1965 *Astrophysics* (Ronald: New York)

Arnold D W, Bradforth S E, Kitsopoulos T N and Neumark D M 1991 *J Chem Phys 958753*

Aschwanden T 1985 *Die Ermittlung Ph ysikalischer Entladungsparame ter in Isolierengasen und Isoliernegemischen mit Einer Verbesserten Swarm Methode* (PhD Thesis, Eidgenossischen Technischen Hoschschule, Zurich)

Atems D E and Wadehra J M 1990 *Phys Rev A 425201*

Atems D E and Wadehra J M 1992 *Chem Phys Lett 797525*

Axford S D T and Hayhurst A N 1990 *23rd Symp Combustion* (Pittsburgh: Combustion Inst) p. 363

Azria R 1984 *Comm At Mol Phys 751*

Azria R, LeCoat Y, Simon D and Tronc M 1980 *J Phys B: A? Mol Phys 731909*

Bacal M and Skinner D A 1990 *Comm At Molec Phys 23283*

Baranov V I and Petrosov V A 1987 Sov *Phys Tech Phys 321037*

Bardsley J N 1968 *J Phys B: Atom Molec Phys 1349*
Bardsley J N and Read F H 1968 *Chem Phys Lett 2333*
Bardsley J N and Wadehra J M 1983 *J Chem Phys 787227*
Bardsley J N, Herzenberg A and Mandl F 1966 *Proc Phys Soc London 89305*
Barnard J A and Bradley J N 1985 *Flame and Combustion* (London: Chapman and Hall) p 171
Barreto E 1979 *Inst Phys Conf No 48135*
Beiting E J, Hildebrandt G F, Kellert F G, Foltz G W, Smith K A, Dunning F B and Stebbings R F 1979 *J Chem Phys 703551*
Bell D E 1993 *Diffusion in Electronegative Gases in Magnetic Fields* (AF Inst Techn Report AFIT/DS/ENP/93-08, Wright-Patterson AFB Ohio),
Bellis F E and O'Neal C O 1957 *Sixth Symp on Combustion (New* York: Reinhold) p *806*
Berlemont P, Skinner D A and Bacal M 1993 Rev *Sci Instr 642721*
Bernhardt P A 1984 *J Geophys Res 893929*
Bernhardt P A, Weber E J, Moore J G, Baumgardner J and Mendillo M 1986 *J Geophys Res 918937*
Bernius M T and Chutjian A 1990 *Aria/ Chem 621345*
Bernius M T and Chutjian A 1989 *J Appl Phys 662783*
Bethe H A 1935 *Phys Rev* 47747
Black J H 1988 *Adv Atom Molec Phys 25477*
Blades A T, Ikonomou M G and Kebarle P 1991 *Aria/ Chem 632109*
Boesten L 1988 *Rev Sci Instr 59233*
Bonani G, Hofman H-J, Morenzoni E, Nessi M, Suter M and Wolfi W 1986 *Radiocarbon 28246*
Boumsellek S, Alajajian S H and Chutjian A 1992 *JAm Soc Mass Spectrom 3243*
Boumsellek S and Chutjian A 1992 *Aria/ Chem 642096*
Boumsellek S and Chutjian A 1993 *Rev Sci Instr 641135*
Branscomb L M and Pagel B E J 1958 *Mon Not Roy Astron Soc 778258*
Branscomb L M and Smith S J 1955 *Phys Rev 981028*
Brewer G R 1967 *Focusing of Charged Particles* (cd: A. Septier New York: Academic) Vol II, Ch. *3.2*
Bronk C R and Hedges R E M 1987 *Nucl Instr Meth 62945*
Buckrnan S J, Brunger M J, Newman D S, Snitchler G, Alston S, Norcross D W, Morrison M A, Saha B C, Danby G and Trail W K 1991 *Phys Rev Lett 653253*
Bunge C F, Galan M and Jauregui E 1982 *Nucl Instr Meth 202299*
Carman H S Jr, Klots C E and Compton R N 1993 *J Chem Phys 991734*
Cavalleri G 1969 *Phys Rev 77986*

Chambers D M, McLuckey S A and Glish G L 1993 *Aria/ Chem 65778*
Chandrasekhar S 1960 *Radiative Transfer* (Dover: New York)
Chandrasekhar S and Breen F H 1946 *Ap J 104430*
Chang E S and Wong S-F 1977 *Phys Rev Lett 381327*
Chang E S 1977a *Phys Rev A 16* 1841
Chang E S 1977b *Phys Rev A 761850*
Chang E S 1983 *Phys Rev A 27709*
Chantry P J 1982 in *Applied Atomic Collision Physics* (eds H S W Massey, E W McDaniel and B Bederson New York: Academic) V 3, p 56
Chapman D A, Balasubramanian K and Lin S H 1988 *Phys Rev A 386098*
Chen C L and Chantry P C 1971 *Bull Am Phys Soc 77406*
Christophorou L G 1971 *Atomic and Molecular Radiation Physics (New* York: Wiley-Interscience)
Christophorou L G, McCorkle D L and Anderson V E 1971 *J Phys B: At Mol Phys 41163*
Christophorou L G, McCorkle D L and Christodoulides A A 1984 *Electron-Molecule /interactions and Their Applications* (ed L G Christophorou New York: Academic) Vol 1, Ch 6
Christophorou L G 1978 Proc 13th Int Conf Phenom Ionized Gases (Berlin: VEB Export-Import)
Christophorou L G, Hunter S R, Pinnaduwage L A, Carter J G, Christodoulides A A and Spyrou S M 1987 *Phys Rev Lett* 581316
Christophorou L G and Pinnaduwage L A 1990 *IEEE Trans Electr Insul 2555*
Christophorou L G, Sauers 1, James D R, Rodrigo H, Pace M O, Carter J G and Hunter S R 1984 *IEEE Trans Electrical Insul EI- 19550*
Chutjian A *1976 J Chem Phys 614279*
Chutjian A 1981 *Phys Rev Lett* 46 1511; 1982 *Phys Rev Lett 48289* (erratum)
Chutjian A 1979 *Rev Sci Instr 50347*
Chutjian A 1982 *J Phys Chem 863518*
Chutjian A and Ajello J M 1977 *J Chem Phys 664544*
Chutjian A and Ajello J M 1980 *Chem Phys Lett 72504*
Chutjian A and Alajajian S H 1985a *Phys Rev A 372885*
Chutjian A and Alajajian S H 1987a *Phys Rev A 354512*
Chutjian A and Alajajian S H 1987b *J Phys B: At Mol Phys 20839*
Chutjian A and Alajajian S H 1985b *J Phys B: At Mol Phys 784159*
Chutjian A, Alajajian S H and Man K-F 1990 *Phys Rev A 47 1311*
Chutjian A, Alajajian S H, Ajello J M and Orient O J 1984 *J Phys B: At Mol Phys 77 L745; 1985 J Phys B: At Mot Phys 183025* (erratum)

Cooke C M and Cookson A H 1978 *IEEE Trans Electr Insul EI-13* 239
Crawford O H and Koch B J D 1974 *J Chem Phys 604512*
Creiz E C 1961 *J Res Nat Bur Stand 65A 389*
Crompton R W and Haddad G N 1983 *Australian J Phys 3615*
Cvejanović D, Andrić L and Hall R I 1993 *J Phys B: At Mol Phys 262899*
Dalgarno A and McCray R A *1973 Ap J 18195*
Darrach M, Boumsellek S and Chutjian A 1994 (work in progress)
Datskos P G, Christophorou L G and Carter J G 1993a *J Chem Phys 987875*
Datskos P G, Christophorou L G and Carter J G 1993b *J Chem Phys 998607*
Dernkov Yu N 1964 Sov *Phys - JETP 19762*
Demkov Yu N 1965 *Phys Lett15* 235
Dettmer J W and Garscadden A 1981 Gaseous Electr Conf (Houston) paper MB5, Abstracts p 27; see also J W Dettmer *Discharge Processes in the Oxygen Plasma* (AFWAL Report TR80-212 Wright-Patterson AFB Ohio)
de Urquijo-Carmona J, Alvarez I and Cisneros C 1986 *J Phys D: App/ Phys 79 L207*
Domcke W 1991 *Phys Rep 20897*
Douglas-Hamilton D H and Mani S A 1973 *App/ Phys Lett 23508*
Douglas-Hamilton D H and Mani S A 1974 *J App/ Phys 454406*
Drukarev G and Pozdneev S A 1980 *J Phys B: At Mol Phys* 732611
Dunning F B 1985 *Am J Phys 53944*
Dunning F B 1987 *J Phys Chem 972244*
Edgely P D and von Engel A 1980 *Proc R Soc (London) A370 375*
Elets 1 S and Kazanskii A K 1982 *Sov Phys JETP 55258*
Elets 1 S and Kazanskii A K 1985 Sov *J Chem Phys 21439*
Emeleus K G and Sayers J 1938 *Proc Roy Irish A cad 2487*
Emeleus and Woolsey 1970 *Discharges in Electronegative Gases (New* York: Barnes and Noble)
Fabrikant I I 1990 *Comments At Mol Phys 2437*
Fabrikant I 1, Kalin S A and Kazansky A K 1992 *J Phys B: At Mo/ Phys 252885*
Fano U 1961 *Phys Rev 7241866*
Fehsenfeld F C 1970 *J Chem Phys 532000*
Feldman H 1990 *J Chem Soc Faraday Trans 862469*
Fenn J B, Mann M, Meng C K and Wong S F 1990 *Mass Spectrom Rev 937*
Ferreiro C M, Gousset G and Touzeau M 1988 *J Phys D: App/ Phys 27 1403*
Foltz G W, Latimer C J, Hilderbrandt G F, Kellert F G, Smith K A, West W P, Dunning F B and Stebbings R F 1977 *J Chem Phys 671352*
Frey M T, Hill S B, Ling X, Smith K A, Dunning F B and Fabrikant I I 1994 *Phys Rev A 50* 3124

Garscadden A and Nagpal R 1995 *ESCAMPIG* (The Netherlands, in press)
Gauyacq J P 1985 *J Phys B: Atom Molec Phys 181859*
Gauyacq J P 1987 *Dynamic of Negative Ions* (World Scientific, Singapore)
Gauyacq J P and Herzenberg A 1984 *J Phys B: At Mol Phys 77 7755*
Geltman S 1962 *Ap J 736935*
Gibson D K, Crompton R W and Cavalleri G 1973 *J Phys B: At Mol Phys* 61118
Godyak V A 1991 *Proc XXth Int Conf Phys Ionized Gases* (Piss, Italy)
Goffer *Z 1980 Archaeological Chemistry (New* York: Wiley Interscience)
Goldberg L and Pierce A K 1959 *Handbuch der Physik* Vol 52 (ed S Flugge, Springer-Verlag: Berlin)
Goretskii V P, Soloshenko I A and Tarasenko A F 1989 Sov *Phys Tech Phys 341360*
Govers T R, Guyon P-M, Baer T, Cole K, Frohlich H and Lavollee M 1984 *J Chem Phys 87* 373
Gresteau F, Hall R 1, Huetz A, Vichon D and Mazeau J 1979 *J Phys B: At Mol Phys 122925*
Guntherschulze A 1927 *Zeit f Phys 42763*
Haas R A 1973 *Phys Rev A 81017*
Hadjiantoniou A, Christophorou L G and Carter J G 1973 *J Chem Soc Far Trans // 691691*
Hall R 1, Čadež 1, Schermann C and Tronc M 1977 *Phys Rev A 75599*
Hall R 1, Čadež 1, Landau M, Pichou F and Schermann C 1988 *Rev Sci Instr 60 337*
Hansen D, Jungblut H and Schmidt W F 1983 *J Phys D: Appl Phys 761623*
Hatano, Y Kimizuka Y-1 and Shimamori H 1982 *Radiat Phys Chem 79255*
Hatfield J V, York T A, Comer J and Hicks P J 1989 *IEEE J Solid State Circuits 24704*
Hayashi M 1981 "Recommended Values of Transport Cross Sections for Elastic Collision and Total Collision Cross Section for Electrons in Atomic and Molecular Gases" (*Inst Plasma Phys Rept IPPJ-AM-19,* Nagoya Univ, Jpn)
Hazi A U, Orel A E and Rescigno T N 1981 *Phys Rev Lett 46918*
Hegerberg R and Crompton R W 1980 *Australian J Phys 33989*
Herd C R, Adams N G and Smith D A 1990 *Astrophys J 349388*
Hettich R L, Compton R N and Ritchie R H 1991 *Phys Rev Lett 671242*
Hickman A P, Olson R E and Pascale J 1983 "Theoretical Approaches to Low-Energy Collisions of Rydberg Atoms with Atoms and Ions", in *Rydberg States of Atoms and Molecules* (eds R F Stebbings and F B Dunning, New York: Cambridge)
Hildebrandt G F, Kellert F G, Dunning F B, Smith K A and Stebbings R F 1978

J Chem Phys 681349

Hilmert H and Schmidt W F 1991 *J Phys D: Appl Phys 24915*

Holmes A J T, Dammertz G and Green T S 1985 *Rev Sci Instr 591697*

Hsia J 1977 *App/ Phys Let? 30101*

Hunter S R and Christophorou L G 1984 *J Chem Phys 806150*

Huxley L G H and Crompton R W 1974 *The Diffusion and Drift of Electrons in Gases (New* York: Wiley Interscience)

Ikonomou M G, Blades A T and Kebarle P 1991 *Aria/ Chem 631989*

Jaffke T, Hashemi R, Christophorou L G, Illenberger E and Baumgärtl H 1993 *Chem Phys Let? 20321*

Jung K, Antoni Th, Mueller R, Kochem K-H and Ehrhardt H 1982 *J Phys B: At Mol Phys 153535*

Kalarnarides A, Goeller L N, Smith K A, Dunning F B, Kimura M and Lane N F 1987 *Phys Rev A 363108*

Kalamarides A, Walter C W, Lindsay, B G, Smith, K A and Dunning, F B 1989 *J Chem Phys 914411*

Kalarnarides A, Marawar R W, Ling X, Walter C W, Lindsay B G, Smith K A and Dunning, F B 1990a *J Chem Phys 921672*

Kalamarides A, Marawar R W, Durham M A, Lindsay B G, Smith K A and Dunning F B 1990b *J Chem Phys 934043*

Kalin S A and Kazansky A K 1990 *J Phys B: At Mo/Phys234377*

Kazanskii A K and Fabrikant I I 1984 Sov *Phys Usp 27607*

Kazansky A K and Yelets I S 1984 *J Phys B: At Mol Phys 174767*

Kebarle P and Tang L 1993 *Aria/ Chem 65 972A*

Khvorostovskaya L E and Yankovsky V A 1991 *Contrib Plasma Phys 3178*

King G C, Zubek M, Rutter P M and Read F H 1987 *J Phys E: Sci Instr 20440*

King G C unpublished results (1991)

Klar D, Ruf M-W and Hotop H 1992a *Chem Phys Let? 789448*

Klar D, Ruf M-W and Hotop H 1992b *Australian J Phys 45263*

Klar D, Ruf M-W and Hotop H 1994 *Meas Sci Technol* (in press)

Klots C E 1976 *Chem Phys Lett 3861*

Kondoq T 1987 *Microclusters* (eds S Sugano, Y Nishana and S Ohnishi, New York: Springer Verlag) p 167

Krishnakumar E and Srivastava S K 1990 *Phys Rev A 412445*

Kurepa M V, Čadež I M and Pejčev V M 1974 *Fizika 6185*

Langevin P 1905 *Ann Chim Phys 5245*

LeCoat Y, Azria R and Tronc M 1985 *J Phys B: At Mol Phys 78809*

LeCoat Y, Guillotin J P and Bouby L 1991 *J Phys B: At Mol Phys 243285*

Lee T G 1963 *J Phys Chem 67360*

Leopold D G, Murray K K, Miller A E S and Lineberger W C 1985 *J Chem Phys 83 4849*

Lewis B and von Elbe G 1961 *Combustion, Flames and Explosions in Gases* (New York: Academic)

Libby, W 1955 *Radiocarbon Dating* (Chicago: Univ. Chicago)

Ling X, Durham M A, Kalamarides A, Marawar R W, Lindsay B G, Smith K A and Dunning F B 1990 *J Chem Phys 938669*

Ling X, Lindsay B G, Smith K A, and Dunning F B 1992 *Phys Rev A* 45242

Ling X, Smith K A and Dunning F B 1993a *Phys Rev A 47* RI

Ling X, Frey M T, Smith K A and Dunning F B 1993b *Phys Rev A 481252*

Loffer S and Homann K H 1990 *23rd Symp Combustion* (Pittsburgh: Combustion Inst) p *355*

Long W H Jr, Bailey W F, Pond D R and Garscadden A 1976 *IEEE Plasma Sciences Conf Record* (Knoxville TN); data illustrated in W L Nighan, *Principles of Laser Plasmas* (ed G Bekefi New York: Wiley) Ch 7

Man K-F, Boumsellek S and Chutjian A 1993 *6th Int. Symp. Exp. Methods for Microgravity Materials Science (1 23rd* TMS Annual Meeting, San Francisco CA)

Marmet P and Kerwin L 1960 *Can J Phys 38787*

Mason E A and McDaniel E W 1973 *Transport Properties of Ions in Gases (New* York: Wiley -Interscience)

Massey H S W 1976 *Negative Ions* (Cambridge University Press: Cambridge)

Massey H S W 1980 *Endeavour 478*

Massey H S W and Bates D R 1940 *Ap J* 91202

Matsuzawa M 1983 "Theoretical Studies of Collisions of Rydberg Atoms with Molecules" in *Rydberg States of Atoms and Molecules* (eds R F Stebbings and F B Dunning, New York: Cambridge)

Mayhew C A and Smith D 1990 *Int J Mass Spectry Ion Process 100737*

McCorkle D L, Christophorou L G, Christodoulides A A and Pichiarella L 1986 *J Chem Phys 851966*

McCorkle D L, Christodoulides A A, Christophorou L G and Szamrej I 1980 *J Chem Phys 724049*

McGeechan J P, O'Neill B C, Prasad A N and Craggs J D 1975 *J Phys D: Appl Phys 8153*

McLuckey S A, Glish G L, Asano K G and Grant B C 1988 *Anal Chem 602220*

McLuckey S A, Glish G L and Asano K G 1989 *Anal Chim Acts 22525*

McLuckey S A, Glish G L, Duckworth D C and Marcus R K 1992 *Anal Chem 641606*

Middleton R, Klein J and Fink D 1989 *Nucl Instr Meth f343 231*

Miller W J 1973 *Proc X/V Int Symp Combust* (Pittsburgh: Combustion Inst) p 307
Mosch W and Hauschild W 1979 *Veb Verlag Technik* (Berlin)
Motz L 1970 *Astrophysics and Stellar Structure* (Ginn: Waltham MA)
Nickel J C, Zetner P W, Shen G and Trajmar S 1989 *J Phys E: Sci Instr 22730*
Nierneyer L, Ulrich L and Wiegart N 1989 */EEE Trans Electr Insul 24309*
Nighan W L 1976 in *Principles of Laser P/asmas* (ed G Bekefi, Wiley: New York) Ch.7
Nighan W L and Wiegand W J 1974 *Phys Rev A 10922*
Nobata and Kando 1979 *J App/ Phys 503956*
O'Malley T F 1966 *Phys Rev 75014*
O'Malley T F and Taylor H S 1968 *Phys Rev 776207*
O'Neill B C and Craggs J D 1973 *J Phys B: Atom Mol Phys 62634*
Olthoff J K, Van Brunt R J, Wang Y, Champion R L and Doverspike L D 1989 *J Chem Phys 91 2261*
Orient O J and Srivastava S K 1987 *J Phys B: At Mol Phys 203923*
Orient O J and Chutjian A 1986 *Phys Rev A 341841*
Orient O J and Srivastava S K 1983 *J Chem Phys 782949*
Orient O J, Chutjian A, Crompton R W and Cheung B 1989 *Phys Rev A 394494*
Orient O J, Chutjian A and Alajajian S H 1985 *Rev Sci Instr 5669*
Orient O J and Srivastava S K 1983 *J Chem Phys 782949*
Orient O J and Srivastava S K 1983 *Phys Rev A* 271209
Osborne M R, Winfield R J and Green J M 1989 *J App/ Phys 655242*
Oskam H J 1958 *Phillips Res Reports 73335*
Pack R T and Hirschfelder J O 1968 *J Chem Phys 494009*
Pedersen A 1989 *IEEE' Trans Electr Insul* 24721
Petrović Z Lj and Crornpton R W 1985 *J Phys B: At Mol Phys 772777*
Phelps A V and Pitchford L C 1985b *JILA Information Center Report No. 26* (Univ. Colorado, Boulder CO)
Phelps A V and Pitchford L C 1985a *Phys Rev A 372932*
Pinnaduwage L A, Christophorou L G and Hunter S R 1989 *J Chem Phys 906275*
Pinnaduwage L A, Christophorou L G and Bitouni A P 1991 *J Chem Phys 95274*
Pinnaduwage L A and Christophorou L G 1993 *Phys Rev Lett 70754*
Pinnaduwage L A and Christophorou L G 1994 *J Appl Phys 7646*
Popovic' D, Čadež 1, Landau M, Pichou F, Schermann C and Hall R I 1990 *Meas Sci Technol 7* 1041
Popple R A, Durham M A, Marawar R W, Lindsay B G, Smith K A and Dunning F B 1992 *Phys Rev A 45247*
Pozdneev S A 1982 *Sov Phys Tech Phys 27919*
Read F H 1968 *J Phys B: At Mol Phys 2893*

Read F H 1975 *J Phys B: At Mol Phys 81034*
Register D F, Trajmar S and Srivastava S K 1980 *Phys Rev A 27* 1134
Rogoff G L 1985 *J Phys D: Appl Phys 781533*
Sabadil H 1973 *Beitr aus der Plasmaphysik 13234*
Schauer S N, Williams P and Compton R N 1990 *Phys Rev Lett 65625*
Schermann C, Čadež 1, Delon P, Tronc M and Hall R I 1978 *J Phys E: Sci Instr 17746*
Scheunemann H-U, Illenberger E and Baugärtl H 1980 *Ber Bunsenges Physik Chem 84580*
Schneider B 1, Le Dourneuf M and Lan Vo Ky 1979a *Phys Rev Lett 431926*
Schneider B 1, Le Dourneuf M and Burke P G 1979b *J Phys B: At Mol Phys 72 L365*
Schulz G J and Asundi R K 1967 *Phys Rev 75825*
Schwartz C 1961 *Phys Rev 1231700*
Shimamori H and Hotta H 1986 *J Chem Phys 85887*
Shimamori H and Hotta H 1984 *J Chem Phys 87 1271*
Shimamori H and Nakatani Y 1988 *Chem Phys Lett 750109*
Shimamori H, Nakatani Y and Ogawa Y 1991 *Joint Symposium on Electron and Ion Swarms and Low Energy Electron Scattering* (Bond Univ, Gold Coast, Australia) abstracts p 28
Shimamori H and Hotta H 1983 *J Chem Phys 781318*
Shimamori H and Hatano Y 1976 *Chem Phys Lett 38242*
Shimamori H and Nakatani Y 1992 *J Chem Phys 961967*
Shimamori H, Tatsumi Y, Ogawa Y and Sunagawa T 1992a *Chem Phys Lett 794 223*
Shimamori H, Tatsumi Y, Ogawa Y and Sunagawa T 1992b *J Chem Phys 976335*
Shimamori H, Tatsumi Y and Sunagawa T 1993 *J Chem Phys 997787*
Smirnov B M 1982 *Negative Ions* (McGraw Hill, NY)
Smith D and Adams N G 1985 *Astrophys J 298827*
Smith D, Adams N G and Alge E 1984 *J Phys B: At Mol Phys 17461*
Smith D and Adams N G 1987 *J Phys B: At Mol Phys 204903*
Smith D, Španěl P and Mayhew C A 1992 *Int J Mass Spectry ion Process 117457*
Smith D and Španěl P 1994 *Adv Atom Molec Opt Phys* (Academic: New York) Vol 32, p 307
Smith D, Herd C R and Adams N G 1989 *Int J Mass Spectry Ion Process 9315*
Smith D and Plumb I C 1972 *J Phys D: Appl Phys 51226*
Smith D and Adams N G 1983 in *Physics of Ion-Ion and Electron-Ion Collisions* (eds F Brouillard and J Wm McGowan, New York: Plenum)
Smith D and Adams N G 1984 *Pure Appl Chem 56* 175

Smith D, Adams N G, Dean A G and Church M J 1975 *J Phys D: App/ Phys 8141*
Smith D, Herd C R, Adams N G and Paulson J F 1990 */nt J Mass Spectry Ion Process 96341*
Smith R D, Barinaga C J and Udseth H R 1988 *Aria/ Chem* 601948
Smith J 1965 *J Geophys Res* 893929
Sohn W, Jung K and Ehrhardt H 1983 *J Phys B: At Mol Phys 16891*
Španěl P, Tichý M and Smith D 1993 *J Chem Phys 988660*
Spence D and Schulz G J 1973 *J Chem Phys* 581800
Spyrou S M, Hunter S R and Christophorou L G 1985 *J Chem Phys 83641*
Spyrou S M and Christophorou L G 1985 *J Chem Phys 822620*
Srivastava S K, Chutjian A and Trajmar S 1975 *J Chem Phys 632659*
Stamatović A and Schulz G J 1970 *Rev Sci Instr 4 1 423*
Stebbings R F 1976 *Science* 193537
Stemmler E A and Hites R A 1988 *Electron Capture Negative Ion Mass Spectra of Environmental Contaminants and Related Compounds (New* York: VCH Publishers)
Swider W 1985 *Handbook of Geophysics and the Space Environment* (ed A F Jursa, USAF)
Tawara H, Itikawa Y, Nishimura H, Tanaka H and Nakamura Y 1990 "Collision Data Involving Hydro-Carbon Molecules" *{Nat Inst Fusion Sci Rept NIFS-DATA-6,* Nagoya, Jpn)
Tawara H, Kato T and Ohnishi M 1985 "Ionization Cross Sections of Atoms and Ions by Electron Impact" (*Inst Plasma Phys Rept IPPJ-AM-37,* Nagoya Univ, Jpn)
Teillet-Billy D and Gauyacq J-P 1984 *J Phys B: At Mo/ Phys 773329*
Thompson J B 1959 *Proc Phys Soc 73818*
Toriumi M and Hatano Y 1985 *J Chem Phys 82* 254
Trajmar S and Register D F 1984 in *Electron-Molecule Collisions* (eds I Shimamura and K Takayanagi, New York: Plenum) p. 427
Trajmar S, Register D F and Chutjian A 1983 *Phys Reports 97219*
Trajmar S and Hall R I 1974 *J Phys B: At Mol Phys 7 L458*
Tronc M, Azria R and Ben Arfa M 1988 *J Phys B: At Mol Phys 272497*
Tronc M, Azria R, LeCoat Y and Simon D 1979 *J Phys B: At Mol Phys 72 L467*
Tronc M, Fiquet-Fayard F, Schermann C and Hall R I 1977 *J Phys B: At Mo/ Phys* 70305
Trump J G 1954 *Dielectric Materials and Their Applications* (ed A R von Hippel New York: Wiley)
Tsendin L D 1989 Sov *Phys Tech Phys 3411*
Van Brunt R J and Herron J T 1990 *IEEE Trans Electrical Insul 25* 75
Van Brunt R J and Kieffer L J 1970 *Phys Rev A 2* 1899

Van Brunt R J and Kieffer L J 1974 *Phys Rev A* 701633
van 0s C F A 1989 Thesis, Univ. Utrecht
van 0s C F A, Heeren R M A and Amersfoort P W 1987 *App/ Phys Lett 57 1495*
Vogt E and Wannier G H 1954 *Phys Rev 951190*
Wadehra J M 1984 *Phys Rev A 29106*
Wadehra J M 1986 in *Nonequilibrium Vibrational Kinetics* (ed M Capitelli, Springer-Verlag, NY)
Wadehra J M 1990 *Phys Rev A 473607*
Wadehra J M and Bardsley J N 1978 *Phys* RevLett47 1795
Walter C W, Lindsay B G, Smith K A and Dunning F B 1989 *Chem Phys Lett 754 409*
Watanabe Y and Shiratani M 1993 *Jpn J Appl Phys 323074*
Watson C H, Wronka J, Laukien F H, Barshick C M and Eyler J R 1993 *Aria/ Chem 65 2801*
Wayne R P 1991 *Chemistry of Atmospheres* (Clarendon: Oxford)
West W P, Foltz G W, Dunning F B, Latimer C J and Stebbings R F 1976 *Phys Rev Lett 36854*
Wigner E P 1948 *Phys Rev 731002*
Wildt R 1939a *Ap J* 89295
Wildt R 1939b *Ap J 90611*
Wildt R 1941 *Ap J 9347*
Yang S H, Pettiette C L, Conceicao J, Cheshnovsky O and Smalley R E 1987 *Chem Phys Lett 739233*
Yang S H, Taylor K J, Craycraft M J, Conceicao J, Pettiette C L, Cheshnovsky O and Smalley R E 1987 *Chem Phys Lett 744431*
Yichen-Wang, Champion R L, Doverspike L D, Olthoff J K and Van Brunt R J 1989 *J Chem Phys 922254*
Zel'dovich Y B 1944 *Theory of Combustion and Detonation in Gases* (Moscow: Acad Sci USSR)
Zheng Z, Smith K A and Dunning F B 1988 *J Chem Phys 896295*
Zollars B G, Higgs C, Lu F, Walter C W, Gray L G, Smith K A, Dunning F B and Stebbings R F 1985 *Phys Rev A 323330*
Zubeck M and King G C 1990 *J Phys B: At Mo/ Opt Phys 23561*
Zubeck M, King G C, Rutter P M and Read F H 1989 *J Phys B: At Mo/ Opt Phys 223411*

FIGURE CAPTIONS

Fig. 1. Representative potential-energy curves for electron capture by molecule AB to form A + B" through ground and negative-ion states described by potentials $V_o(R)$ and V"(R), respectively,

Fig. 2. Schematic of the high-Rydberg collisional ionization apparatus (Kalamarides *et al 1990),*

Fig. 3. The Kr photoionization apparatus used to measure attachment channels, lineshapes, and temperature dependencies (Chutjian and Alajajian 1985a),

Fig. 4. Magnetically-confined, trochoidal monochromator system (Scheunemann *et a/ 1980).*

Fig. 5. Time-of-Flight apparatus for measurement of negative-ion products and lifetimes (Hadjiantoniou *et a/ 1973).*

Fig. 6. The Reversal Electron Attachment Detector (*READ*) used for generating low-energy electrons and extracting the product negative ions (Bernius and Chutjian 1989, Boumsellek and Chutjian 1992).

Fig. 7. The Cavalleri Electron-Density Sampling (*CEDS*) apparatus for measuring attachment rate constants and temperature dependencies (Orient *et a/ 1989,* Crompton and Haddad 1983).

Fig. 8. Schematic of the drift-tube swarm apparatus (Spyrou and Christophorou 1985),

Fig. 9. The Flowing-Afterglow/Langmuir-Probe (*FALP*) apparatus for measuring attachment channels and rate constants (Smith *et a/ 1984),*

Fig. 10. Schematic of the Microwave-Cavity /Pulsed-Radiolysis (*MCPR*) apparatus with additional cavity heating (Shimamori *et a/ 1992a,* 1992b).

Fig. 11. Schematic of the 127° electrostatic monochromator and analyzer system (Jung *et a/ 1982),*

Fig. 12. The 127° electrostatic analyzer system used to detect threshold photoelectrons (King *et al 1987),*

Fig. 13. Combination of 127° electrostatic monochromator and fixed-angle (90°) quadruple mass analyzer for energy-loss measurements of outgoing negative ions (Hall *et al 1988).*

Fig. 14. Magnetically-confined pulsed electron gun and quadruple mass analyzer system for negative-ion detection (Krishnakumar and Srivastava 1990).

Fig. 15. Enhanced O^- signal with laser excitation of SO_2 in single-collision electron attachment (Jaffke *et al 1993).*

Fig. 16. Calculated (--) and measured (o) dissociative attachment signals in DI relative to HI (Chutjian *et al 1990).*

Fig. 17. Potential energy curves for HI and DI: (a) and (b), schematic curves drawn with a $^2\Sigma^+$ resonance-attachment interpretation (Chutjian *et al 1990);* (c) diabatic capture model, with the diabatic correction shown as (- · - -) (Crawford and Koch 1974); (d) *ab initio* resonance capture calculation (Chapman *et al 1988).*

Fig. 18. Dissociative attachment cross sections in F_2 (Chutjian and Alajajian *1987),*

Fig. 19. Calculated and measured rate constants for attachment in SF_6 to produce SF_6 and $SF_5 + F$ (Orient and Chutjian 1986).

Fig. 20. Comparison of calculated and measured rate constants for attachment in $CFCl_3$ to produce Cl^- (Orient *et al* 1989).

Fig. 21. Normalized negative-ion density profile g_n and electron density profile g_e for condition of attachment frequency/ionization frequency = 2, and detachment frequency/ionization frequency = 1 (after Bell 1992).

Fig. 22, Variation ΔE of electron affinity in an atom as a function of metal-atom distance. Surface conversion occurs at some optimal distance Z.

Fig. 23. **Reflex-type high current negative-ion source (Goretskii et *al 1989).* Vibrational excitation of molecules occurs in the discharge column by higher-energy, magnetically-confined electrons. The molecules then diffuse radially to undergo dissociative attachment by slower electrons** in the periphery.

Fig. 24. **Mass spectrum of the explosives molecule PETN using the *READ* technique (Boumsellek eta*l 1991* b).**

Fig. 25. **Absorption coefficients (and cross sections) for a hydrogen plasma. The theoretical absorption coefficient of H^- per hydrogen atom is also illustrated for a chosen LTE condition of 6300 K (– –- –, after Chandrasekar 1960).**

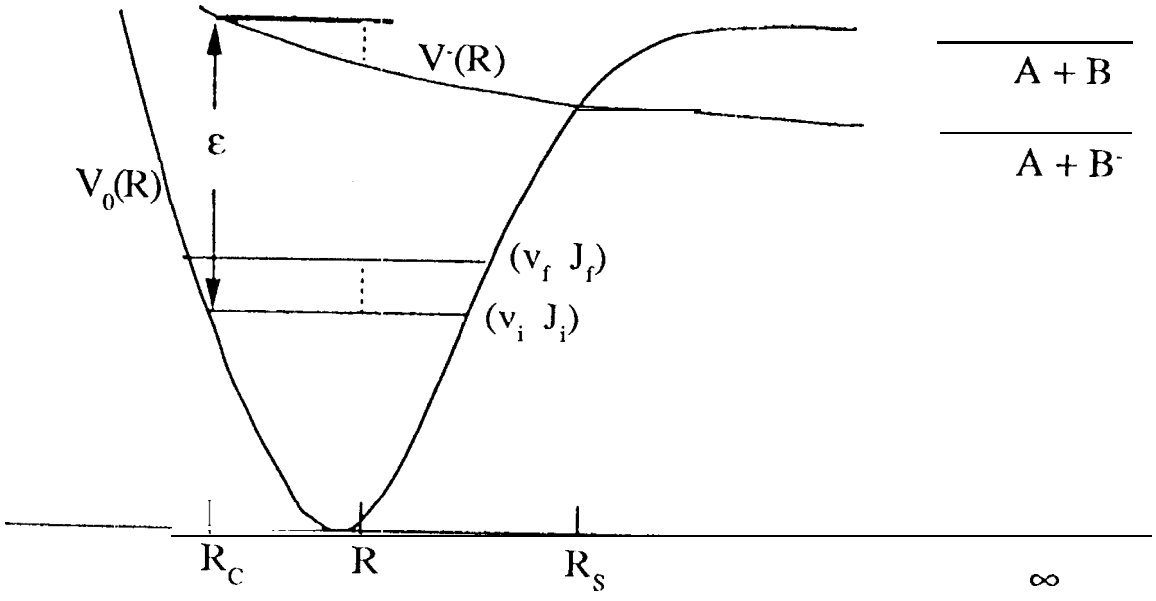

INTERNUCLEAR SEPARATION R

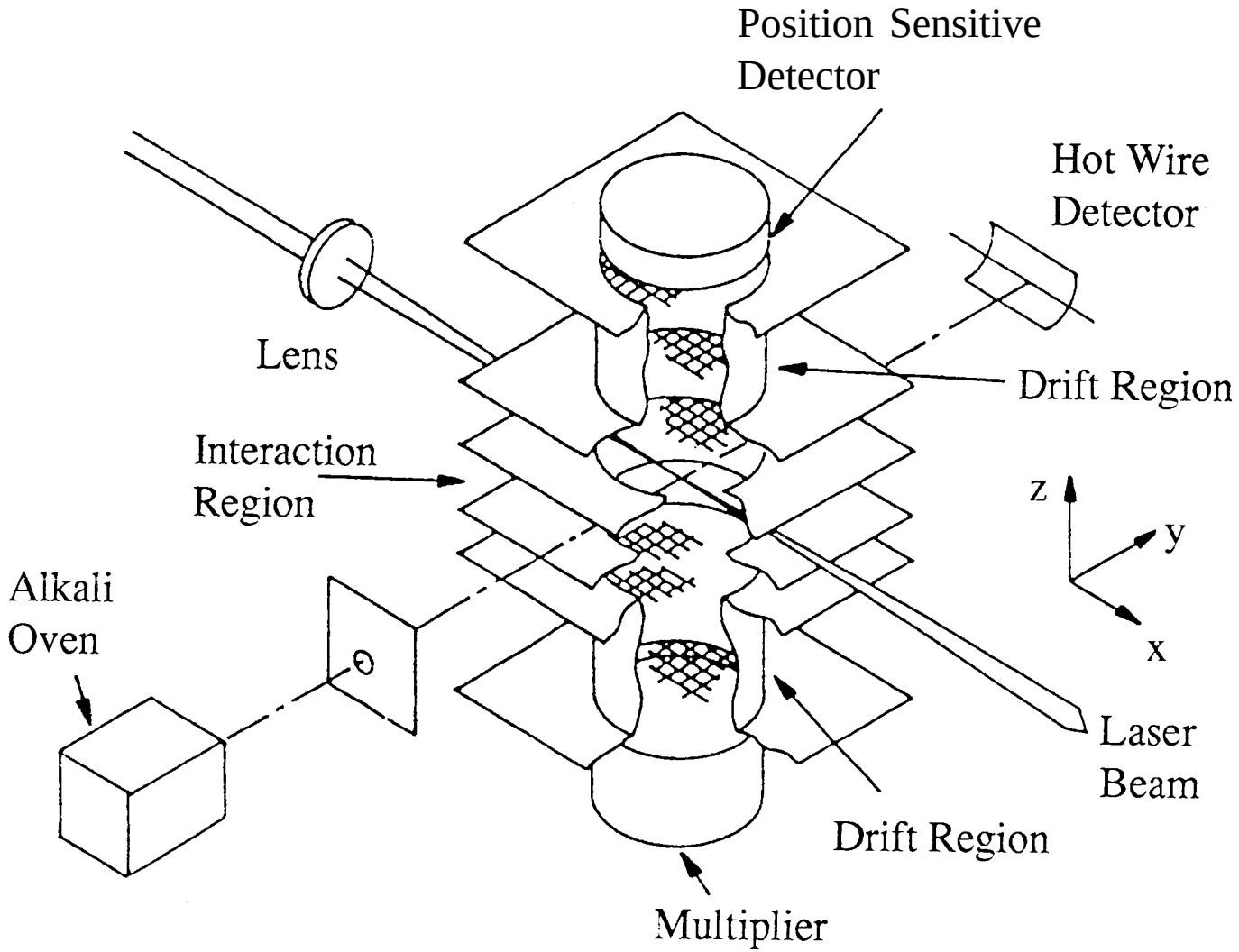
Position Sensitive
Detector
Hot Wire
Detector
Lens
Drift Region
Interaction
Region
z
y
x
Alkali
Oven
Laser
Beam
Drift Region
Multiplier

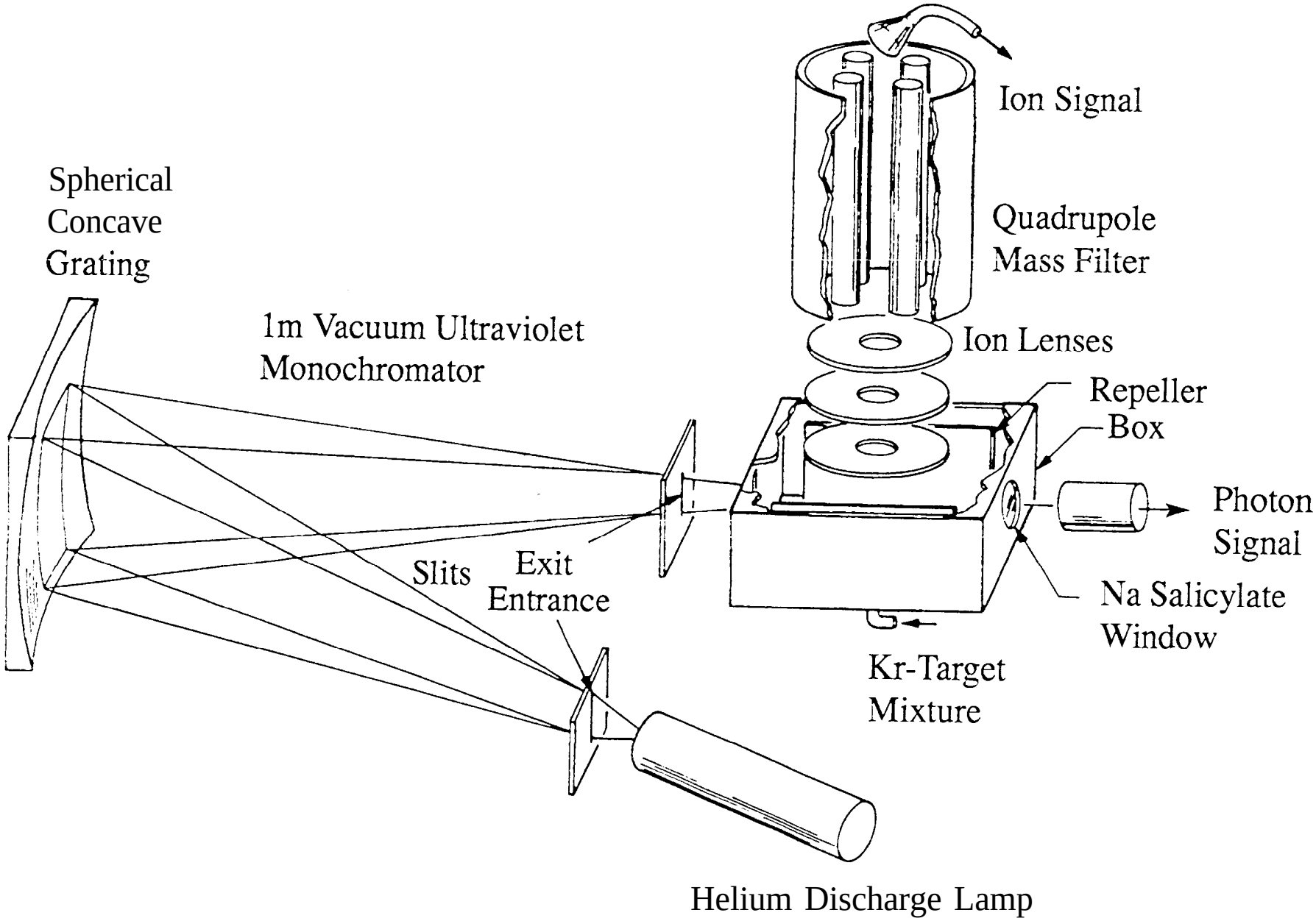
Ion Signal
Spherical
Concave
Grating
Quadrupole
Mass Filter
1m Vacuum Ultraviolet
Monochromator
Ion Lenses
Repeller
Box
Photon
Signal
Slits
Exit
Entrance
Na Salicylate
Window
Kr-Target
Mixture
Helium Discharge Lamp

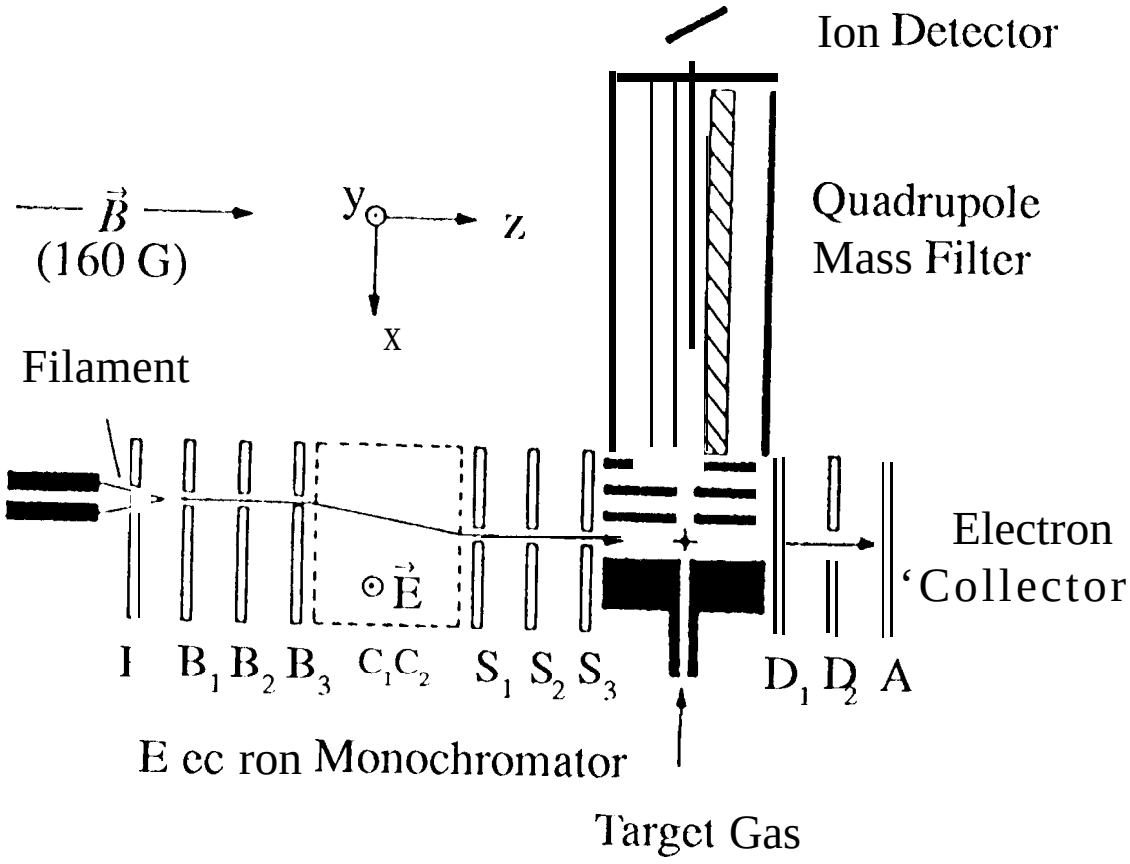
Ion Detector
$\vec{B}$
(160 G)
y
z
x
Quadrupole
Mass Filter
Filament
$\vec{E}$
Electron
'Collector
I B_1 B_2 B_3 C_1 C_2 S_1 S_2 S_3 D_1 D_2 A
E ec ron Monochromator
Target Gas

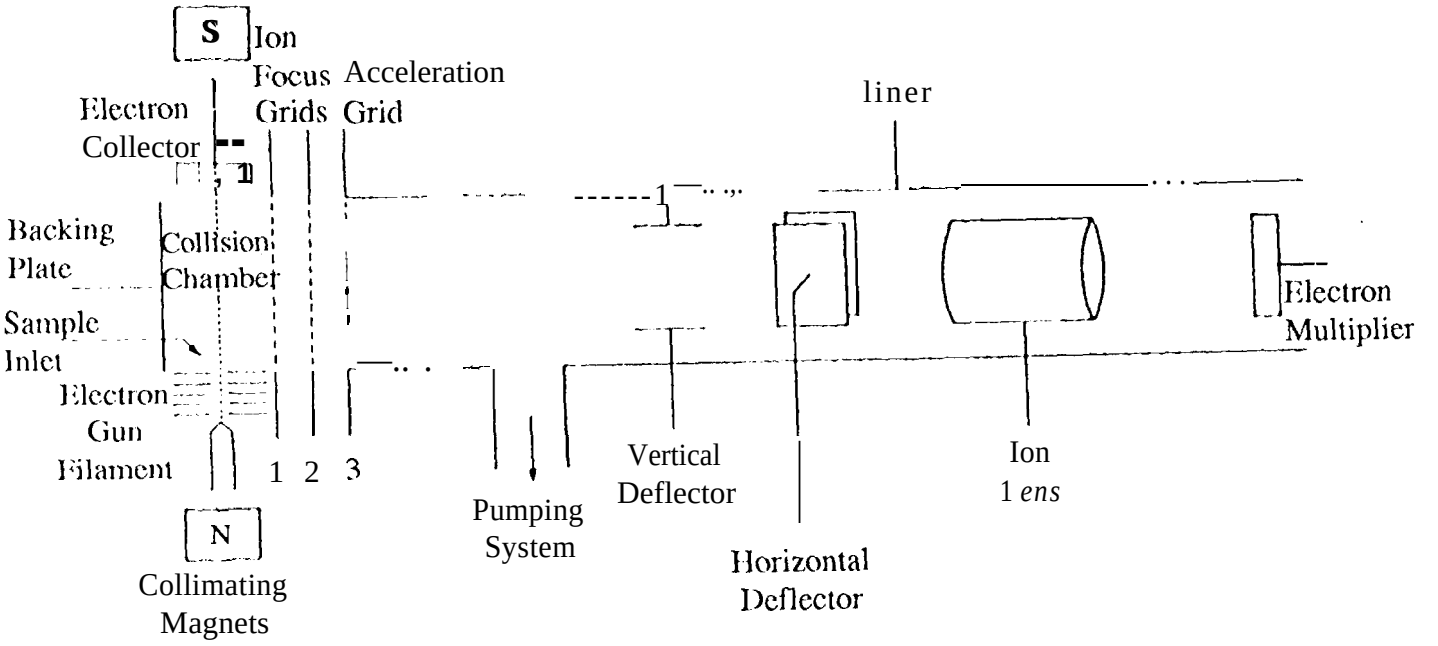
S
Ion
Focus Grids
Acceleration Grid
liner
Electron Collector
Backing Plate
Collision Chamber
Sample Inlet
Electron Gun Filament
1 2 3
N
Collimating Magnets
Pumping System
Vertical Deflector
Horizontal Deflector
Ion 1 ens
Electron Multiplier

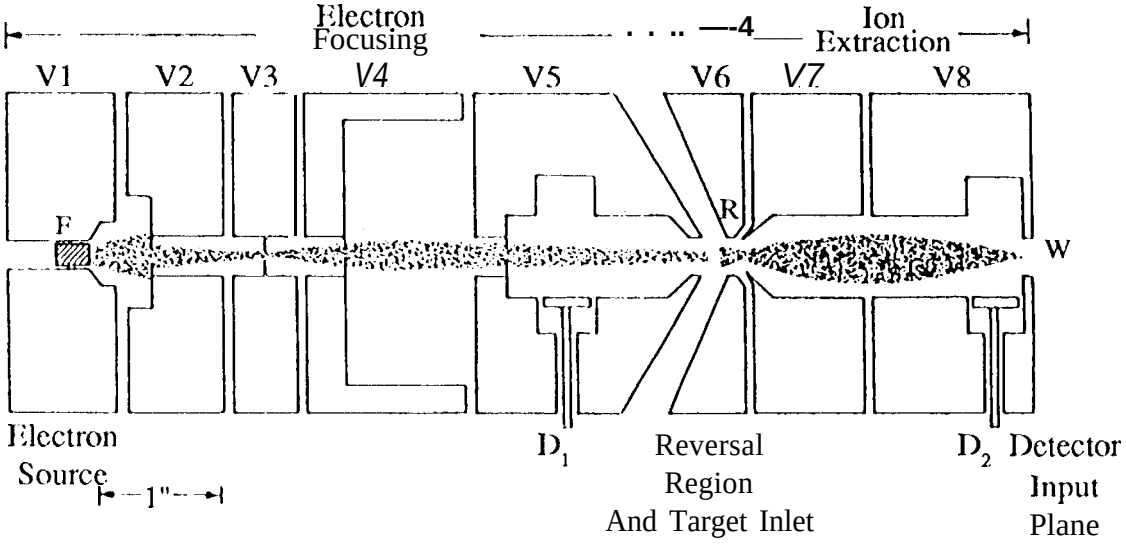
Electron
Focusing
Ion
Extraction
V1
V2
V3
V4
V5
V6
V7
V8
F
R
W
Electron
Source
1"
D1
Reversal
Region
And Target Inlet
D2
Detector
Input
Plane

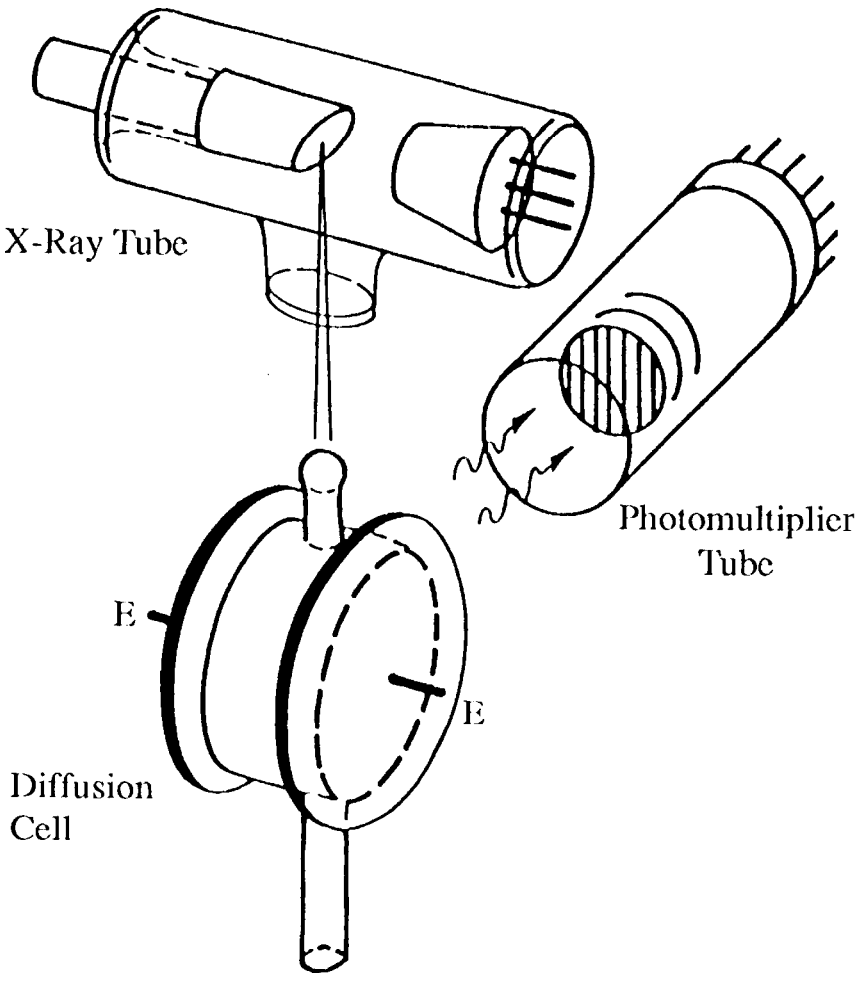
X-Ray Tube
Photomultiplier
Tube
E
E
Diffusion
Cell

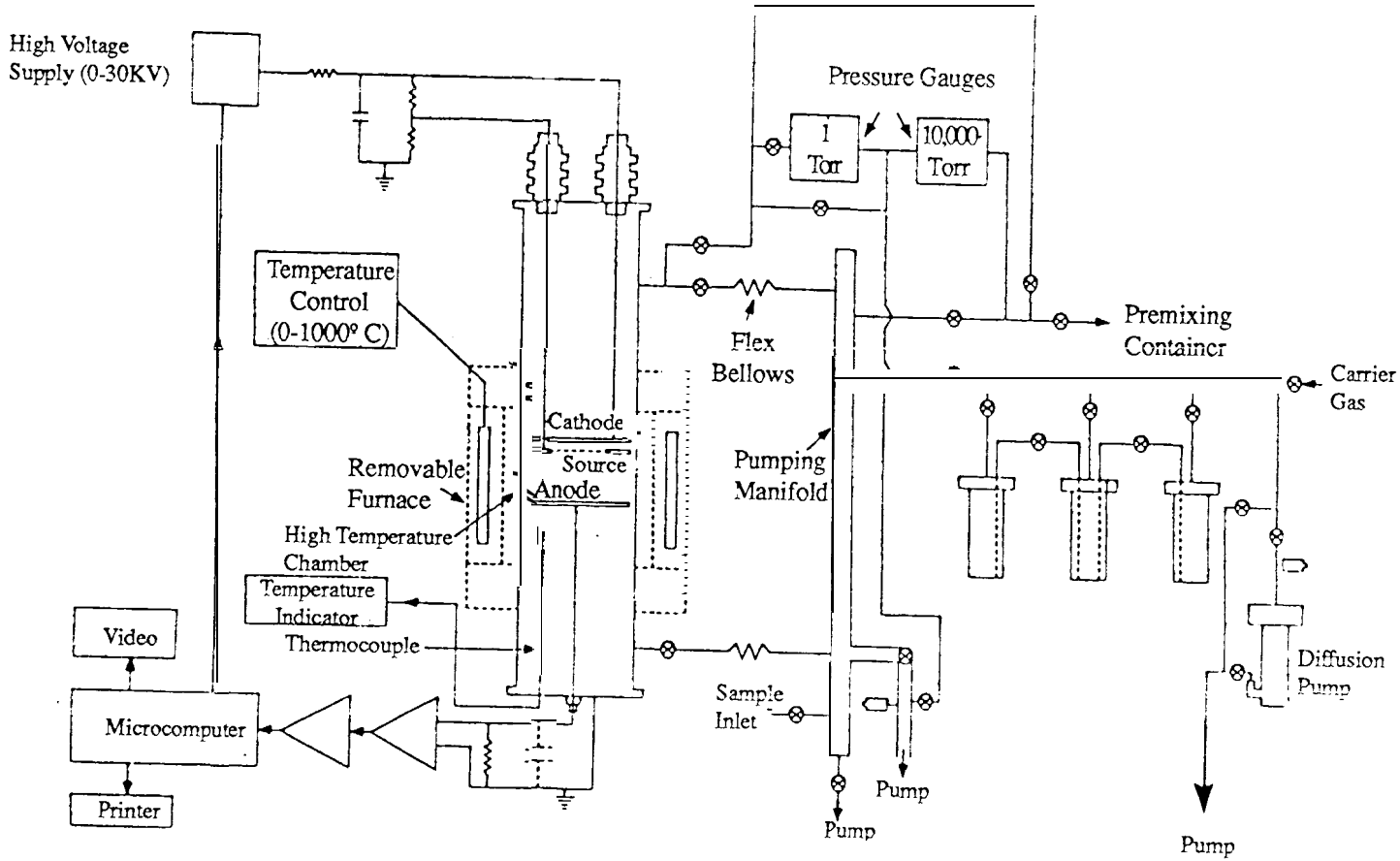
High Voltage
Supply (0-30KV)
Pressure Gauges
1
Torr
10,000
Torr
Temperature
Control
(0-1000° C)
Flex
Bellows
Premixing
Container
Carrier
Gas
Cathode
Source
Anode
Removable
Furnace
Pumping
Manifold
High Temperature
Chamber
Temperature
Indicator
Thermocouple
Video
Microcomputer
Printer
Sample
Inlet
Pump
Pump
Pump
Diffusion
Pump

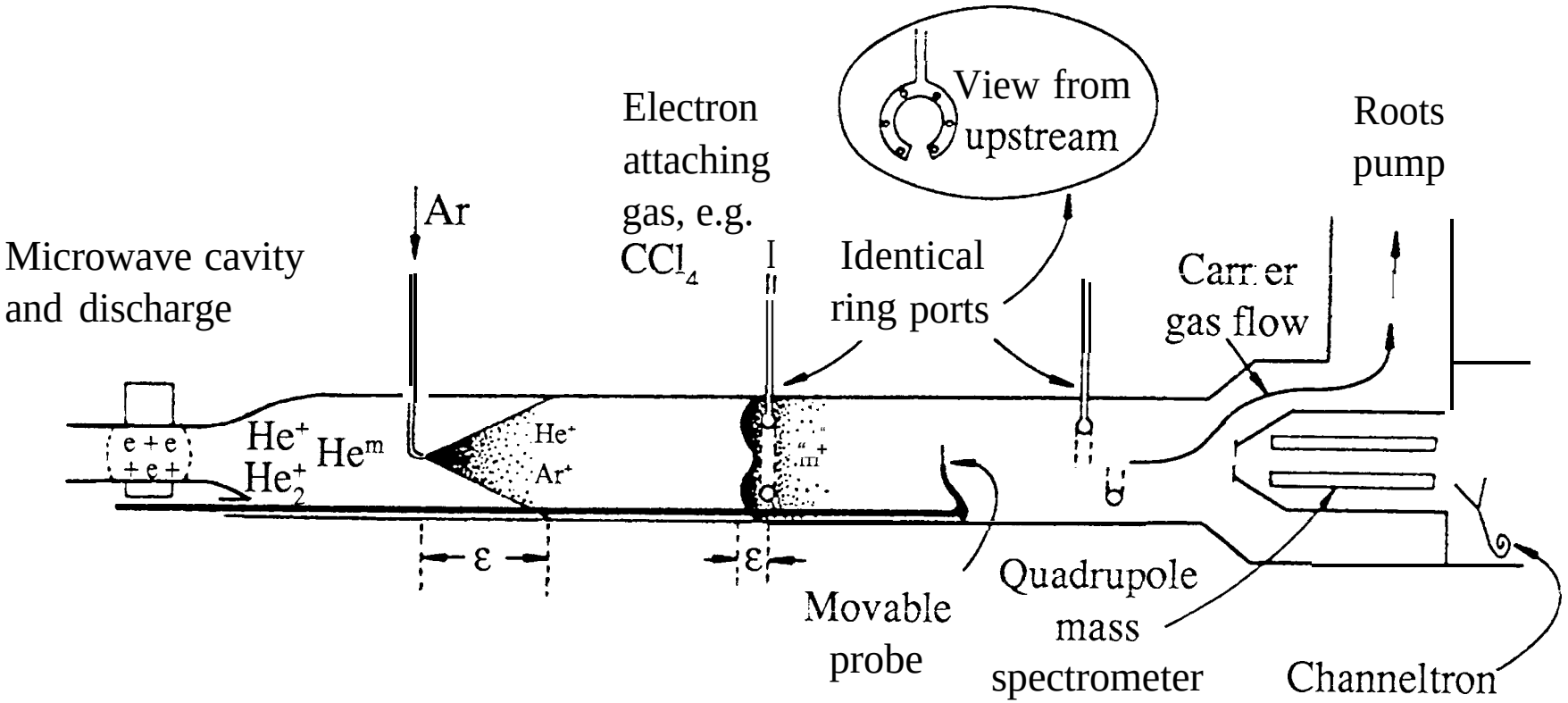
Microwave cavity
and discharge
Ar
Electron
attaching
gas, e.g.
CCl_4
View from
upstream
Identical
ring ports
Roots
pump
Carrier
gas flow
e + e
+ e +
He^+
He_2^+
He^m
He^+
Ar^+
ε
ε
Movable
probe
Quadrupole
mass
spectrometer
Channeltron

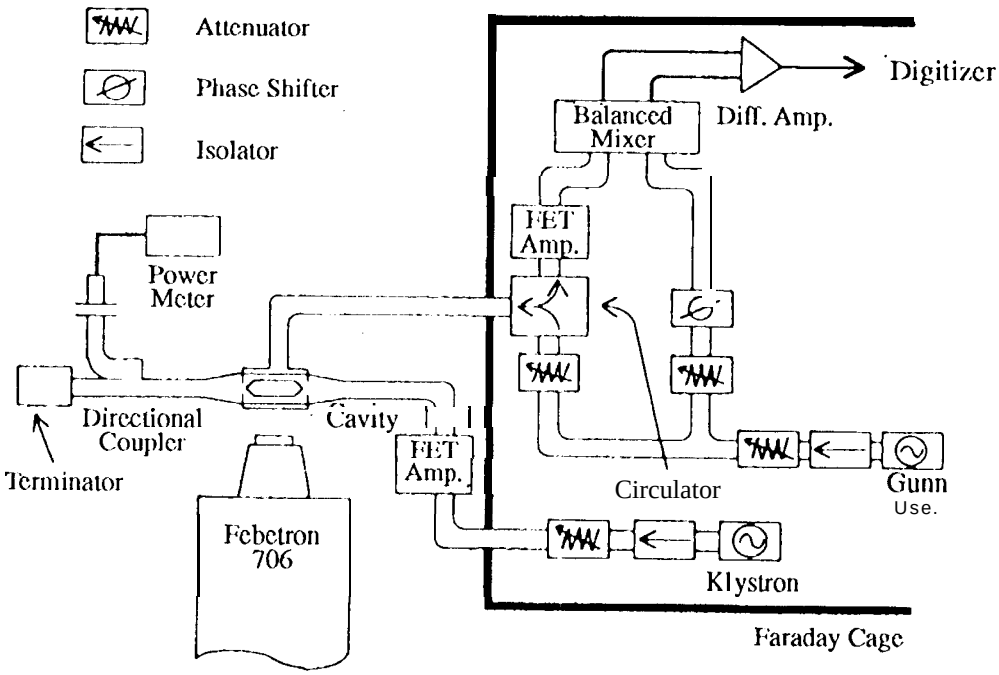
Attenuator
Phase Shifter
Isolator
Digitizer
Balanced Mixer
Diff. Amp.
FET Amp.
Power Meter
Directional Coupler
Cavity
Terminator
FET Amp.
Circulator
Gunn Use.
Fabetron 706
Klystron
Faraday Cage

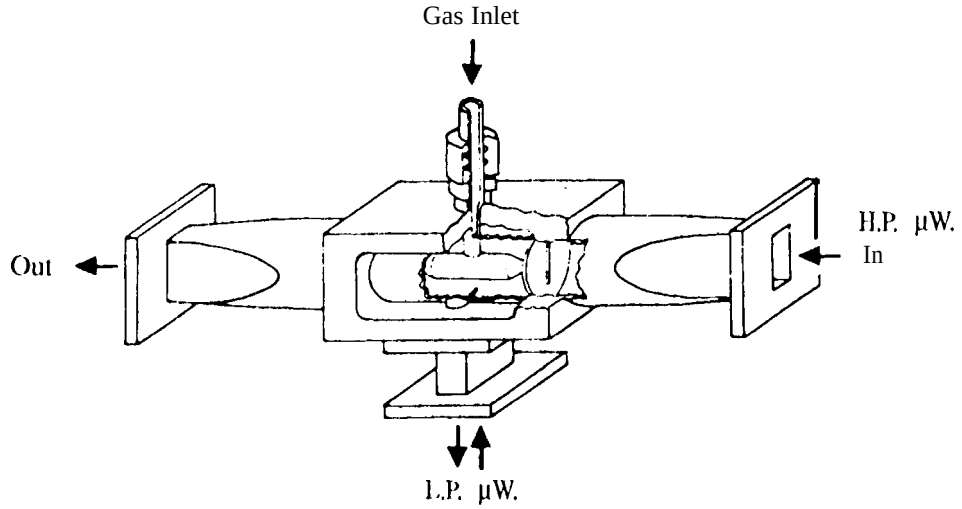
Gas Inlet
Out
H.P. µW. In
L.P. µW.

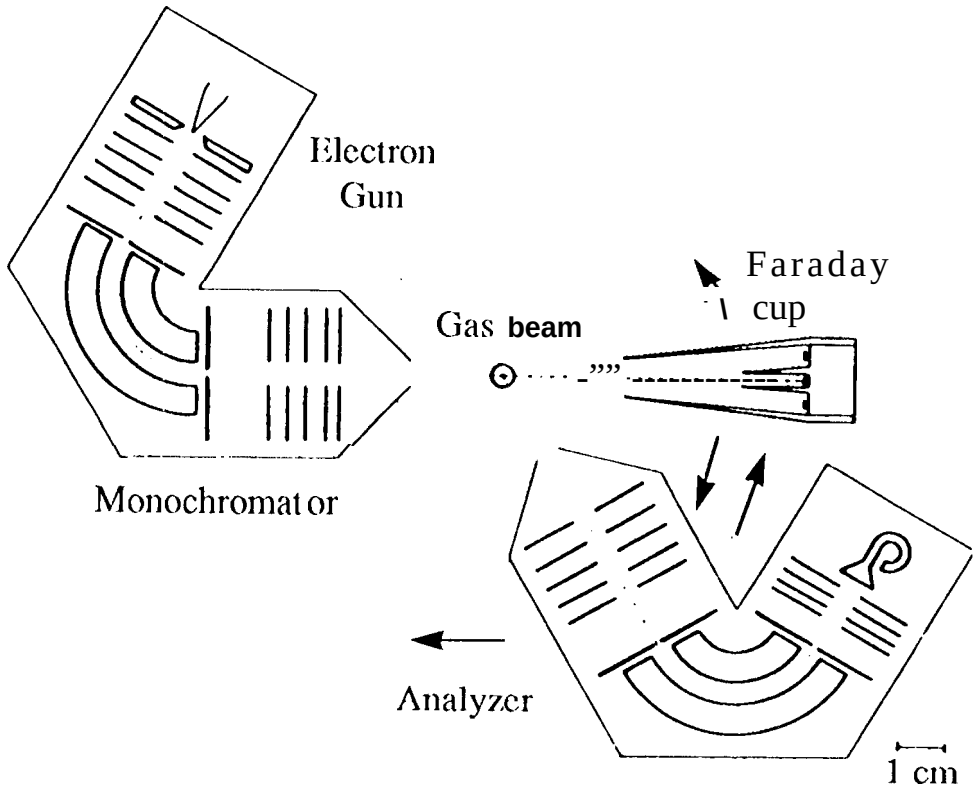
Electron
Gun
Faraday
cup
Gas beam
Monochromator
Analyzer
1 cm

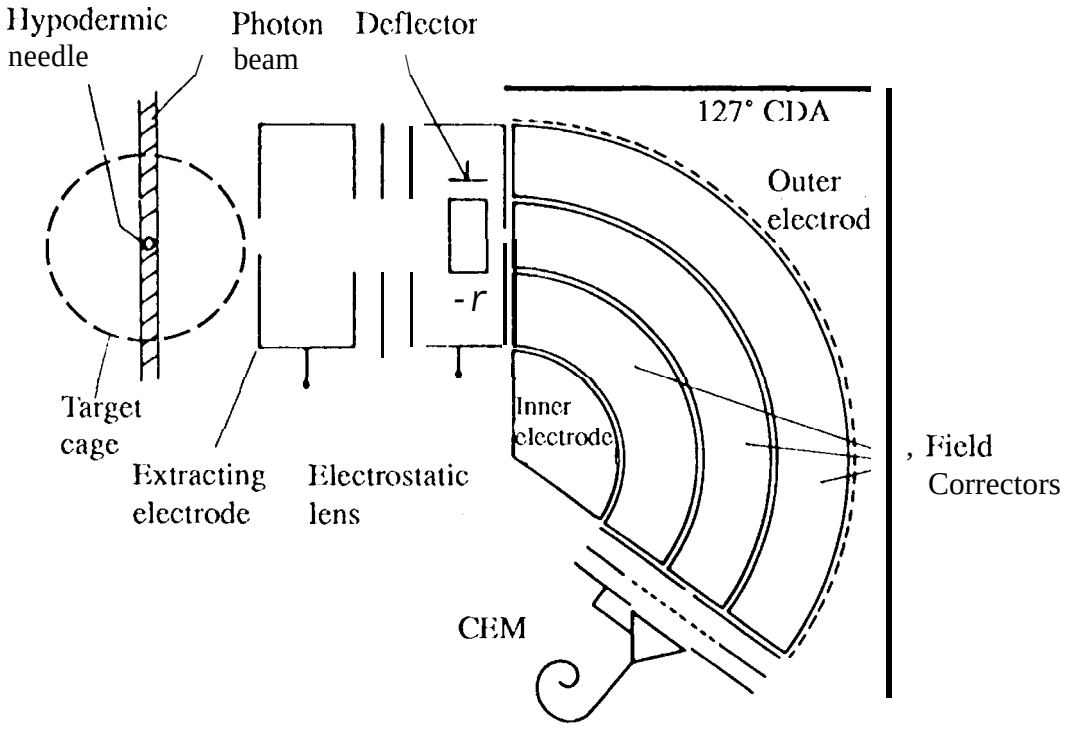
Hypodermic needle
Photon beam
Deflector
127° CDA
Outer electrod
-r
Target cage
Extracting electrode
Electrostatic lens
Inner electrode
, Field Correctors
CEM

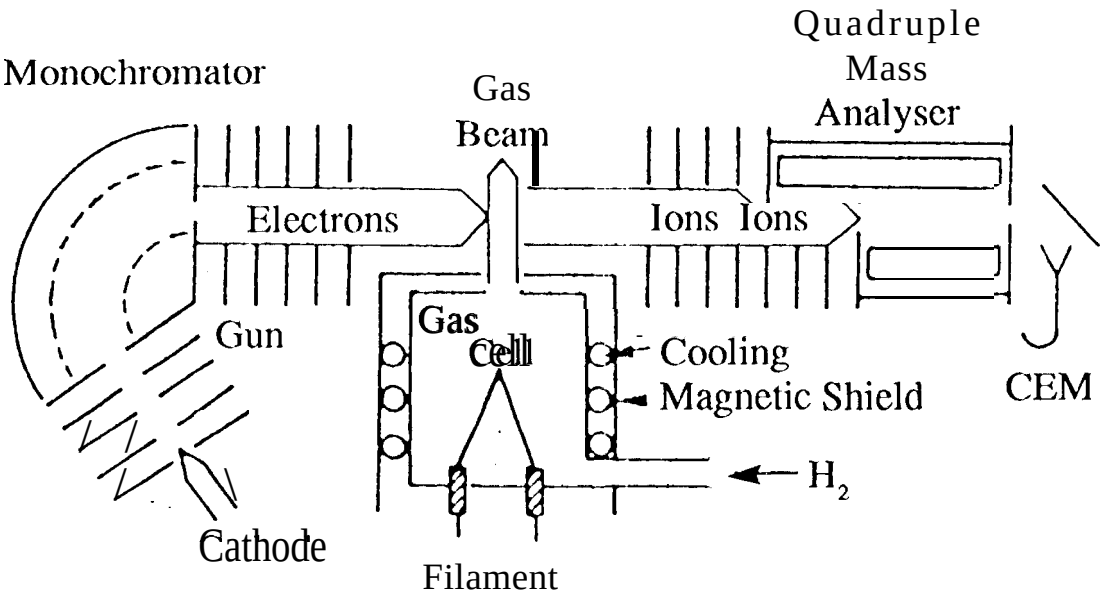
Monochromator
Gas
Beam
Quadruple
Mass
Analyser
Electrons
Ions
Ions
Gun
Gas
Cell
Cooling
Magnetic Shield
CEM
H_2
Cathode
Filament

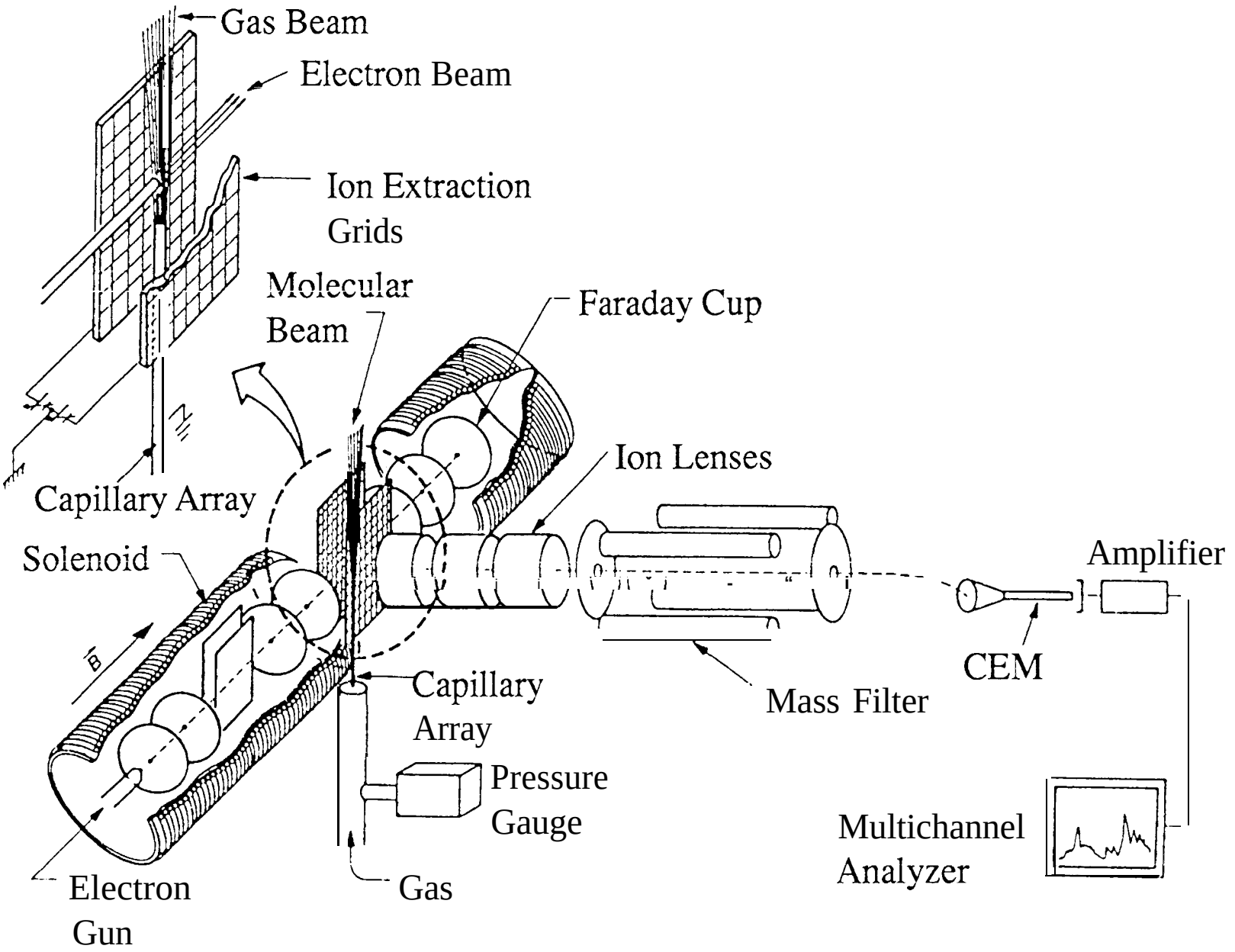
Gas Beam
Electron Beam
Ion Extraction Grids
Molecular Beam
Faraday Cup
Ion Lenses
Capillary Array
Solenoid
Amplifier
CEM
Mass Filter
Capillary Array
Pressure Gauge
Multichannel Analyzer
Electron Gun
Gas

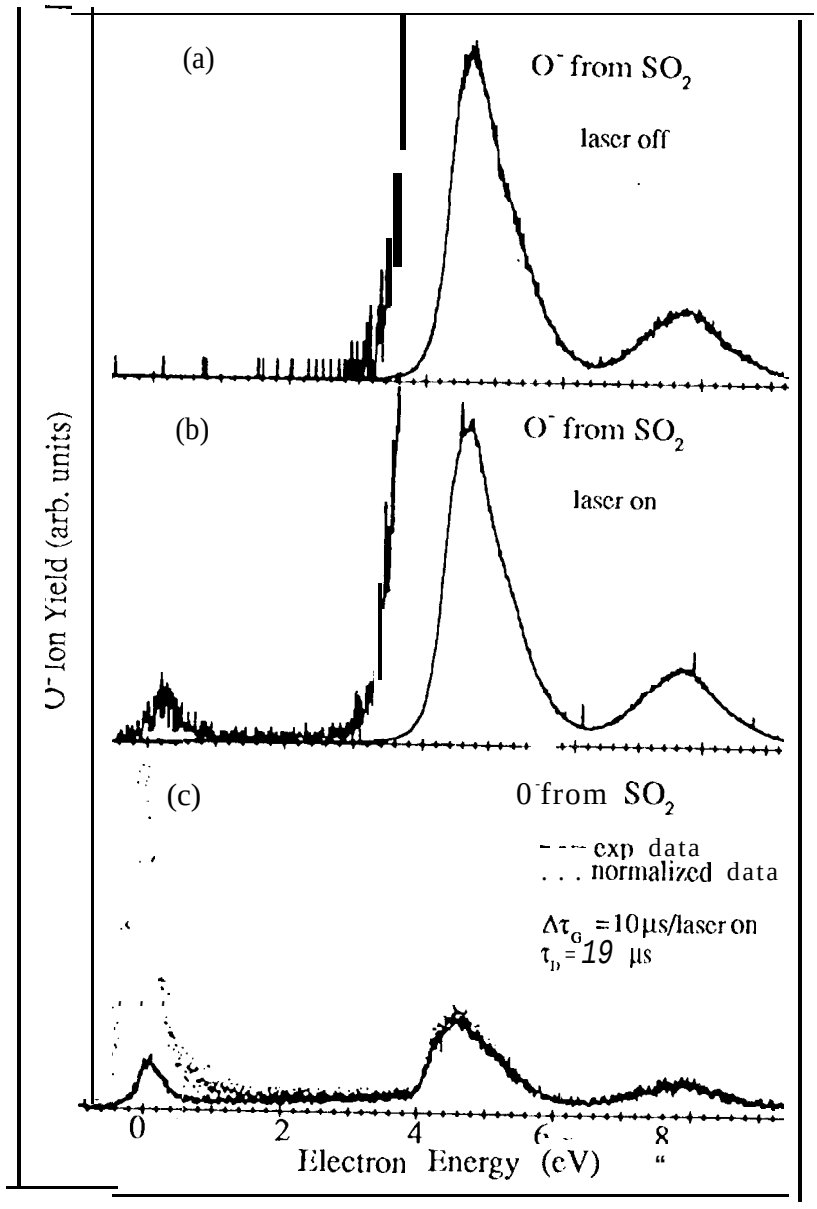
(a)
O⁻ from SO2
laser off
(b)
O⁻ from SO2
laser on
O⁻ Ion Yield (arb. units)
(c)
O⁻ from SO2
- - - exp data
. . . normalized data
Δτ_G = 10 μs/laser on
τ_D = 19 μs
0
2
4
8
Electron Energy (eV)

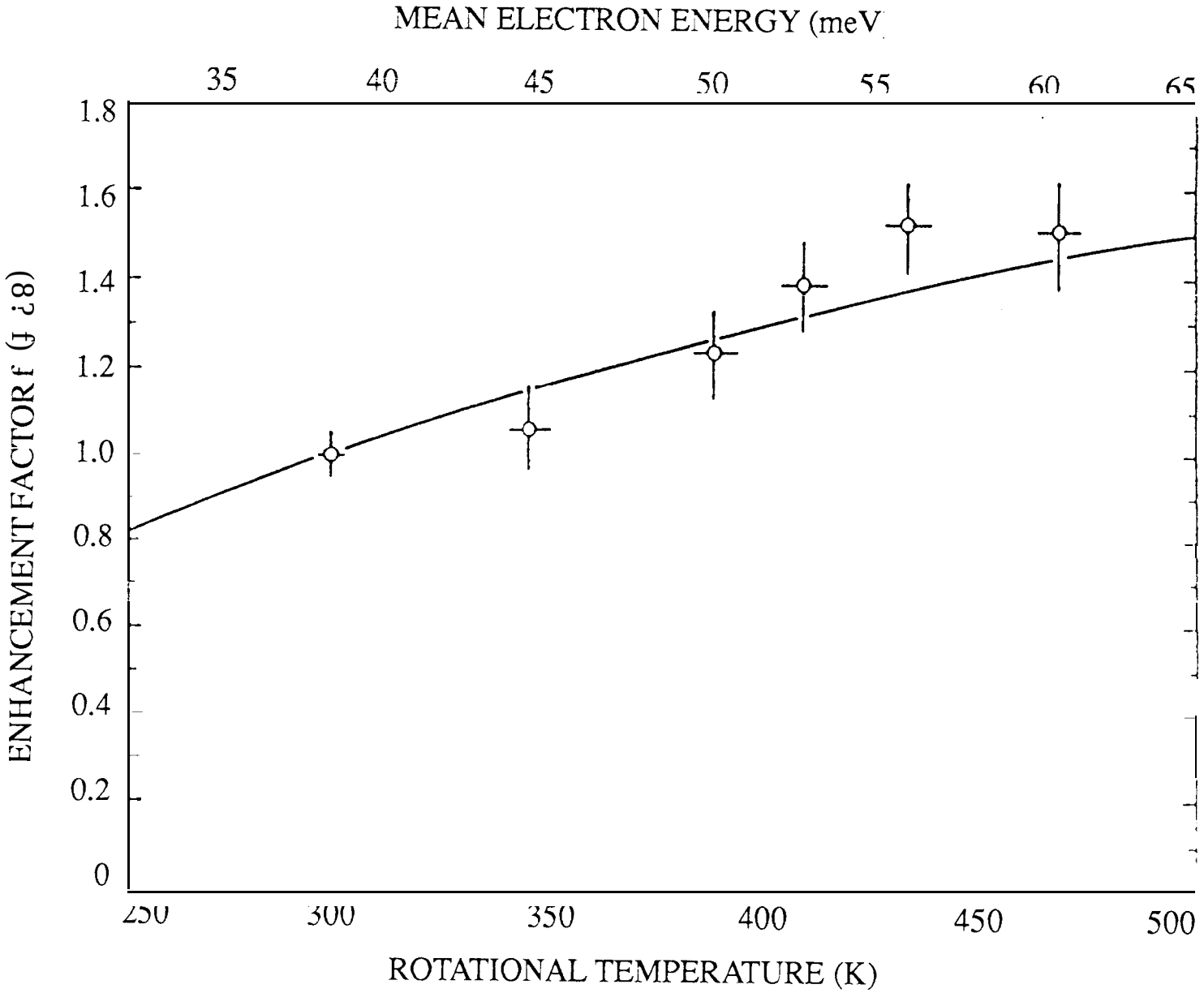
MEAN ELECTRON ENERGY (meV
35
40
45
50
55
60
65
1.8
1.6
1.4
1.2
1.0
0.8
0.6
0.4
0.2
0
ENHANCEMENT FACTOR f (g, g8)
250
300
350
400
450
500
ROTATIONAL TEMPERATURE (K)

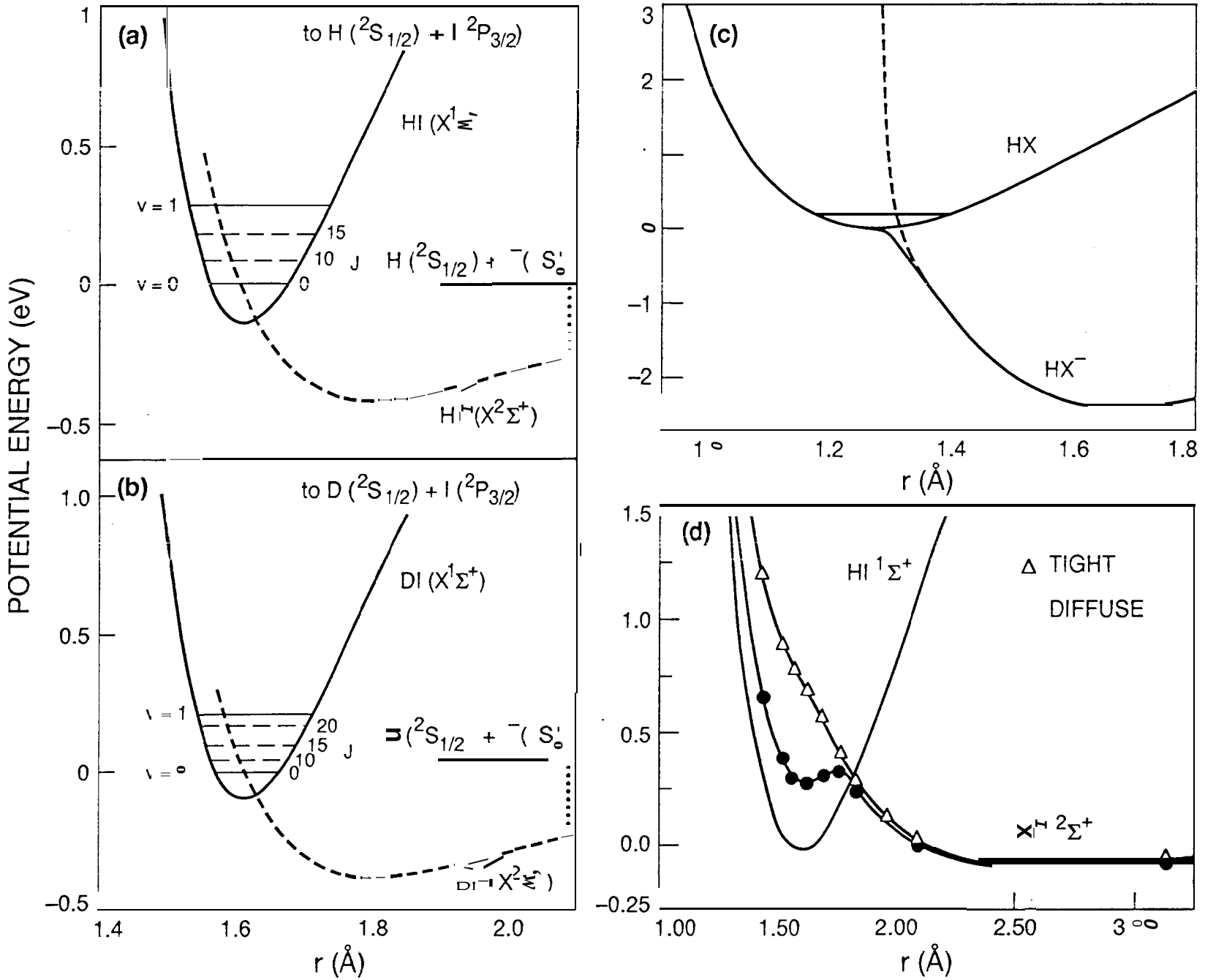
(a)
to H ($^2S_{1/2}$) + I $^2P_{3/2}$)
HI ($X^1\Sigma^+$)
v = 1
v = 0
15
10
0
J
H ($^2S_{1/2}$) + $^-$(S_o'
H$^+$H($X^2\Sigma^+$)
(b)
to D ($^2S_{1/2}$) + I ($^2P_{3/2}$)
DI ($X^1\Sigma^+$)
20
15
10
0
J
D$^+$I($X^2\Sigma^+$)
POTENTIAL ENERGY (eV)
r (Å)
(c)
HX
HX$^-$
r (Å)
(d)
HI $^1\Sigma^+$
Δ TIGHT
DIFFUSE
X$^+$H $^2\Sigma^+$
r (Å)

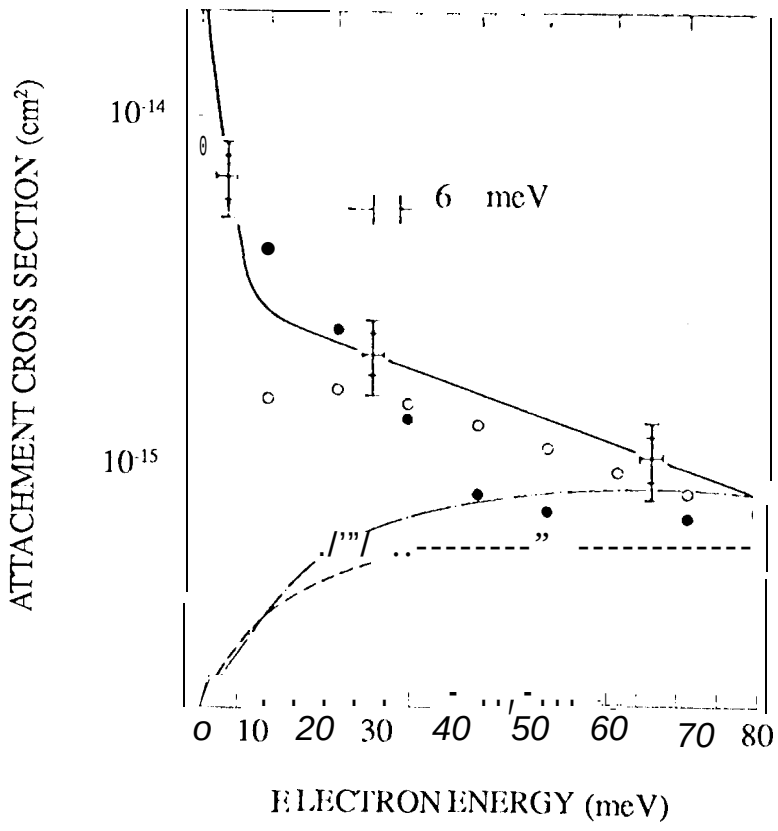
ATTACHMENT CROSS SECTION (cm²)
10⁻¹⁴
10⁻¹⁵
6 meV
0 10 20 30 40 50 60 70 80
ELECTRON ENERGY (meV)

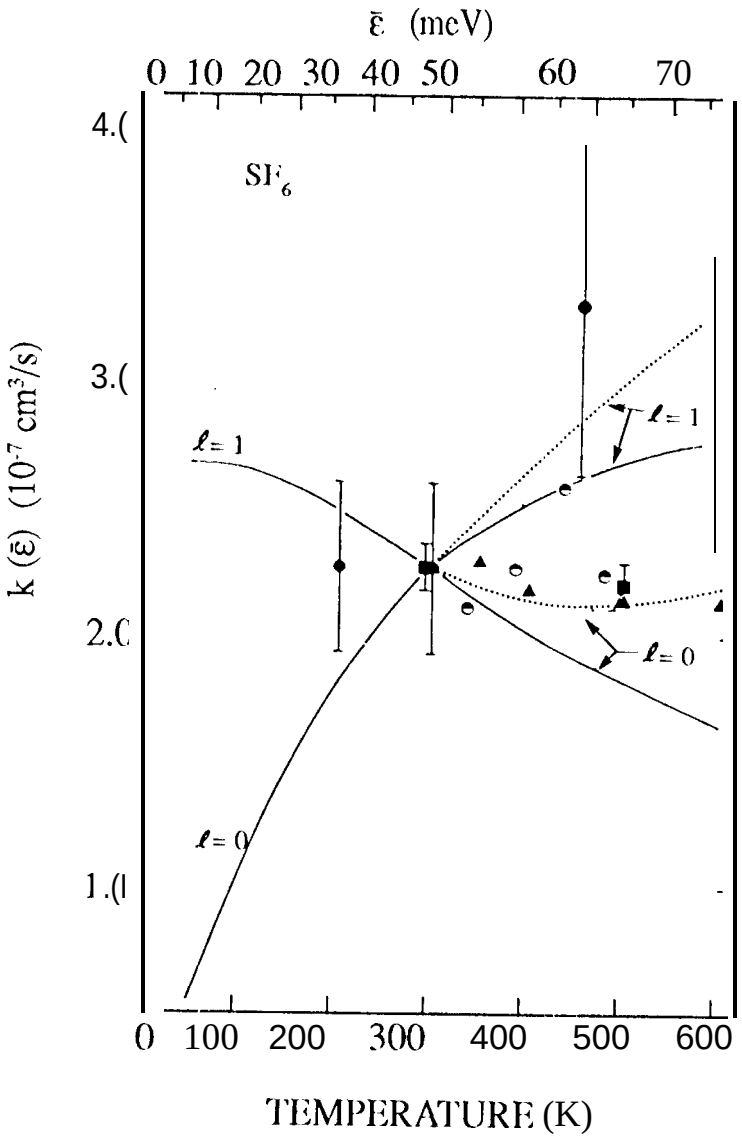
ε̄ (meV)
0 10 20 30 40 50 60 70
4.(
3.(
2.C
1.(
SF6
ℓ = 1
ℓ = 1
ℓ = 0
ℓ = 0
k (ε̄) (10-7 cm3/s)
0 100 200 300 400 500 600
TEMPERATURE (K)

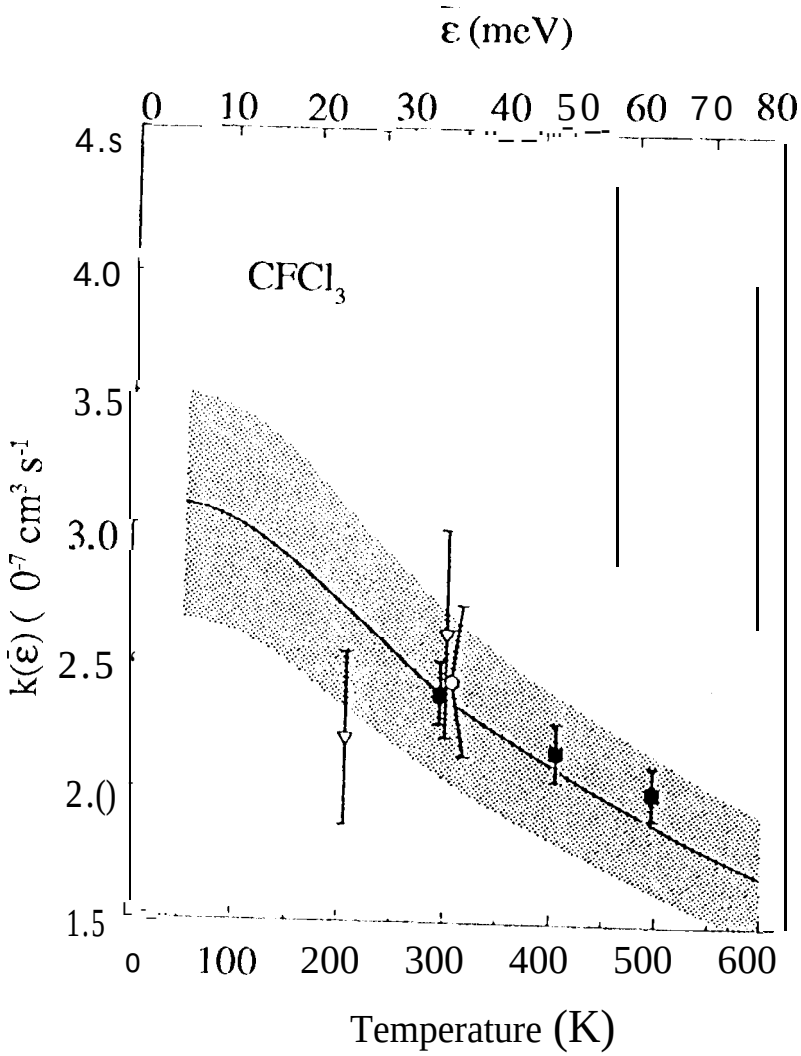
ε (meV)
0 10 20 30 40 50 60 70 80
4.s
4.0
3.5
3.0
2.5
2.0
1.5
CFCl3
k(ε) (0-7 cm3 s-1
0 100 200 300 400 500 600
Temperature (K)

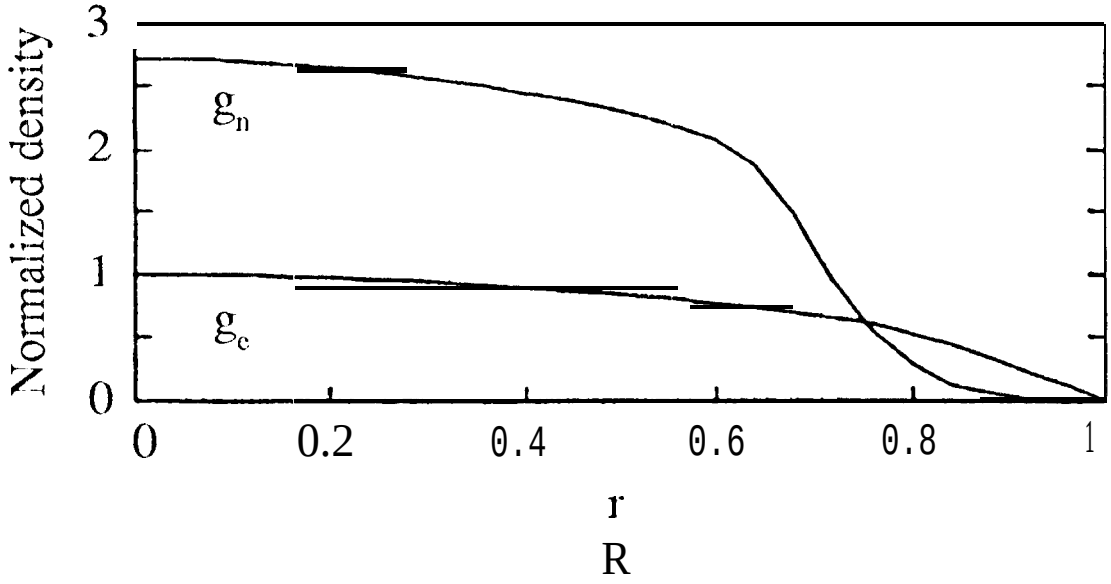
Normalized density
3
2
1
0
g_n
g_c
0
0.2
0.4
0.6
0.8
1
r
R

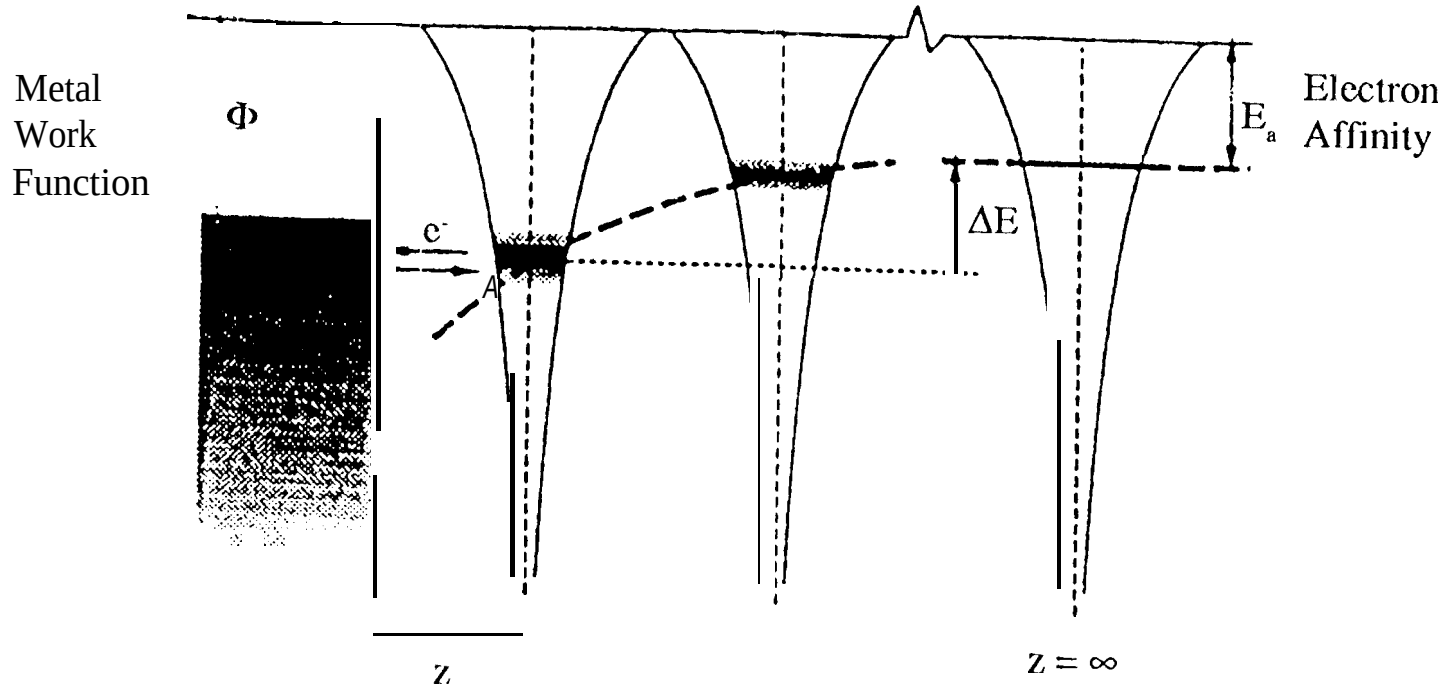
Metal
Work
Function
Φ
e⁻
A
ΔE
E_a
Electron
Affinity
z
z = ∞
DISTANCE FROM SURFACE

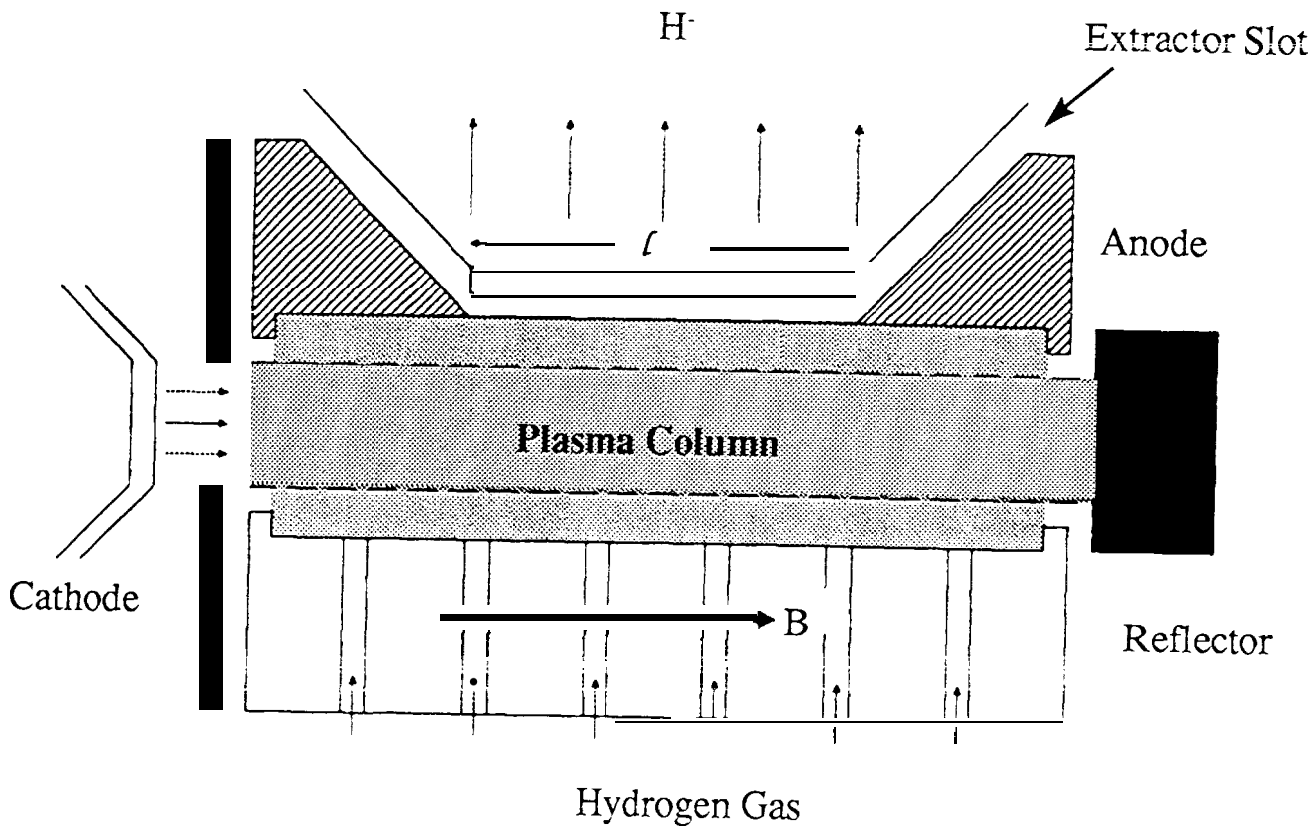
H-
Extractor Slot
Anode
Plasma Column
Cathode
B
Reflector
Hydrogen Gas

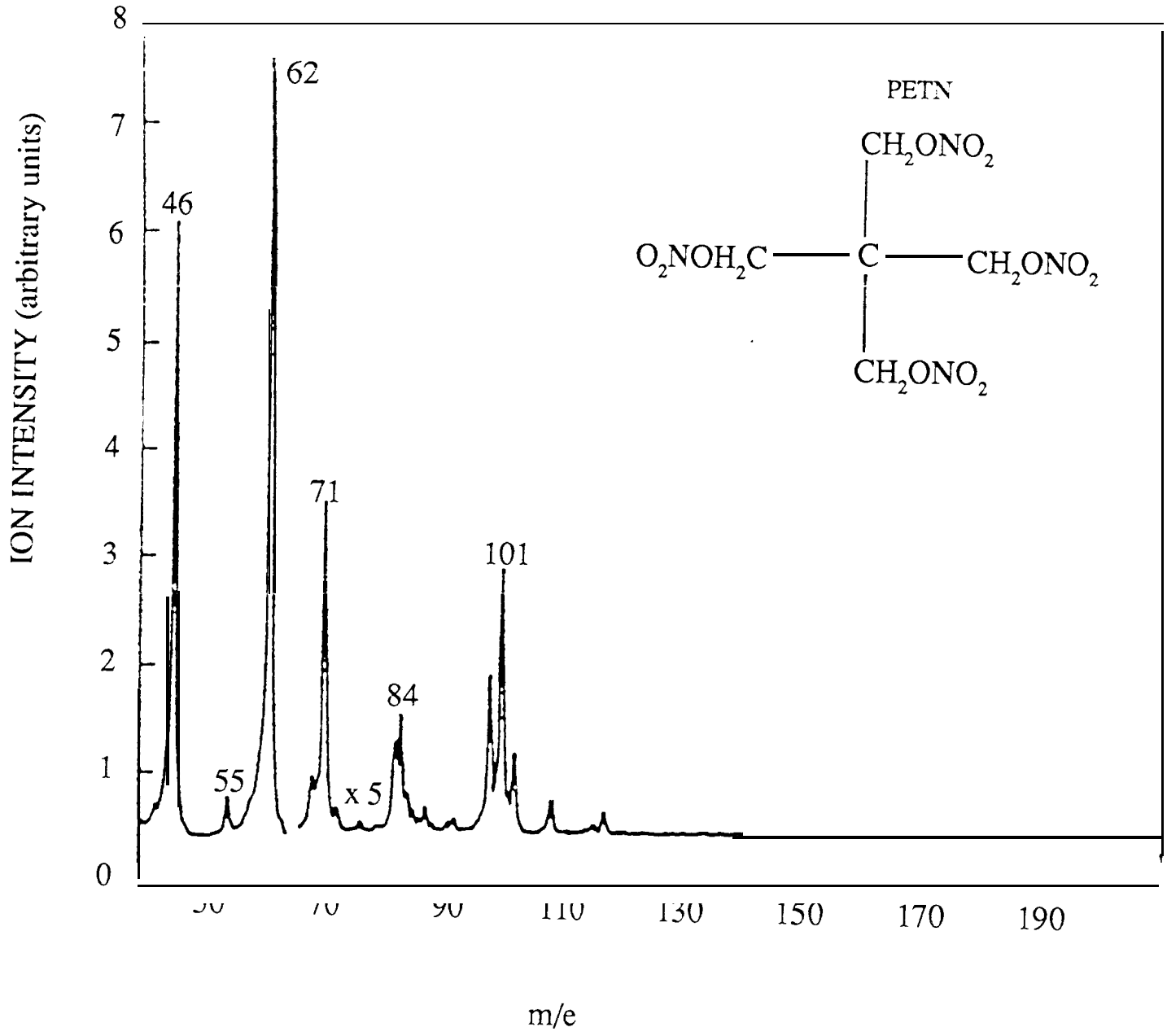
ION INTENSITY (arbitrary units)
8
7
6
5
4
3
2
1
0
46
62
71
55
x 5
84
101
PETN
CH_2ONO_2
O_2NOH_2C
C
CH_2ONO_2
CH_2ONO_2
70
90
110
130
150
170
190
m/e

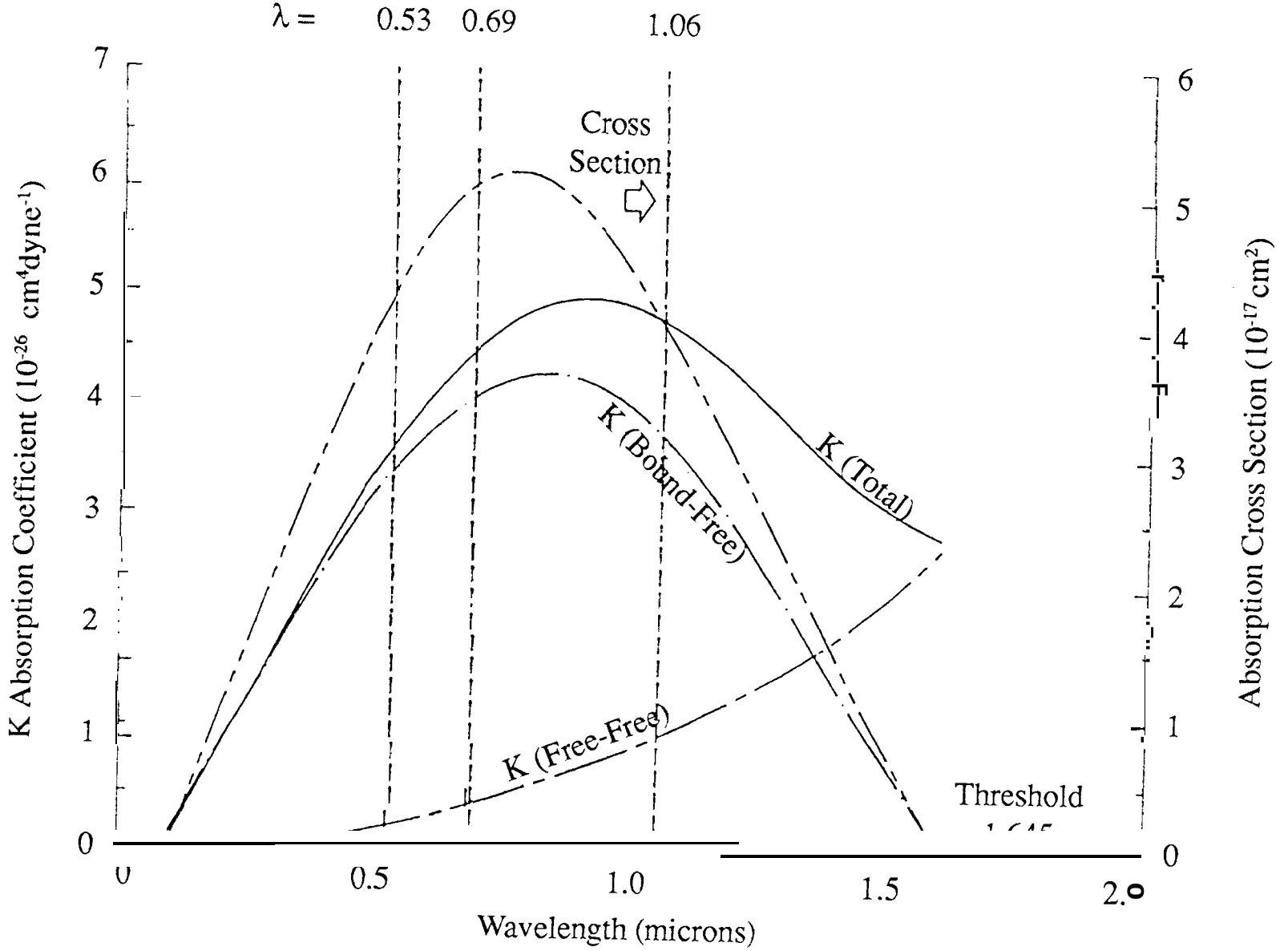
λ = 0.53 0.69 1.06
Cross Section
K (Total)
K (Bound-Free)
K (Free-Free)
Threshold
K Absorption Coefficient (10^{-26} cm^{4}dyne^{-1})
Absorption Cross Section (10^{-17} cm^2)
Wavelength (microns)
0
0.5
1.0
1.5
2.0
1
2
3
4
5
6
7